Analysis of the extracellular battlefield of potato blight disease

Laura Ossorio Carballo



Wolfson college

Department of Biology

University of Oxford

Supervised by Professor Renier A.L. van der Hoorn

Thesis submitted for the degree of *Doctor of Philosophy*

September 2022

Laura Ossorio Carballo

Wolfson college

Department of Biology

University of Oxford

Supervised by Professor Renier A.L. van der Hoorn

Thesis submitted for the degree of *Doctor of Philosophy*

September 2022

Abstract

Antagonistic interactions between plant and pathogens trigger plant immune responses that rely on complex signalling networks in which molecules and proteins of diverse nature interact to avoid pathogen colonisation. On their side, plant pathogens have developed mechanisms to suppress plant immunity. Secreted hydrolases play a key role in early plant immunity as they can release pathogen molecules in the apoplast that can be sensed by plant receptors and pathogens secrete inhibitors to supress their activity. This suppression of hydrolase activities can help the pathogen to overcome plant defences and establish a compatible interaction causing disease.

In this thesis we investigated apoplastic hydrolytic activities during infection by the causal agent of potato blight disease: the oomycete *Phytophthora infestans*. In chapter 2, we monitored the impact of leaf detachment in infection assays in the model organism *Nicotiana benthamiana*. We addressed the hydrolytic activity changes on the apoplast upon detachment and we used proteomics to examine protein changes in apoplast and total extract. We then assessed the impact of detachment in specific immune responses triggered by pathogen-associated molecular patterns and effectors. In chapter 3, we used ABPP coupled with mass spectrometry to study the active proteome of the tomato apoplast during early infection of *P. infestans*. We compared abundance and activity data to identify putative post translational regulation of apoplastic hydrolases activity. Additionally, we performed convolution ABPP coupled with mass spectrometry to discover novel suppressed tomato hydrolases upon *P. infestans* infection. Finally in chapter 4, we characterised a novel secreted cysteine protease from *P. infestans* using transient expression *in* planta. We confirmed the activity of the novel *P. infestans* protease and its inhibition by protease secreted inhibitors from *P. infestans*

using ABPP and substrate-specific activity assays. Furthermore, we compared the expression patterns of the *P. infestans* protease and inhibitors throughout the time course of infection. Altogether, the present thesis provides an overview of how plant immunity is affected in detached leaves infection assays. It also provides evidence for novel apoplastic hydrolytic activity in the context the potato blight disease and dwells into the impact of apoplastic proteases in immunity.

Acknowledgements

This thesis would not have been possible without the help and encouragement of so many people. That is why, all the sentences are constructed using the first person of the plural. Few times those "we" have had such a strong meaning, and I dedicate this thesis to all those who directly or indirectly, have been part of this scientific and extraordinary journey.

First of all, a huge thanks to my supervisor and fundamental pillar of this work: Prof Renier A L van der Hoorn. Without his infinite patience and his guidance this thesis would not have been possible. Moreover, it is him who has helped and guided me to become the scientist I am now a days. I will never forget the first time I visited the so-called Plant Sciences department (now Biology department) to meet him and his team for the interviews. I knew from the very beginning that was the place where I wanted to become a PhD, and four years later that dream has culminated in this thesis. Eternal thanks, Renier.

Thanks also to Marie Sklodowska-Curie Actions for their supporting funds, the European Union for making possible this program and to all the people within PROTECTA network. Regardless the pandemic and the limitations it imposed, it has been a pleasure to meet you all.

Thanks to the lab members Urzula and Sarah for their amazing technical support. Your help has been fundamental to our research.

Also, to my collaborators in the mass spectrometry facility of Essen, specially to Dr Farnusch Kaschani.

A huge thanks to all the current and former lab members with which I shared these fantastic years in Oxford:

- Pierre: Thanks so much for all the guidance and patience you had teaching me all the techniques used in the lab when I arrived. I will never forget those evenings doing ABPP while playing some R&R in the speakers.
- Philippe: I want to thank you for being a reference point and a truly scientific inspiration for me, but moreover I am even more grateful I could call you friend and you and Helene

know that whenever I am, you will find your home. For many more years of friendship and scientific adventures!

- Judith: Thanks you so much for being so inspiring to me and for being there for some evening pints!
- Kyoko: I am really grateful I get to know you and for being the representation of great science and hard work. I wish you the best in all the future adventures, you have been a truly example of what is an excellent scientist!
- Mariana: gracias por haber sido una compañera dentro y fuera del trabajo, y port u apoyo en lo bueno y en lo malo, que realmente me ayudó. Mis mejores deseos para el futuro.
- Emma: pequeña patatita, you have been one of the most amazing and intelligent humans I had the pleasure to meet in my life. I cannot express with words how grateful I am for all those moments we have spent together inside and outside the lab, and how much you have helped me to overcome difficulties. You have left a permanent fingerprint in my heart and you have a friend in me for the rest of the years to come!
- Maria: POTATO TE QUIERO, es un amor de potato a potato tan intenso que no tengo palabras para expresarlo. Siempre estuviste ahí cuando más lo necesite, y para lo bueno nunca pediste in raincheck. No puedo esperar a celebrar contigo y con Jose tantas cosas que tenemos que celebrar… ☺
- Tee: Thank you so so much for always being there ready to give a hand with any problem I could have in the lab (or with the scripts!) and for our friendship, and all those super deep conversations we had sometimes late in the evenings in the office. And obviously for all those amazing moments outside the lab, chicken wings are not and will never the same without you.
- Jiorgos: My friend, thank you so much for all the science, pints and amazing moments we shared with the crew, you really represent the spirit of what Oxford experience has been to me, and you know you have a friend in me. It has been a pleasure and I make a toast for many years of friendship to come.
- Pollito (Marcel): Pio pio pio. Quién me iba a decir que aquella llamada que te hice desde Barna iba a ser el principio de esta aventura maravillosa. Sabes que te voy a estar eternamente agradecida por haber sido el principal agente causal de que yo me fuese a Oxford, y sabes que siempre siempre vas a tener una amiga allí donde yo esté. Esta tesis no hubiese podido suceder sin tí, tu apoyo, y todos los buenos momentos que vivimos. A tí te la dedico especialmente.

- Felix: Thanks so much having always a smile and warm words ready every morning, and for your support and discussions about data (also for those couple of breakfast at Brasenose and the unforgettable formal dinners!). It has been a pleasure to meet you and to have you as a colleague!
- Alice: You have been a truly amazing colleague, and I cannot be more sure you have amazing things waiting for you in the years to come.
- Issy: Thank you so much for all those conversations and good moments we had in the office. I wish you the best in your future adventures!

To other member of the department that have also been an essential part of this work:

- Hayley: I cannot express how lucky I feel I get to know you and become your friend. You have been there in some of the most amazing moments and memories I have from Oxford, and you also have been always there to listen and support whenever I needed it. I will be there always for you ;)
- Bea: Gracias infinitas por todas las conversaciones y apoyo que me brindaste, eres una persona increíble y te mereces absolutamente y solamente lo mejor. Me siento tremendamente afortunada de haberte conocido.
- Riccardo: I see you in Rome man! You are such a inspiring person and scientist, and I will never forget the unforgettable amazing moments we shared in Oxford!

Estas son líneas dedicadas a aquellas personas que aun estando fuera de Oxford, fueron actores principales también de esta tesis:

- Mi querida amiga Mariana Bustamante: desde el día en que te conocí, te admiré tanto como persona como científica. Para mi has sido siempre y seguirás siendo un modelo de vida en todos los aspectos, no solo por tu éxito profesional, sino sobre todo por esa Fortaleza mayúscula que posees y esa naturaleza generosa y buena que te define. No cambies nunca, todo lo que tienes te lo mereces con creces, y espero poder seguir formando parte de tu órbita en los años que nos queden.
- Mi amigo y compañero Xurde: Siempre has sido un referente para mí desde que nos conocimos hace ya unos añinos en la facultad. Fueron de los mejores días de mi vida y nunca olvidaré todas aquellas tardes en la biblioteca del BOS. Sabes que no hay océano que diluya nuestra amistad, y estoy deseando que vuelvas a los continentes europeos para

poder verte más a menudo y compartir charlas interminables con unos culinos. Gracias por todo, siempre te llevo en el pensamiento.

- Mi amiga Laura: gracias por haber estado ahí desde hace tanto tiempo y tan incondicionalmente. Tú has formado parte de mi vida en lo bueno y en lo malo y jamás estaré agradecida lo suficiente a ese maldito curso Erasmus por haber sido lo que nos acercó. Eres una persona maravillosa, inteligentísima y espero poder compartir contigo muchas más aventuras en el futuro.

Un agradecimiento especial también para todos los brillantes profesores que tuve durante los años como estudiante de biología en la Universidad de Oviedo, porque ellos forjaron la base de la científica que soy ahora. Especialmente al doctor José María Pérez Freije, porque él me enseñó los secretos de las hidrolasas, por haberme transmitido la pasión por la ciencia y la curiosidad por aquellas elegantes enzimas y por haber sido un ser humano excepcional dentro y fuera del aula. Nunca me olvidaré de tus lecciones.

Y por último pero obviamente no menos importante, quiero dedicar esta tesis enteramente a mis padres. Ellos son los que lo han dado todo por mí, los que me cogieron de la mano cuando me caí y la constante base sobre la que he forjado mis principios. Sin ellos y sin su apoyo, nada de ésto hubiese pasado. Gracias a su amor incondicional, puedo estar orgullosa de lo que soy hoy. Gracias a su apoyo, he podido llegar más lejos. Gracias a sus consejos, he podido superar las adversidades. Gracias a su paciencia, he podido aprender de mis errores. Gracias a su entrega, he sentido que podía alcanzar mis metas. En definitiva, gracias a ellos, soy lo que soy. Esta tesis, que es parte de mí, es vuestra. Os quiero, siempre.

GRACIAS, THANK YOU.

Laura.

Table of Contents

CHAPTER 1: GENERAL INTRODUCTION. THE APOPLAST AS THE EXTRACELLULAR BATTLEFIELD IN PLANT-PATHOGEN INTERACTIONS. 10

THE PLANT EXTRACELLULAR SPACE IS SURVEYED BY PLANT IMMUNE SYSTEM ... 10
EXTRACELLULAR RECEPTORS SENSE APOPLASTIC MOLECULES ... 12
THE ROLE OF APOPLASTIC SERINE AND CYSTEINE HYDROLASES IN IMMUNE RESPONSES ... 13
SOLANACEAE FAMILY IN PHYTOPATHOLOGY: THE MODEL *N. BENTHAMIANA* AND THE CROP *S. LYCOPERSYCUM* ... 14
ABPP FOR STUDYING PLANT IMMUNITY ... 16
AIM OF THE THESIS ... 17
BIBLIOGRAPHY ... 18

CHAPTER 2: LEAF DETACHMENT IMPACTS *N. BENTHAMIANA* IMMUNE RESPONSES. 26

INTRODUCTION ... 26
RESULTS ... 27
Leaf detachment affects extracellular protein accumulation and subtilase activity, and impacts principal cellular processes. 27
Detachment significantly delays ROS burst associated with elicitor flg22 sensing ... 31
Detachment impacts P. syringae infection phenotype of N. benthamiana leaves ... 32
Cell death tiggered by P. infestans secretome is impaired upon detachment and in sobir1 mutants ... 33
P. infestans infects similarly WT and sobir1 mutant N. benthamiana detached leaves. ... 34
DISCUSSION ... 37
Protein accumulation dynamics upon leaf detachment ... 37
Detachment impacts responses triggered by P. syringae ... 39
PAMP Sensing and immunity against P. infestans are compromised upon detachment. ... 40
MATERIALS AND METHODS ... 41
N. benthamiana and P. infestans growth conditions ... 41
Apoplastic fluid extraction and fluorescent ABPP and SDS-PAGE ... 42
FASP sample preparation for mass spectrometry analysis ... 42
Proteomic analysis ... 43
Oxidative burst luminol assay ... 43
WT and ΔhopQ P. syringae DC3000 spot infiltrations ... 43
P. infestans secretome collection ... 44
P. infestans infection biomass analysis ... 44
BIBLIOGRAPHY ... 45
SUPPLEMENTARY MATERIALS ... 49

CHAPTER 3: LARGE-SCALE ACTIVITY-BASED PROTEIN PROFILING OF APOPLAST REVEALS HYDROLASE MANIPULATION UPON INFECTION BY *PHYTOPHTHORA INFESTANS*. 51

INTRODUCTION ... 51
RESULTS ... 52
Tomato apoplastic proteome changes upon P. infestans infection ... 52
ABPP-MS unveils P. infestans and tomato apoplastic activome during infection. ... 58
Seven tomato hydrolase protein groups might be subject of post-translational regulation during infection. ... 61
Convolution ABPP-MS reveals a tomato SCPL as a possible inhibited hydrolase upon infection. ... 63
DISCUSSION ... 67
MATERIALS AND METHODS ... 72
Money Maker tomato plants infection with P. infestans spores. ... 72
Apoplastic fluid isolation ... 72
In-solution trypsin digestion of total proteomes ... 73
Labelling of active apoplastic hydrolases and affinity purification ... 73
Convolution ... 74
On-bead digestion and peptide purification ... 74
LC-MS analysis ... 75
Data analysis ... 75

Fluorescent ABPP *76*
BIBLIOGRAPHY 77
SUPPLEMENTARY MATERIALS 84

CHAPTER 4: CHARACTERISATION OF PAIN1A: A NOVEL PAPAIN1-LIKE CYSTEINE PROTEASE SECRETED BY *PHYTOPHTHORA INFESTANS*. 108

INTRODUCTION 108
RESULTS 110
Selection of P. infestans secreted proteases for heterologous expression *110*
Pain1a is conserved in Phytophthora genus. *112*
Pain1a does not affect flg22 signalling. *114*
Pain1a activity is inhibited by EPICs of P. infestans. *115*
Opposite expression pattern of Pain1a and EPICs. *116*
DISCUSSION 117
MATERIAL AND METHODS 120
Pain1a orthologs search and alignment *120*
RNAseq expression analysis *120*
Phytophthora infestans and Nicotiana benthamiana growth conditions *120*
Cloning *121*
Agrobacterium-mediated in planta expression *121*
ABPP and SDS-page *122*
ROS burst assays *122*
EPIC2B E. coli expression and protein purification *123*
Plate reader inhibition assays *123*
Alphafold2 structural prediction *123*
BIBLIOGRAPHY 124
SUPPLEMENTARY MATERIALS 130

CHAPTER 5: GENERAL DISCUSSION, CONCLUSIONS AND FUTURE PERSPECTIVES. 131

IMPACT OF LEAF DETACHMENT IN PLANT IMMUNITY: CONCLUSIONS AND FUTURE PERSPECTIVES. 131
TOMATO APOPLASTIC PROTEOME AND ACTIVOME CHANGES UPON *P. INFESTANS* INFECTION: CONCLUSIONS AND FUTURE PERSPECTIVES. 132
A ROLE FOR PAIN1A IN *P. INFESTANS* PATHOGENICITY: CONCLUSIONS AND FUTURE PERSPECTIVES. 134
CONCLUSION 136

Chapter 1: General introduction. The apoplast as the extracellular battlefield in plant-pathogen interactions.

The plant extracellular space is surveyed by plant immune system

The space located between the plant cell membrane and the cell wall is referred as apoplast. The term was introduced by E. Münch in the 20th century, and it refers to the plant extracellular space (*apo-* prefix meaning "away" and *plast* meaning "living structure").

Biotic and abiotic stresses signals can confluence in the apoplast as a result of tissue damage and other pathogen-derived molecules release[1–5] (**Figure 1**). Consequently, the apoplast is a dynamic environment with a diverse molecular composition. Among apoplastic soluble molecules we can find components of the cell wall, signal transducing hormones, secreted proteins and other molecules such as reactive oxygen species[1,2,6–8].

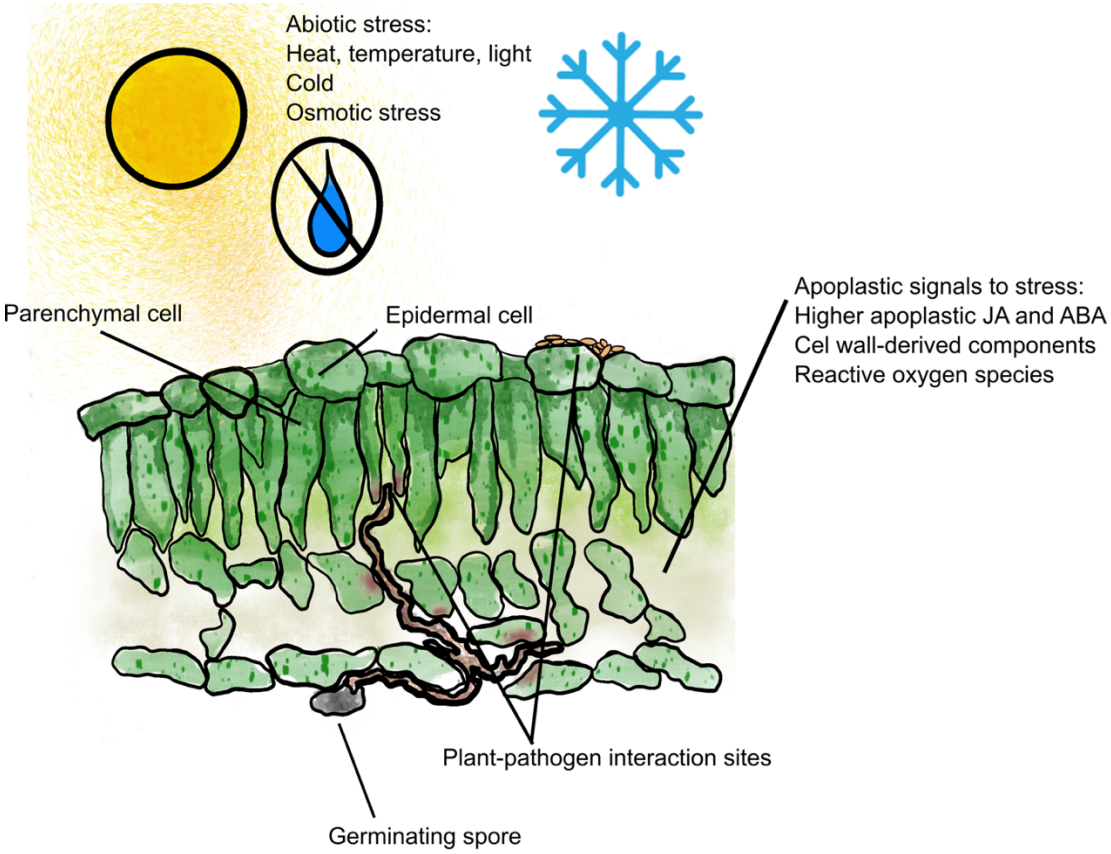


Figure 1. The apoplastic battlefield. Represented in the figure, different stresses that can confluence in apoplastic signals. For instance, heat stress, osmotic stress, bacterial growth or germinating pathogens colonising the apoplast. Laura Ossorio Carballo, 2022©.

The cell wall is an ever-changing structure that responds to plant developmental changes and to stresses of different nature such as pathogen attacks or wounding. It acts as a primary physical barrier against pathogen colonisation and adjustments in its composition are tightly regulated and often involve the release of cell wall derived-molecules into the apoplast[1,9]. Some pathogens can secrete galacturonases that degrade the primary cell wall component oligogalacturonides[10]. The released cell wall components can elicit plant defence responses when they are sensed by specific receptors. For instance, cell wall associated WAK receptors can bind to pectin molecules and unleash a phosphorylation cascade resulting in the activation of a stress response[9].

The apoplast is also a place where distal hormonal signalling occurs. For instance, jasmonic acid is secreted from the cells into the apoplast during abiotic stress. There it can move from the roots to the shoots inducing a systemic response and promoting plant stress resilience[2]. Phosphatidic acid (PA) is another example of an apoplastic molecule that transduces stress signals. The hormone abscisic acid promotes the activity of apoplastic phospholipases that results in the accumulation of apoplastic phosphatidic acid ultimately inducing stomatal closure[11].

The apoplast contains an important number of secreted proteins. As such, apoplastic pathogenesis-related proteins (PR) are components of the plant immune system and they play a key role in act against pathogen colonisation[12]. For instance, apoplastic thaumatins and osmotins belong to the PR5 class and are associated with osmotic stress. They also have antifungal activity presumably due to membrane permeabilisation that leads to the rupture of fungal hyphae[13,14]. An example is tobacco osmotin II AP24 that induces lysis of *P. infestans* hyphae and impairs the growth of the oomycete[15].

Pathogen Related-9 (PR-9) family comprises proteins with peroxidase activity triggered upon pathogen colonisation. Peroxidases are abundant in the apoplast and they promote the generation of oxygen radicals or reactive oxygen species (ROS) during biotic stress[16]. ROS toxicity can hamper pathogen growth and also damage cellular components such as DNA or lipids which serves as a signalling mechanism that triggers further immune responses such as hypersensitive response (HR)[17,18].

Another prominent example of apoplastic PR proteins are chitinases. Chitinases hydrolyse a major component of fungal cell walls (chitin) and they classify into different PR classes (PR-3, 4, 8 and 11) depending on their protein domains and activity[12].

Overall, the soluble fraction of plant apoplast has a complex composition that can change rapidly as a response of different external stimulus.

Extracellular receptors sense apoplastic molecules

Plant pattern recognition receptors (PRRs) survey the apoplastic space with their extracellular domains that bind to self and non-self molecules. Tissue damage and pathogen molecular patterns can be sensed by PRRs during abiotic and biotic stress[19–22]. The extracellular domain of PRRs determines the binding specificity. For instance, extracellular leucine-rich repeat (LRR) domain found in receptor FLS2 can bind the immunogenic peptide flg22 derived from bacteria flagellin in a BAK1 coreceptor dependent manner[23,24]. Likewise, LRR domain of the receptor-like protein ELR from the wild relative of tomato *Solanum microdontum* recognises *P. infestans* elicitor INF1, promoting cell death[25]. PRRs containing LysM domain such as CERK1 recognise chitin and peptidoglycans during fungal pathogens colonisation[26–28]. Pathogens such as *Zymoseptoria triciti* secrete LysM domains that mimic plant LysM receptors sequestering chitin and avoiding immune responses[29].

PRRs act in a orchestrated way with other receptors to trigger downstream immune signalling. Co-receptor BRASSINOSTEROID INSENSITIVE 1-associated receptor kinase 1 (BAK1) and related SOMATIC EMBRIOGENESIS RECEPTOR kinases (SERKs) are required to activate downstream immune responses of FLS2 and ELR receptors (**Figure 2**), and BAK1/SERK is considered an immune hub in which different immune stimuli converge[30–32].

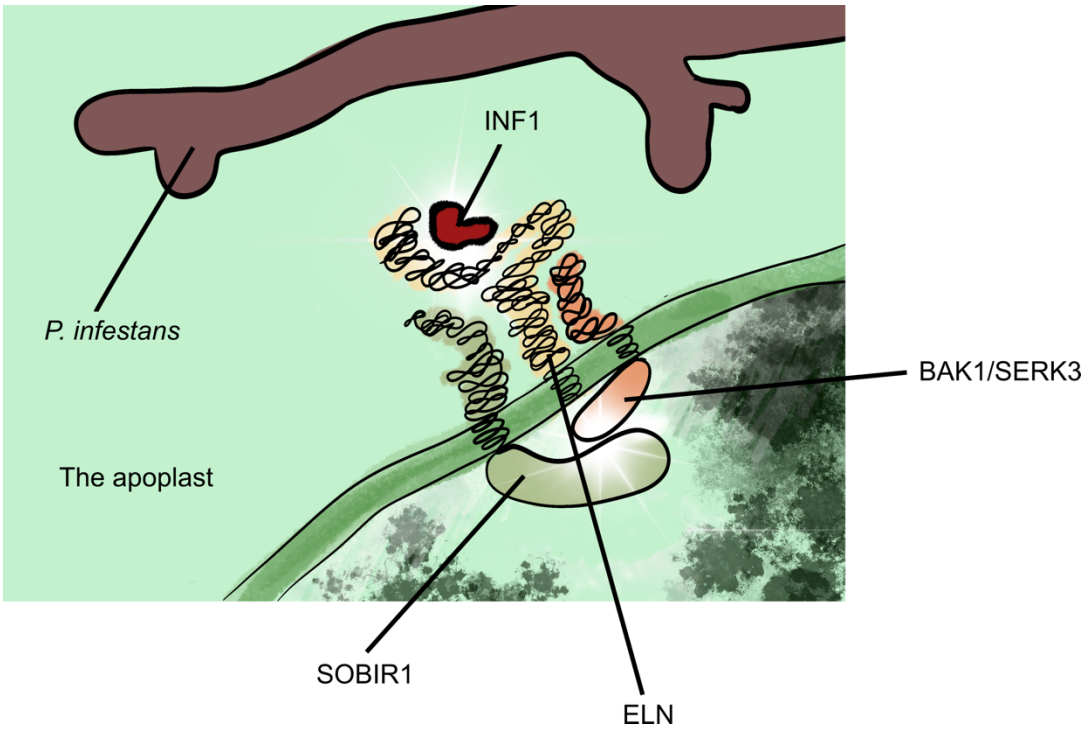


Figure 2. Elicitin INF1 triggering an immune response upon INF1 recognition. The receptor ELN can recognise the effector INF1 from *P. infestans* and develop a SOBIR1 BAK1/SERK3 dependent immune response that culminates in HR and cell death. Laura Ossorio Carballo 2022©.

The role of apoplastic serine and cysteine hydrolases in immune responses

Serine hydrolases (SH) are enzymes that possess a nucleophilic serine residue necessary for the hydrolysis of their substrates. The family comprises enzymes with protease, lipase and esterase activities[33]. In plants, serine hydrolases can be found abundantly in the apoplast and their functions are varied. The most abundant family of apoplastic serine hydrolases are subtilases. Subtilases are proteases that belong to the family/clan S8 of the MEROPS classification and they have an autoinhibitory domain that acts as a chaperone regulating proteolytic activity[34]. Apoplastic subtilases such as the P69 family participate in plant immune responses[35]. An extracellular leucin-rich protein induced during disease is processed by P69C in tomato[36], ultimately contributing to the induction of jasmonic acid (JA) synthesis and the subsequent innate immunity response[37]. Moreover, tomato P69B is a serine protease that cleaves and activates the immune protease Rcr3 as part of a proteolytic cascade[38].

Serine carboxypeptidases are enzymes that cleave amino acids from the C-termini of their substrates and they belong to the MEROPS family S10. Plant extracellular serine carboxypeptidases can participate in the allocation of nitrogenated compounds during developmental processes such as cell elongation[39]. They are also known to regulate ABA signalling,

promoting seed germination in rice[40]. They are commonly secreted in digestive tracks of animals including plant parasitic insects. Plants produce carboxypeptidases inhibitors as a defence against herbivorous[41–43].

Another example of secreted serine hydrolases are methyl and carboxy esterases. Methyl esterases participate in the degradation of cell-wall components. During infection, induction of pectin methylesterases can promote infection of necrotrophic pathogens such as *Botrytis cinerea*[44]. Carboxyesterases are implicated in JA, SA and indolacetic acid synthesis and activation[45]. Moreover, esterases are also involved in the release of volatile compounds in tomato that confers these fruits their characteristic flavour[46].

Apoplastic papain-like cysteine proteases (PLCPs) contain a reactive cysteine at their active site and participate in plant immunity. During *Ustilago maydis* infection, maize apoplastic PLCPs and SA undergo a positive feedback loop of induction promoting immunity[47].

Another prominent example of immunity-PLCP is tomato Rcr3. This protease can bind inhibitors secreted by the pathogen *Cladosporium fulvum* such as Avr2, and act as a coreceptor with receptor-like protein Cf-2 triggering tomato immune responses in tomato[48]. Rcr3 also confers resistance against *P. infestans* and it is targeted by the *P. infestans*-derived cystatin-like inhibitors EPIC1 and EPIC2B[49].

Also the depletion of the tomato PLCP inhibited by *P. infestans* Pip1 induces susceptibility to unrelated pathogens such as *C. fulvum*, *P. infestans* and *Pseudomonas syringae*, suggesting that this protease acts as a hub for immunity[50]. Close homologs of tomato C14 in *N. benthamiana* and potato confer resistance against *P. infestans* and are inhibited by secreted EPIC effectors[51–53]. Moreover, C14 secretion is prevented by the *P. infestans* effector Avrblb2[52].

Solanaceae family in phytopathology: the model *N. benthamiana* and the crop *S. lycopersycum*

Nicotiana benthamiana is an endemic species of Australian continent that belongs to the *Solanaceae* family. This species has unique features that made it become a model organism in phytopathology. Firstly, *N. benthamiana* is very susceptible to viral infection such as tomato spotted wilt virus, possibly due to a mutation in an RNA-dependent RNA polymerase gene[54]. *N. benthamiana* is also suitable for the application of genetic manipulation techniques such as virus-induced gene silencing (VIGS)[55] and agrobacterium-mediated transient expression[56].

Another major advantage of *N. benthamiana* is that it is closely related to several crop species of social and economic interest such as *Solanum lycopersicum* (tomato), *Solanum tuberosum* (potato), *Solanum melongena* (aubergine) and *Solanum capsicum* (pepper). This taxonomic and evolutionary relationship has allowed researchers to perform functional characterisation of crop genes taking advantage of *N. benthamiana*. For instance, Kourelis *et al.* (2020)[57] developed a transient hypersensitive response assay to study Rcr3 of *Solanum pimpinellifollium* role in immunity. In the assay, the transient expression of *Sp*Rcr3 in *N. benthamaiana* leaves along with Cf2 receptor and the *C. fulvum* effector Avr2 triggers an hypersensitive response (HR). Further experiments showing the inhibition of Rcr3 by Avr2 by activity-based protein profiling (ABPP) and the lack of HR response when key residues for the interaction of these proteins confirms the interaction of these three proteins. Another good example of *N. benthamiana* versatility can be seen in the study conducted by Brendolise *et al.* (2017) in which the authors generate a library of antisense hairpin mRNA for silencing a set of *N. benthamiana* nucleotide-binding site and leucine-rich repeat proteins (NBS-LRR). These proteins are able to recognise intracellular effectors and start the effector triggered immunity (ETI) that often involves HR[58]. Using the antisense mRNA library in *N. benthamiana*, pathogen effectors of interest can be expressed in the silenced plants. A lack of HR would indicate a possible NBS-LRR interactor as both components are required for such response[59].

N. benthamiana is also used to perform infection phenotypic studies of pathogens that cause major diseases in crops such as the causal agent of potato blight disease, *Phytophthora infestans*. *P. infestans* is a filamentous organism closely related to brown algae and diatoms that can reproduce sexually and asexually[60,61]. Its life cycle comprises differentiated stages and during infection it behaves as an hemibiotroph. Motile zoopores released from multinucleated sporangia can be dispersed in droplets by the wind or can swim in flooded soils. Once a zoospore arrives to roots, tubers, leaves or stems of a host they germinate and mycelia colonises host tissue during the biotrophic phase. *P. infestans* is able to deliver effectors and obtain nutrients using haustoria[62]. These structures are formed during the biotrophic phase after a local digestion of the cell wall and is in close proximity with the host cell membrane[63]. This biotroph stage of *P. infestans* infection is characterised by the suppression of host defences, followed by an orchestrated necrotrophic phase in which host tissue dies and it is digested by the pathogen[62]. The active suppression of plant immunity during biotrophic phase is partially carried out by apoplastic and haustorial effectors secreted by *P. infestans*. For instance, *P. infestans* show a reduced expression of apoplastic elicitins during biotrophic phase, presumably to avoid recognition and the subsequent strong HR triggered by these conserved effectors[64,65]. Apoplastic small cysteine rich (SCP) proteins secreted by *P. infestans*

such as PC2 can be processed by apoplastic immune subtilases and develop a immune response. *P. infestans* might avoid this processing and subsequent recognition by secreting kazal-like EPI1 and EPI10 subtilase inhibitors during infection[66–68].

Moreover, *P. infestans* suppresses immunity related to PLCP activity at three levels. First, secreted cystatine -like EPIC inhibitors bind directly to host PLCPs suppressing their activity in the apoplast[49,51]. Secondly, the haustorial Avrblb2 effector prevents the secretion of the immune protease C14[52]. Thirdly, P69B inhibition by EPIs prevents Rcr3 maturation and subsequent Rcr3-dependant immune response[38].

Activity-based protein profiling (ABPP) for studying plant immunity

Activity-based protein profiling is a technique that is widely used in medical research and that allows to monitor changes in activity of a complex mix of proteins[69–71]. It is based on the use of small molecules that bind covalently to the active site of hydrolases. These probes can be attached to a fluorescent or to an affinity tag such as biotin. Fluorescent probes can be used to monitor activity changes of a protein sample when the labelled hydrolases are separated on a protein gel and scanned for fluorescence[72]. This ABPP-SDS page technique has been applied to the plant pathology field allowing the identification and characterisation of hydrolytic activity related to immune responses. For instance, in Sueldo *et al.* (2014) the authors identify significant activity changes prior to the development of HR in tomato seedlings, including the increase of P69B subtilase activity[73]. ABPP can also be used to discover and confirm novel inhibitor-hydrolase interactions. Convolution ABPP is a variant of the conventional ABPP protocol in which two samples are mixed and incubated prior to the labelling step. If one of those samples contains an inhibitor, the resulting fluorescent signal would be less than the average of the control and treatment fluorescence separately[74]. In the study conducted by Buscall *et al.* (2019), convolution ABPP is used to detect suppression of β-galactosidase activity suppression during *P. syringae* infection[75].

Probes attached to an affinity tag facilitate enrichment and purification of the active hydrolases in a sample, or activome. The purified activome can then be analysed with mass spectrometry allowing the identification of many of proteins at a time[76] (**Figure 3**). One prominent example of

successful application of ABPP-MS to the field of plant pathology is the detection of over 30 apopastic differential hydrolases of tomato during *Ralstonia solanacearum* infection[77].

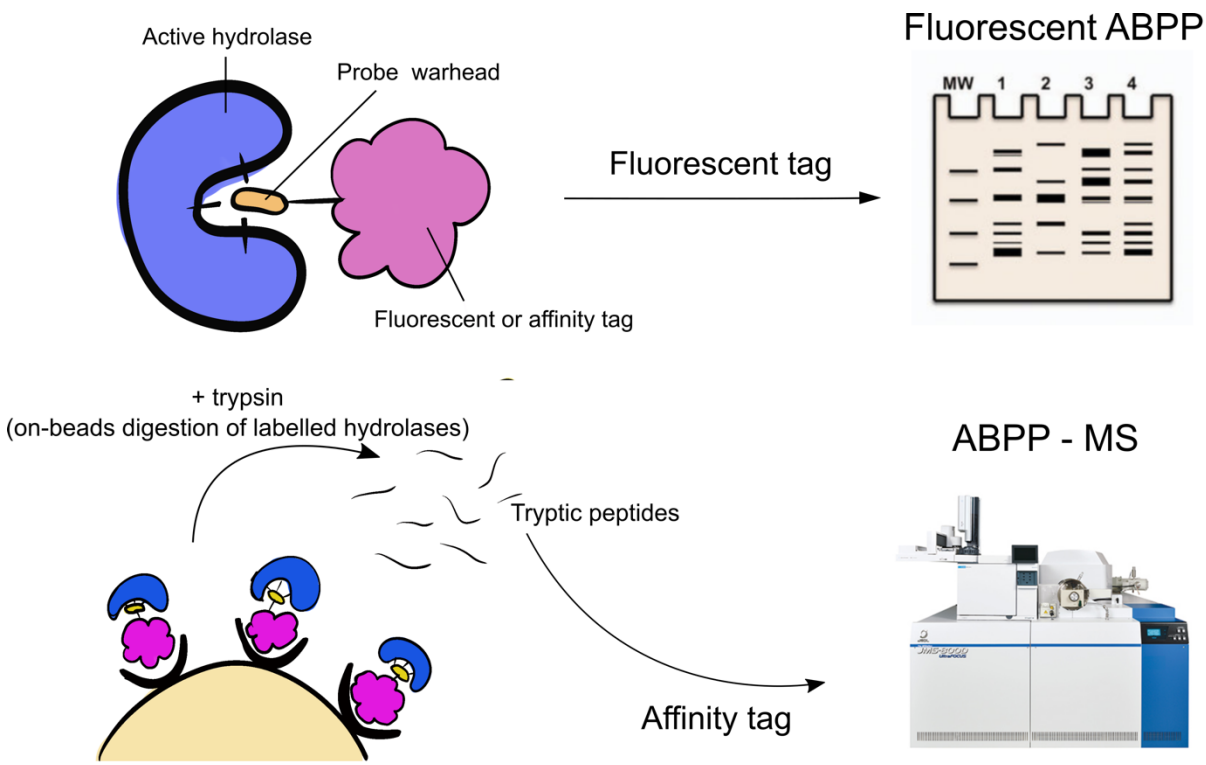


Figure 3. Fluorescent and affinity ABPP, summarised. ABPP probes can bind covalently the active site of hydrolases. These probes can be fluorescent and after SDS-PAGE separation, protein activities can be observed as fluorescent bands in the protein gel. Probes containing affinity tags such as the ones attached to biotin, make possible to purify and enrich a complex activome in a sample. Then, ABPP can be coupled with mass spectrometry for proteomic analysis. Laura Ossorio Carballo 2022©.

The recent advances in MS technology have improved greatly the number and confidence of protein identification in proteomics. Ultimately, these advances will allow plant pathologists to study plant activomes thoughtfully during the coming years.

Aim of the thesis

The general aim of this thesis is to study antagonistic interactions in the apoplast upon *P. infestans* infection. The thesis contains three experimental chapters addressing the following objectives:

Chapter 2: The objective of this chapter is to identify the impact of leaf detachment apoplastic immunity. The research in this chapter is motivated by the general use of detached leaves in infection assays and the fact that previous studies have demonstrated that leaf immunity can be compromised in Arabidopsis, potato and strawberries upon detachment[78–80]. The aim is to provide a broad picture of the general protein changes occurring upon detachment in the apoplast and to address how much these changes can affect PTI and ETI.

Chapter 3: The objective of the second chapter is to provide a comprehensive snapshot of the hydrolytic landscape in the tomato apoplast upon *P. infestans* infection, and to monitor hydrolytic activity changes that could derive from pathogen inhibitors or other post translational regulation. For this aim, we performed a large-scale shotgun and convolution ABPP on apoplastic fluids of infected tomato plants.

Chapter 4: Finally, in this chapter we will study the activity and regulation of a *P. infestans*-secreted protease. We will analyse *in silico* predicted PLCPs in *P. infestans* secretome and we will select a candidate to be core effector. Then, we will study the biochesmitry of the selected candidates *in vitro* using ABPP and inhibition assays.

Bibliography

1. Hamann, T. Plant cell wall integrity maintenance as an essential component of biotic stress response mechanisms. *Front. Plant Sci.* **3**, (2012).

2. Ali, Md. S. & Baek, K.-H. Jasmonic acid signaling pathway in response to abiotic stresses in plants. *Int. J. Mol. Sci.* **21**, 621 (2020).

3. Ali, S. *et al.* Pathogenesis-related proteins and peptides as promising tools for engineering plants with multiple stress tolerance. *Microbiol. Res.* **212–213**, 29–37 (2018).

4. Fujii, H. & Zhu, J.-K. Osmotic stress signaling via protein kinases. *Cell. Mol. Life Sci.* **69**, 3165–3173 (2012).

5. Miller, R. N. G., *et al.* Plant immunity: unravelling the complexity of plant responses to biotic stresses. *Ann. Bot.* **119**, 681–687 (2017).

6. Godson, A. & van der Hoorn, R. A. L. The front line of defence: a meta-analysis of apoplastic proteases in plant immunity. *J. Exp. Bot.* **72**, 3381–3394 (2021).

7. Smith, J. M. & Heese, A. Rapid bioassay to measure early reactive oxygen species production in Arabidopsis leave tissue in response to living *Pseudomonas syringae*. *Plant Methods* **10**, 6 (2014).

8. Cornish, K. & Zeevaart, J. A. D. Movement of abscisic acid into the apoplast in response to water stress in *Xanthium strumarium* L. *Plant Physiol.* **78**, 623–626 (1985).

9. Kohorn, B. & Kohorn, S. The cell wall-associated kinases, WAKs, as pectin receptors. *Front. Plant Sci.* **3**, (2012).

10. Humphrey, T. V., Bonetta, D. T. & Goring, D. R. Sentinels at the wall: cell wall receptors and sensors. *New Phytol.* **176**, 7–21 (2007).

11. Saucedo-García, M., *et al.* Long-chain bases, phosphatidic acid, MAPKs, and reactive oxygen species as nodal signal transducers in stress responses in Arabidopsis. *Front. Plant Sci.* **6**, (2015).

12. Sudisha, J., *et al.* Pathogenesis related proteins in plant defense response. *Plant Defence* **379–403** (2012).

13. Breiteneder, H. Thaumatin-like proteins – a new family of pollen and fruit allergens. *Allergy* **59**, 479–481 (2004).

14. Vigers, A. J. *et al.* Thaumatin-like pathogenesis-related proteins are antifungal. *Plant Sci.* **83**, 155–161 (1992).

15. Woloshuk, C. P *et al.* Pathogen-induced proteins with inhibitory activity toward *Phytophthora infestans*. *Plant Cell* **3**, 619–628 (1991).

16. Bestwick, C. S., *et al.* Localized changes in peroxidase activity accompany hydrogen peroxide generation during the development of a nonhost hypersensitive reaction in lettuce. *Plant Physiol.* **118**, 1067–1078 (1998).

17. Torres, M. A. ROS in biotic interactions. *Physiol. Plant.* **138**, 414–429 (2010).

18. Passardi, F., *et al.* Peroxidases have more functions than a Swiss army knife. *Plant Cell Rep.* **24**, 255–265 (2005).

19. Monaghan, J. & Zipfel, C. Plant pattern recognition receptor complexes at the plasma membrane. *Curr. Opin. Plant Biol.* **15**, 349–357 (2012).

20. Brustolini, O. J. B *et al.* Bioinformatics analysis of the receptor-like kinase (RLK) superfamily. *Plant Pattern Recognition Receptors.* 123–132 (2017

21. Jaillais, Y., *et al.* Extracellular leucine-rich repeats as a platform for receptor/coreceptor complex formation. *Proc. Natl. Acad. Sci. U. S. A.* **108**, 8503–8507 (2011).

22. Smakowska-Luzan, E. *et al.* An extracellular network of Arabidopsis leucine-rich repeat receptor kinases. *Nature* **553**, 342–346 (2018).

23. Chinchilla, D. *et al.* A flagellin-induced complex of the receptor FLS2 and BAK1 initiates plant defence. *Nature* **448**, 497–500 (2007).

24. Li, L. *et al.* Activation-dependent destruction of a co-receptor by a *Pseudomonas syringae* effector dampens plant immunity. *Cell Host Microbe* **20**, 504–514 (2016).

25. Domazakis, E. *et al.* The ELR-SOBIR1 complex functions as a two-component receptor-like kinase to mount defense against *Phytophthora infestans*. *Mol. Plant-Microbe Interactions* **31**, 795–802 (2018).

26. Hu, S.-P. *et al.* Lysin Motif (LysM) proteins: interlinking manipulation of plant immunity and fungi. *Int. J. Mol. Sci.* **22**, 3114 (2021).

27. Miya, A. *et al.* CERK1, a LysM receptor kinase, is essential for chitin elicitor signaling in Arabidopsis. *Proc. Natl. Acad. Sci.* **104**, 19613–19618 (2007).

28. Tanaka, K., *et al.* Role of LysM receptors in chitin-triggered plant innate immunity. *Plant Signal. Behav.* **8**, (2013).

29. Tian, H. *et al.* Three LysM effectors of *Zymoseptoria tritici* collectively disarm chitin-triggered plant immunity. *Mol. Plant Pathol.* **22**, 683–693 (2021).

30. Chaparro-Garcia, A. *et al.* The receptor-like kinase SERK3/BAK1 is required for basal resistance against the late blight pathogen *Phytophthora infestans* in *Nicotiana benthamiana*. *PLoS ONE* **6**, (2011).

31. Chinchilla, D. *et al.* A flagellin-induced complex of the receptor FLS2 and BAK1 initiates plant defence. *Nature* **448**, 497–500 (2007).

32. Chinchilla, D *et al.* One for all: the receptor-associated kinase BAK1. *Trends Plant Sci.* **14**, 535–541 (2009).

33. Sieber, S. A., *et al.* Small molecules as versatile tools for ativity-based protein profiling experiments. *Comprehensive Natural Products* **629–674** (2010).

34. Meyer, M., *et al.* Functional characterization of propeptides in plant subtilases as intramolecular chaperones and inhibitors of the mature protease. *J. Biol. Chem.* **291** (2016).

35. Schaller, A. *et al.* From structure to function – a family portrait of plant subtilases. *New Phytol.* **218**, 901–915 (2018).

36. Tornero, P. *et al.* Characterization of LRP, a leucine-rich repeat (LRR) protein from tomato plants that is processed during pathogenesis. *Plant J.* **10**, 315–330 (1996).

37. Figueiredo, J., Sousa Silva, M. & Figueiredo, A. Subtilisin-like proteases in plant defence: the past, the present and beyond. *Mol. Plant Pathol.* **19**, 1017–1028 (2018).

38. Paulus, J. K. *et al.* Extracellular proteolytic cascade in tomato activates immune protease Rcr3. *Proc. Natl. Acad. Sci.* **117**, 17409–17417 (2020).

39. Bienert, M. D., *et al.* NtSCP1 from tobacco is an extracellular serine carboxypeptidase III that has an impact on cell elongation. *Plant Physiol.* **158**, 1220–1229 (2012).

40. Li, Z. *et al.* Serine carboxypeptidase 46 regulates grain filling and seed germination in rice (*Oryza sativa* L.). *PLoS ONE* **11**, e0159737 (2016).

41. Bayés, A. *et al.* Structural basis of the resistance of an insect carboxypeptidase to plant protease inhibitors. *Proc. Natl. Acad. Sci.* **102**, 16602–16607 (2005).

42. Huang, X., *et al.* Cloning and characterization of the first serine carboxypeptidase from a plant parasitic nematode, *Radopholus similis*. *Sci. Rep.* **7**, 4815 (2017).

43. Quilis, J. *et al.* A potato carboxypeptidase inhibitor gene provides pathogen resistance in transgenic rice. *Plant Biotechnol. J.* **5**, 537–553 (2007).

44. Raiola, A. *et al.* Pectin methylesterase is induced in *Arabidopsis* upon infection and is necessary for a successful colonization by necrotrophic pathogens. *Mol. Plant-Microbe Interactions* **24**, 432–440 (2011).

45. Yang, Y. *et al.* Inactive methyl indole-3-acetic acid ester can be hydrolyzed and activated by several esterases belonging to the AtMES esterase family of Arabidopsis. *Plant Physiol.* **147**, 1034–1045 (2008).

46. Goulet, C. *et al.* Role of an esterase in flavor volatile variation within the tomato clade. *Proc. Natl. Acad. Sci. U. S. A.* **109**, 19009–19014 (2012).

47. van der Linde K, *et al.* A maize cystatin suppresses host immunity by inhibiting apoplastic cysteine proteases. *Plant Cell.* 24(3):1285-300 (2012).

48. Rooney, H. C. E. *et al.* Cladosporium Avr2 inhibits tomato Rcr3 protease required for Cf-2-dependent disease resistance. *Science* **308**, 1783–1786 (2005).

49. Tian, M. *et al.* A *Phytophthora infestans* cystatin-like protein targets a novel tomato papain-like apoplastic protease. *Plant Physiol.* **143**, 364–377 (2007).

50. Ilyas, M. *et al.* Functional divergence of two secreted immune proteases of tomato. *Curr. Biol.* **25**, 2300–2306 (2015).

51. Kaschani, F. & Van der Hoorn, R. A. A model of the C14-EPIC complex indicates hotspots for a protease-inhibitor arms race in the oomycete-potato interaction. *Plant Signal. Behav.* **6**, 109–112 (2011).

52. Bozkurt, T. O. *et al. Phytophthora infestans* effector AVRblb2 prevents secretion of a plant immune protease at the haustorial interface. *Proc. Natl. Acad. Sci.* **108**, 20832–20837 (2011).

53. Kaschani, F. *et al.* An effector-targeted protease contributes to defense against *Phytophthora infestans* and is under diversifying selection in natural hosts. *Plant Physiol.* **154**, 1794–1804 (2010).

54. Yang, S.-J., *et al.* A natural variant of a host RNA-dependent RNA polymerase is associated with increased susceptibility to viruses by *Nicotiana benthamiana. Proc. Natl. Acad. Sci. U. S. A.* **101**, 6297–6302 (2004).

55. Thomas C.L., *et al.* Size constraints for targeting post-transcriptional gene silencing and for RNA-directed methylation in *Nicotiana benthamiana* using a potato virus X vector. *Plant J.* **25**(4):417-25 (2001).

56. Wydro, M., Kozubek, E. & Lehmann, P. Optimization of transient Agrobacterium-mediated gene expression system in leaves of *Nicotiana benthamiana*. *Acta Biochim. Pol.* **53**, 289–298 (2006).

57. Kourelis, J. *et al.* Evolution of a guarded decoy protease and its receptor in solanaceous plants. *Nat. Commun.* **11**, 4393 (2020).

58. Zhai, K. *et al.* NLRs guard metabolism to coordinate pattern- and effector-triggered immunity. *Nature* 1–7 (2021).

59. Brendolise, C. *et al.* A novel hairpin library-based approach to identify NBS–LRR genes required for effector-triggered hypersensitive response in *Nicotiana benthamiana*. *Plant Methods* **13**, 32 (2017).

60. Garry, G. *et al.* Genetic diversity and host differentiation among isolates of *Phytophthora infestans* from cultivated potato and wild solanaceous hosts in Peru. *Plant Pathol.* **54**, 740–748 (2005).

61. Goss, E. M. *et al.* The Irish potato famine pathogen *Phytophthora infestans* originated in central Mexico rather than the Andes. *Proc. Natl. Acad. Sci.* **111**, 8791–8796 (2014).

62. Boevink, P. C., *et al.* Devastating intimacy: the cell biology of plant–*Phytophthora* interactions. *New Phytol.* **n/a**,.

63. Whisson, S. C *et al.* The cell biology of late blight disease. *Curr. Opin. Microbiol.* **34**, 127–135 (2016).

64. Du, J. *et al.* Elicitin recognition confers enhanced resistance to *Phytophthora infestans* in potato. *Nat. Plants* **1**, 1–5 (2015).

65. Kamoun, S., *et al.* Resistance of *Nicotiana benthamiana* to *Phytophthora infestans* Is mediated by the recognition of the elicitor protein INF1. *Plant Cell* **10**, 1413–1425 (1998).

66. Wang, S. *et al.* Cleavage of a pathogen apoplastic protein by plant subtilases activates immunity. *bioRxiv,* doi:10.1101/2019.12.16.878272 (2019).

67. Tian, M., *et al.* Second Kazal-like protease inhibitor from *Phytophthora infestans* inhibits and interacts with the apoplastic pathogenesis-related protease P69B of tomato. *Plant Physiol.* **138**, 1785–1793 (2005).

68. Tian, M. & Kamoun, S. A two disulfide bridge Kazal domain from *Phytophthora* exhibits stable inhibitory activity against serine proteases of the subtilisin family. *BMC Biochem.* **6**, 15 (2005).

69. Kozarich, J. W. Activity-based proteomics: enzyme chemistry redux. *Curr. Opin. Chem. Biol.* **7**, 78–83 (2003).

70. Wang, S. *et al.* Advanced activity-based protein profiling application strategies for drug development. *Front. Pharmacol.* **9**, (2018).

71. Lee, K. Y., *et al.* Drugging the undruggable: activity-based protein profiling offers opportunities for targeting the KLK activome. *Cancer Biol. Ther.* **23**, 136–138 (2022).

72. Hong, T. N. & van der Hoorn, R. A. L. DIGE-ABPP by click chemistry: pairwise comparison of serine hydrolase activities from the apoplast of infected plants. *Plant-Pathogen Interactions,* **183–194** (2014).

73. Sueldo, D. *et al.* Dynamic hydrolase activities precede hypersensitive tissue collapse in tomato seedlings. *New Phytol.* **203**, 913–925 (2014).

74. Chandrasekar, B., Hong, T. N. & van der Hoorn, R. A. L. Inhibitor discovery by convolution ABPP. *Activity-Based Proteomics: Methods and Protocols*, **47–56** (2017).

75. Buscaill, P. *et al.* Glycosidase and glycan polymorphism control hydrolytic release of immunogenic flagellin peptides. *Science* **364**, eaav0748 (2019).

76. Lovell, S. Unlocking the KLK activome in drug-resistant prostate cancer : biomarker discovery and target validation. *Imperial College London,* doi:10.25560/89910 (2019).

77. Planas-Marquès, M. *et al.* Protease activities triggered by *Ralstonia solanacearum* infection in susceptible and tolerant tomato lines. *Mol. Cell. Proteomics MCP* **17**, 1112–1125 (2018).

78. Miller-Butler, M. A., *et al.* Comparison of whole plant and detached leaf screening techniques for identifying anthracnose resistance in strawberry plants. *Plant Dis.* **102**, 2112–2119 (2018).

79. Liu, G. *et al.* Detached and attached *Arabidopsis* leaf assays reveal distinctive defense responses against hemibiotrophic *Colletotrichum* spp. *Mol. Plant. Microbe Interact.* **20**, 1308–1319 (2007).

80. Orlowska, E., Llorente, B. & Cvitanich, C. Plant integrity: an important factor in plant-pathogen interactions. *Plant Signal. Behav.* **8**, e22513 (2013).

Chapter 2: Leaf detachment impacts *N. benthamiana* immune responses.

Laura Ossorio Carballo[1], Pierre Buscall[1], Philippe Jutras[1], Farnusch Kaschani[2], Markus Kaiser[2], Renier A. L. van der Hoorn[1].

[1] The Plant Chemetics Laboratory, Department of Plant Sciences, University of Oxford, Oxford, UK.

[2] University of Kaiserslautern, Department of Biology, Germany.

Introduction

N. benthamiana is a plant species endemic of Australian continent and member of the Solanaceae family. In the past years, it has gained considerable attention as a model plant for molecular biology research in the field of plant pathology. *N. benthamiana* susceptibility to virus combined with the development of virus-induced gene silencing and the possibility of transiently express genes using *Agrobacterium tumefaciens* infiltration made this species a powerful tool for molecular biology research[1]. These natural advantages for research of *N. benthamiana* served to improve throughput of reverse genetic approaches and the characterisation of resistance genes-pathogen effector interactions. For instance, in the study published by Kourelis *et al.* (2020)[2] the authors explore the evolutionary history of a Solanaceae receptor and its decoy recognition using a hypersensitive response assay in *N. benthamiana*. Furthermore, the biochemical plasticity of *N. benthamiana* makes it an ideal model organism for phenotypic infection assays. Characterisation of resistance genes (*R*-genes) often requires infecting overexpressing plants to demonstrate the implication of the gene of interest in pathogenicity. One example is transcription factor *Nb*ERF173. When overexpressed, *Nb*ERF173 enhances resistance against *Phytophthora parasitica* infection in *N. benthamiana* leaves[3]. Transient expression of papain-like cysteine protease C14 of tomato reduces *P. infestans* colonisation in *N. benthamiana*[4].

In crops, infection assays are routinely performed using detached leaves to preserve germplasm of resistant individuals, maximise throughput and ensure containment[5]. In research, detached leaves are also often the plant material of choice for infection assays[6]. Nevertheless, several studies have reported significant differences in susceptibility between intact plants and detached leaves. In Arabidopsis, detached leaves showed enhanced susceptibility against the hemibiotroph *Colletotrycum* spp[7]. In potato, an elegant study published by Orlowska *et al.* (2012) demonstrates that detached leaves are infected faster by *P. infestans* than whole plants as a consequence of the lost

shoot and roots signalling required for systemic immunity[8]. It is easy to imagine the metabolic stress inflicted by detachment of leaves, as the main source of water and nutrient transport is discontinued. In Guosheng *et al.* (2007)[7] the authors could establish a link between the enhanced susceptibility and senescence in detached leaves. Many stress responses converge with immunity in plants as they share common regulatory elements. For instance, damage-associated molecules can be sensed by membrane receptors and trigger ROS bursts, ion calcium fluxes and MAP kinase signalling cascades in similar ways as pathogen-derived molecular patterns (PAMPs)[9]. Hormones also play a central role in the cross-talk between immunity and abiotic stress, as both processes can activate systemic hormonal signalling pathways[10]. The appropriate orchestration of immune responses in leaves dictates compatibility or incompatibility of plant-pathogen interactions. Despite the noteworthy evidence of leaf immunity impairment upon detachment, there are very few studies addressing in depth this question and surprisingly, no studies at all on *N. benthamiana* despite its detached leaves are frequently used for infection assays.

In the present chapter we study the impact of leaf detachment in *N. benthamiana* from an immunity perspective. For the first time, enzymatic and proteomic changes upon detachment are addressed in a comprehensive description using activity-based protein profiling (ABPP) and mass spectrometry. Moreover, we also explored the level of impact in the different layers of plant immunity: the early and mild PTI and the more drastic effector triggered immunity (ETI). Finally, we combine both pathogen and *N. benthamiana* mutants lacking genes involved in pathogenicity to shed light on the biological implications of leaf detachment on plant-pathogen interactions.

Results

Leaf detachment affects extracellular protein accumulation and subtilase activity, and impacts principal cellular processes

To address changes in the apoplastic hydrolytic landscape upon detachment, we performed ABPP of serine hydrolases on apoplastic fluid (AF) of *N. benthamiana* intact plants and detached leaves (**Figure 1A**). AF was isolated from intact plants in a humid container and from detached leaves kept in sealed petri dishes with the petiole imbibed in wet cotton. Both samples were kept under those conditions for three days prior to AF isolation.

AF from detached leaves showed a strong reduction in subtilases activity compared to intact plants (**Figure 1B**). These results exposed a major impact of detachment on extracellular subtilase activity and served as reason to further investigate the impact of detachment.

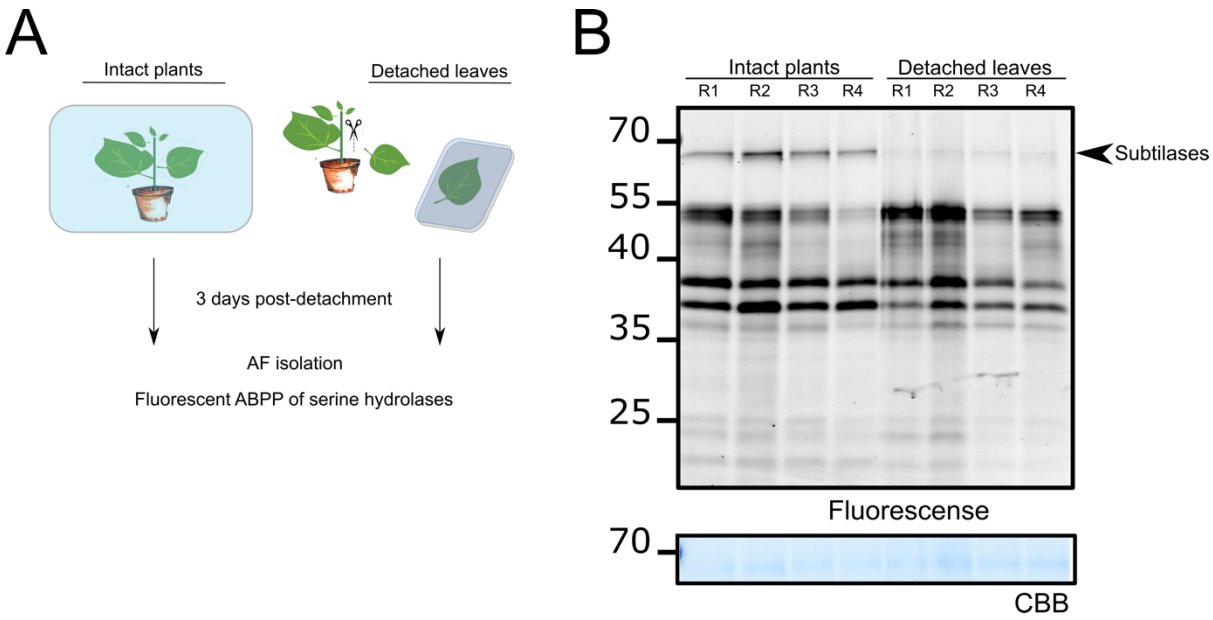


***Figure 1*. Detachment of *Nicotiana benthamiana* leaves reduces apoplastic subtilase activity. A, Experimental design.** *N. benthamiana* plants were placed in a transparent plastic box holding 90% relative humidity (approx.) for three days. Detached leaves from were placed in petri dishes with a bed of wet tissue for three days. Then, AF was extracted from half leaves and the other half was snap freezed in liquid nitrogen for further analysis. **B, Serine hydrolases activity profiles of AF isolated from intact plants or detached leaves.** AF samples were labelled with FP-TAMRA for one hour in darkness. Five volumes of cold acetone were used to precipitate the proteins before separation with SDS-PAGE and Cy3 laser scanning. The arrow points to the band corresponding to apoplastic subtilases (69 kDa) (n = 4).

To obtain a detailed analysis of protein changes in *N. benthamiana* leaves upon detachment, we analysed AF and total extract (TE) proteins obtained from the samples used for ABPP with mass spectrometry (MS). AF and TE were extracted from leaves of intact plants and leaves that were detached. Proteomes were digested with LysC/trypsin using filter-aided sample preparation (FASP). Prior to quantitative analysis, we removed suspected contaminants and only proteins containing signal peptide were considered in AF samples. A total of 250 AF proteins and 3612 TE proteins were robustly identified. Principal component analysis of both sets of samples showed a treatment-dependent clustering of all biological replicates (n = 4, **Figure 2A**).

Comparative analysis of the normalised protein intensities revealed significant changes upon detachment in AF and TE samples (**Figure 2B**). In AF, levels of 32 proteins were increased and

17 decreased upon detachment. In TE samples, levels of 432 proteins were increased and 395 decreased as a consequence of detachment.

Amongst protein families that accumulate in AF are five members of the PR-5/thaumatin-like family showed significant changes in AF as a consequence of detachment with four thaumatins up-regulated (NbD014181.1, NbD011220.1, NbD043610.1 and NbD024221.1) and one down-regulated (NbD00788.1) (**Figure 2C**). The levels of one subtilase were increased upon detachment (NbD007252.1) whereas three abundant subtilases were depleted (NbE03059263.1, NbD038132.1 -P69F homolog- and NbD038072.1). Two GDSL lipases/esterases (NbD032055.1 and NbD043094.1) showed a strong depletion in AF of detached leaves. Altogether, our AF proteome analysis demonstrate that the apoplast undergoes significant protein changes upon leaf detachment with a possible impact in immunity.

To obtain a comprehensive interpretation of the protein changes in TE of detached leaves, we analysed gene ontology (GO) enrichment among up and down regulated proteins (**Figure 2D**). GO terms on translation, protein folding, and photosynthesis processes are significantly reduced upon detachment whereas GO terms on vesicle transport, signal transduction and carbohydrate metabolic processes are increased. These data indicate that detachment affects protein homeostasis and transport as well as central metabolic processes such as photosynthesis. A full table with all proteins and scripts used for the proteomics analysis and functional clustering can be found in Supplementary files 1 and 2.

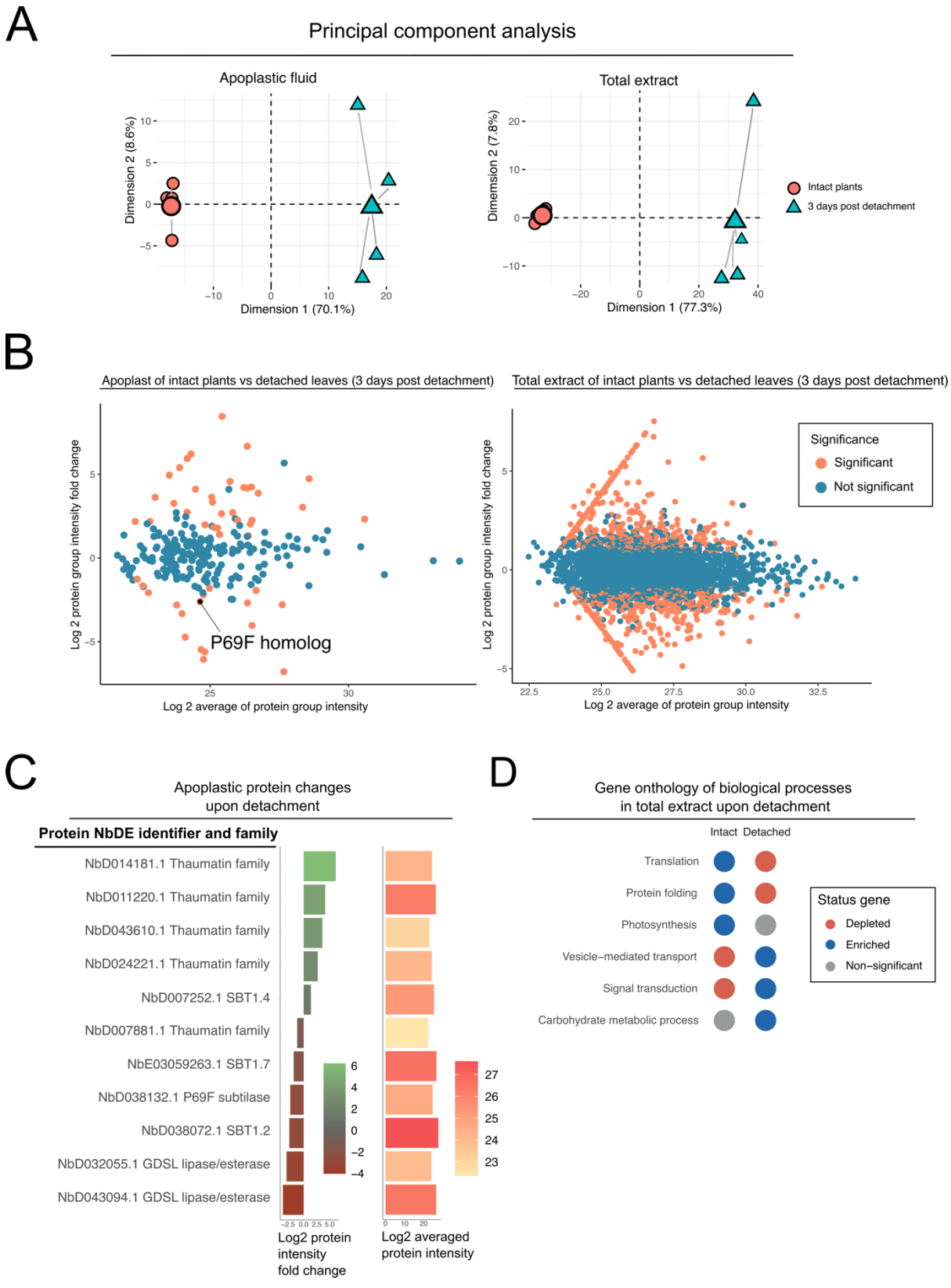


Figure 2. Significant changes in benthamiana protein levels upon detachment. **A, Principal component analysis of *N. benthamiana* AF and TE samples.** Clustering of all samples correlates with the type of samples as expected (n = 4). Samples were averaged. **B, Protein abundance changes in AF and TE.** Only proteins presenting a predicted signal peptide were considered in AF analysis. In MA plots, X axis represents the log2 averaged protein ion intensity for each experiment, y axis

represents the log2 of the fold change. Proteins represented by orange dots showed significant differences in accumulation upon detachment (n = 4, significance with BH corrected p-value < 0.05). **C, Several apoplastic protein families with possible role in immunity show differential accumulation upon detachment.** Left hand side panel shows the protein fold change upon detachment and the right hand side panel represent the log2 of the ion intensity for each of the proteins found in AF samples. **D, Gene ontology enrichment analysis of TE proteins.** Gene ontology clustering analysis was performed in TE significantly up and down regulated proteins upon detachment. A hypergeometric test was used to evaluate significance of GO terms enrichment (significance with BH corrected p-value < 0.005).

Detachment significantly delays ROS burst associated with elicitor flg22 sensing

To explore possible impact of leaf detachment on PTI, we investigated the flg22-associated ROS burst in leaf discs from intact plants and detached leaves using a luminol assay[11]. Statistical comparison of the time points with maximum luminescence value revealed a significant delay in the ROS burst associated with flg22 sensing in *N. benthamiana* detached leaves (pairwise t-test p-value < 0.05, **Figure 3A**). However, comparison of the integrated area under the curves did not reveal significant differences (**Figure 3B**). These results indicated that leaf detachment might have a general impact on PTI. Scripts and files used for the analysis can be found in Supplementary files 3.

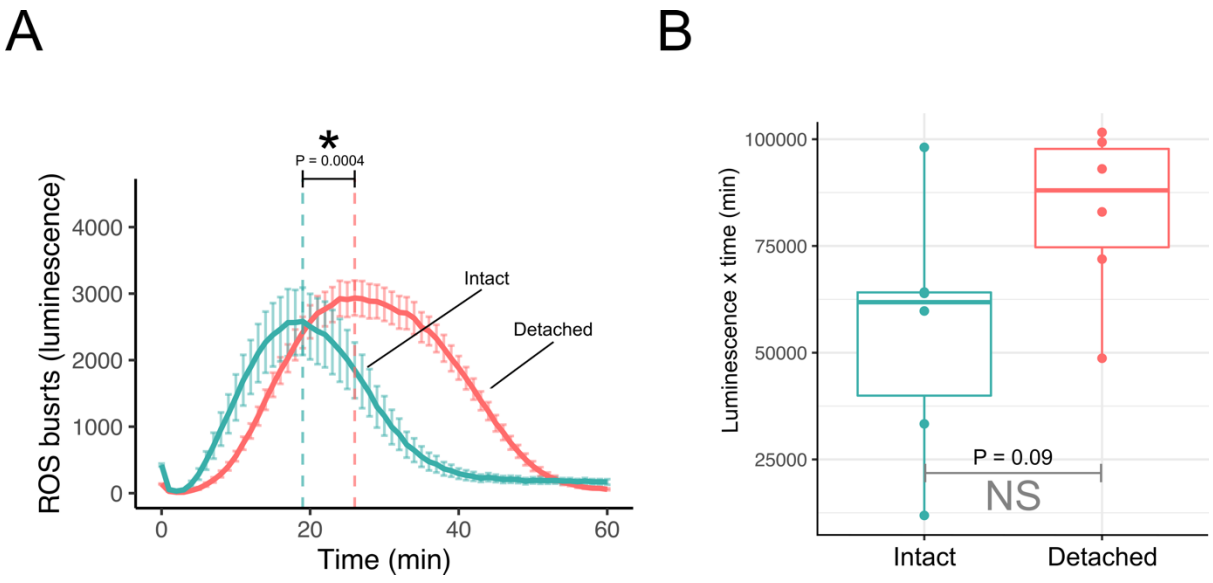


***Figure 3. ROS burst associated with flg22 sensing is delayed upon leaf detachment*. A, ROS measure over time after flg22 induction**. *N. benthamiana* leaf discs from intact plants and detached leaves were placed on top of a solution containing luminol and horse radish peroxidase. Right after adding the flg22 solution, ROS burst was monitored by chemoluminescense measures over the time using a plate reader. Error bars indicate the standard error of the mean (n = 6, T- test, significance when p-value < 0.05). Vertical dotted lines represent the average time point in which highest levels of luminesces are recorded**. B, Integrated areas under ROS burst chemoluminesce curves from intact plants and detached leaves.** Statistical anlaysis did not show significant differences between both treatments (T- test, significance when p-value < 0.05).

Detachment impacts *P. syringae* infection phenotype of N. benthamiana leaves

To evaluate if detachment impacts *N. benthamiana* ETI, we infiltrated *Pseudomonas syringae* pv. tomato DC3000 WT and mutants lacking effector HopQ (ΔhopQ)[12] in intact plants and in leaves detached immediately after infiltration. Three days after spot inoculation, leaves were scanned with a laser and leaf fluorescence was measured in the infiltrated area using ImageJ software. Data from two experiments with four and six biological replicates were combined in a randomised blocked design. Detachment and *P. syringae* genotype effect on the normalised fluorescence was analysed using two-way ANOVA. Significant differences were observed in normalised fluorescence intensity measured with a laser scanner in detached leaves versus leaves from intact plants (**Figure 4B**). Remarkably, there is a higher fluorescence in intact plants infected with WT *P. syringae* strain compared to those infected with ΔhopQ that will need to be confirmed in future. These results demonstrate that detachment affects drastically *P. syringae* infection phenotype in *N. benthamiana*. Moreover, fluorescent scans indicate that intact plants could potentially show differences between ΔhopQ and WT *P. syringae* infection but not in detached leaves, pointing towards an impact of detachment in ETI. Leaf scans of all replicates and analysis scrips can be found in Supplementary files 4 and 5.

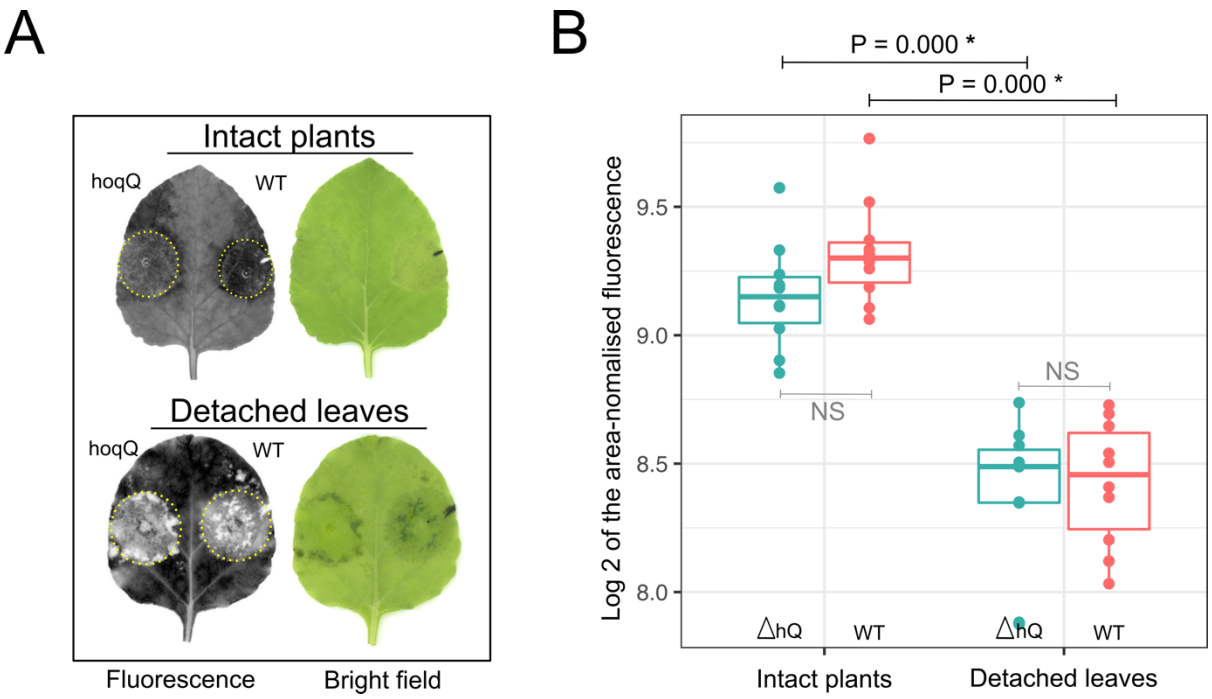


Figure 4. Detachment affects P. syringae infection phenotype of Nicotiana benthamiana leaves. **A, Fluorescent scans of *N. benthamiana* leaves infiltrated with *P. syringae* WT and ΔhopQ strains.** Half leaves were infiltrated with OD = 0.001 of *P. syringae* and plants were kept intact or leaves were detached immediately after infiltration. Scans were taken using a Typhoon scanner

with Cy5 laser three days after infiltration (n = 4 and n = 6 in two indepenent experiments). **B, Fluorescence intensity of the infiltrated area in detached leaves and intact plants.** Fluorescence intensity was measured using ImageJ software and normalised by the area of the measurement. Intensities were compared using ANOVA statistical test and significance between the groups was assessed using Tukey's HSD post hoc test (sig. p-values < 0.05). Not significant differences are marked as NS.

Cell death tiggered by *P. infestans* secretome is impaired upon detachment and in sobir1 mutants

To further investigate the impact of leaf detachment in the sensing of pathogen-derived molecules, we isolated the secretome of filtered axenic culture of *P. infestans* and infiltrated this into leaves of *N. benthamiana* plants that were kept intact, or leaves were immediately detached after infiltration (**Figure 5A**). Then we qualitatively assessed the presence or absence of cell death in the infiltrated area using fluorescent scanning of the leaves using a similar method to the one described in Yuxuan Xi *et al.* (2021)[13]. Diluted V8 culture media was used as a negative control.

Intact plants infiltrated with *P. infestans* secretome showed cell death within the area of infiltration in all replicates (n = 7). However, cell death in detached leaves was only observed in a dispersed speckled pattern and not covering infiltration area in six biological replicates. A representative image of one replicate is shown in **figure 5A**. No cell death was detected in control half-leaves were V8 culture media was infiltrated. We can conclude that cell death triggered by *P. infestans* secretome in *N. benthamiana* is affected upon leaf detachment.

We tested whether *sobir1* mutant lines[14] had the capacity to trigger cell death upon *P. infestans* secretome infiltration knowing that the membrane immune receptor SOBIR1 is required to trigger cell death upon *P. infestans* elicitin INF1 perception in *N. benthamiana*[15] and INF1 is an abundant protein in the *P. infestans* secretome[16]. Half leaves of WT, *sobir1-1* and *sobir1-2* were infiltrated with *P. infestans* secretome and V8 culture media as a negative control. Cell death was observed in WT plants, while no response was observed in any *sobir1-1* and *sobir1-2* mutants for all biological replicates (n = 4, **Figure 5B**).

These data shows that cell death responses to the *P. infestans* secretome are lost upon detachment and that loss is sobir1 dependent. Raw images of all biological replicates can be found in Supplementary files 6 and 7.

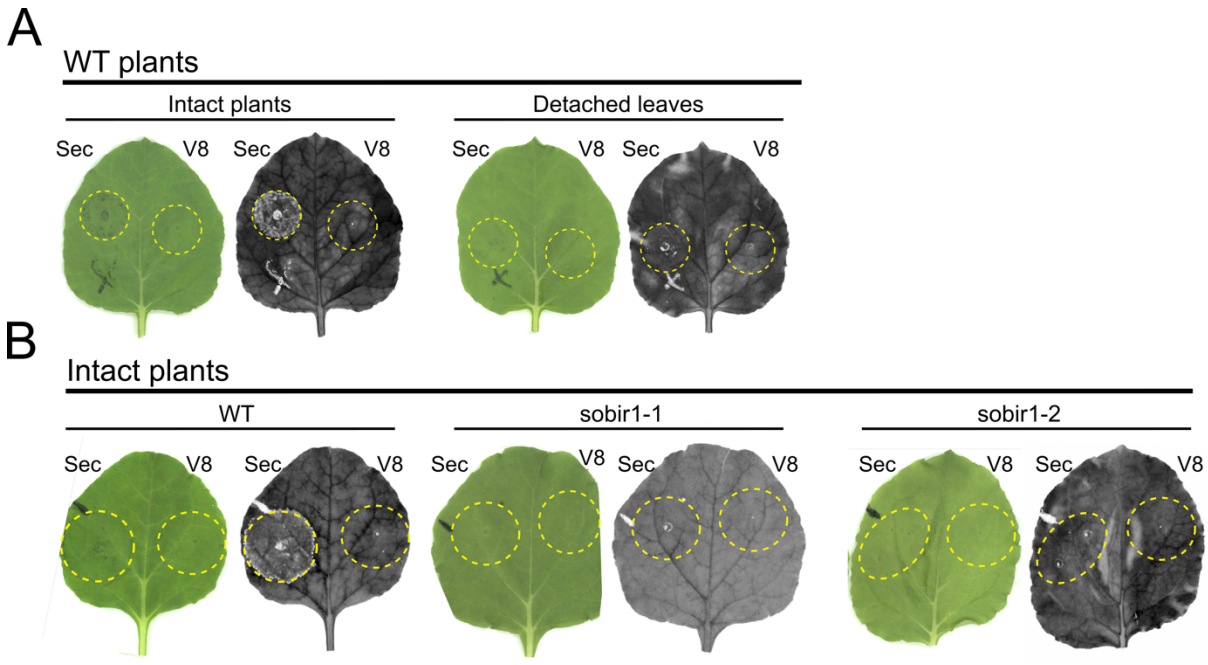


Figure 5. Cell death triggered by P. infestans secretome is impaired in upon detachment and in sobir mutants. **A, Impact of leaf detachment in secretome-triggered cell death.** *N. benthamiana* half leaves were infiltrated with *P. infestans* secretome and with V8 empty media as a negative control. Plants were then kept inatct or leaves were detached right after infiltration. Scans were taken using a Typhoon scanner (Amersham 29187191) with Cy5 laser three days post infiltration (n = 7). **B, sobir1 mutant lines do not develop cell death upon *P. infestans* secretome infiltration.** *P. infestans* 88069 secretome was collected in the same way as described in section A of current caption. Half leaves of WT and *sobir1* mutant plants were infiltrated with *P. infestans* secretome and with V8 empty media and scans were taken three days post infiltration as described before.

P. infestans infects WT and *sobir1* mutant *N. benthamiana* detached leaves similarly.

To further investigate a possible impairment of SOBIR1 signalling in detached leaves, we performed spray inoculation of *P. infestans* 90128 isolate zoospores on *N. benthamiana* WT, *sobir1-1* and *sobir1-2* mutants, both on intact plants and detached leaves. At six days post infection, pictures of intact plants were taken, and leaves were scanned for fluorescence. Two leaf discs from each leaf were collected and relative quantity of *P. infestans* genomic DNA (gDNA) was measured and adjusted to similar levels in all the samples. *N. benthamiana* and *P. infestans* gDNA relative quantity was measured using ΔCT method with quantitative PCR. Ratios of *N. benthamiana* ΔCt values / *P. infestans* ΔCt values were calculated and used as a proxy for *P. infestans* biomass measurement.

WT plants infected with *P. infestans* showed clear cell death lesions compared to *sobir1* mutants, which only showed minor or no infection signs (**Figure 6A**). Quantitative gDNA analysis of infected intact plants revealed an increased *P. infestans* biomass in WT compared to *sobir1* mutant plants (**Figure 6B**). gDNA ratios can be affected by host cell death, however this effect does not

impact gDNA levels from the pathogen and ratio normalisation is intended to account for this effect.

Conversely, *P. infestans* biomass remained unaltered on both detached leaves and intact plants (**Figure 6B**). This observation is supported by fluorescent scans of the leaves. These data demonstrate that detached leaves of *N. benthamiana* WT and *sobir1* have equal *P. infestans* susceptibility to *P. infestans* (**Figure 6A**).

We also compared the effect of detachment in each of the genotypes separately. Statistical comparisons showed that *P. infestans* biomass was significantly increased in all genotypes upon detachment (**Figure 6B**).

Altogether, our data demonstrate that detached leaves from WT and *sobir1* mutants are equally susceptible to *P. infestans*. However, susceptibility to *P. infestans* decreases significantly in intact plants and in this case, *sobir1* mutants are more resistant than *N. benthamiana* WT plants, presumably by recognising INF1 and perhaps other secreted effectors. Thus, leaf detachment results in loss of SOBIR1 dependent resistance.

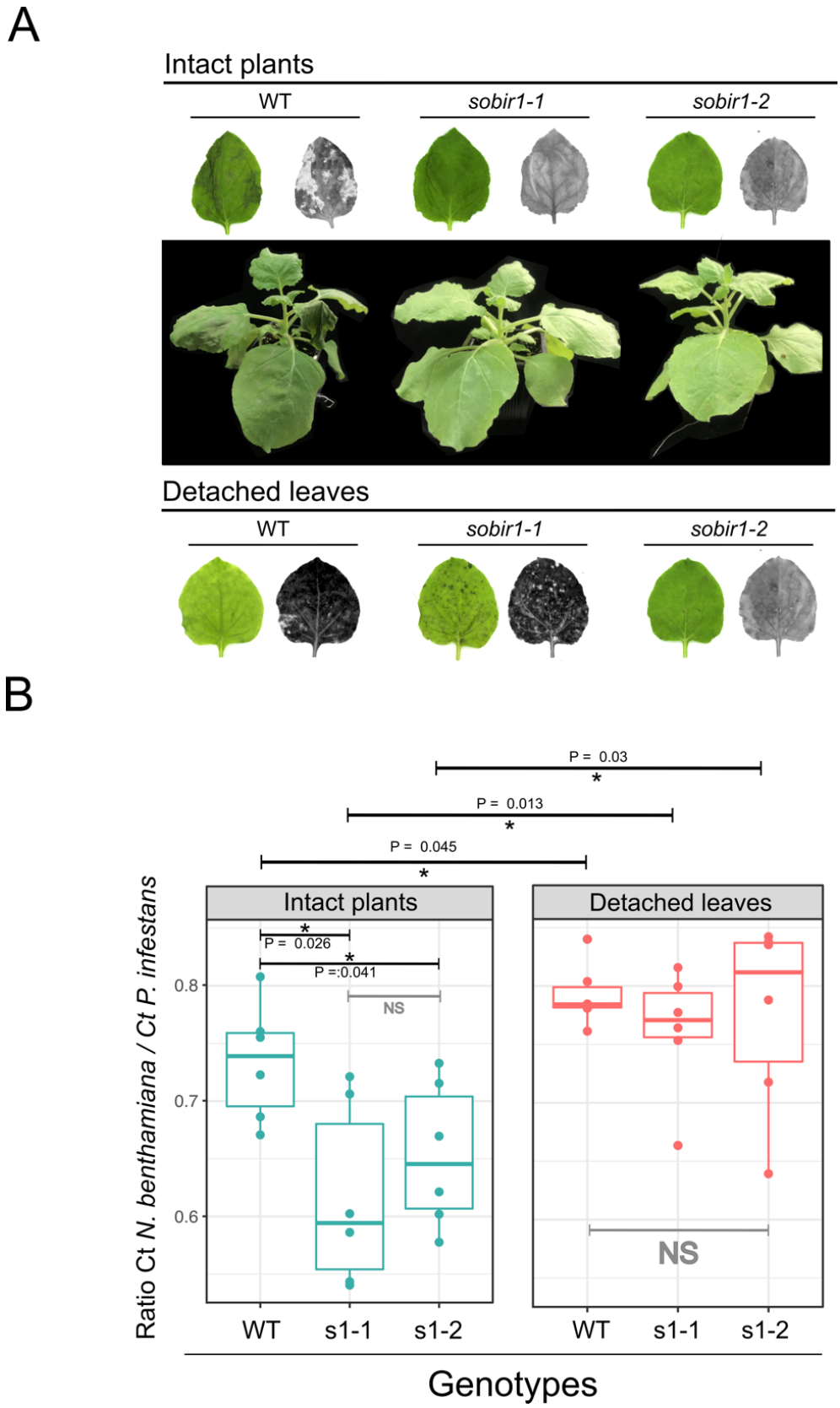


Figure 6. Effect of detachment in P. infestans infection phenotype of Nicotiana benthamiana WT and sobir1 K.O mutants. **A, Leaf infection imaging**. WT and two independent *sobir1* mutants of *N. benthamiana* intact plants and detached leaves were spray infected with 10^5 *P. infestans* zoospores/ml of 90128 strain. Intact plants were kept in a sealed box with 90% of relative humidity

(approx.) and detached leaves were placed in sealed petri dishes with a bed of wet tissue. Scans were taken at 6 dpi with a Typhoon scanner (Amersham 29187191) using Cy5 laser (n = 6). **B, relative *P. infestans* gDNA quantification in WT and sobir1 *N. benthamiana* plants upon detachemnt.** Leaf discs from previously scanned leaves were collected and gDNA was extracted using Qiagen DNeasy plant kit 69104. *P. infestans* tubulin and *N. benthamiana* elongation factor 1 alphra sequences were specifically amplified from gDNA using primers specified in Supplementary table S1.

Discussion

Protein accumulation dynamics upon leaf detachment

In the present chapter, we provide a comprehensive analysis of which biological processes are impacted by leaf detachment in *N. benthamiana*. First, we addressed hydrolytic activity changes in the apoplast upon detachment. ABPP of serine hydrolases revealed a decrease in the protein activity at 69 kDa in detached leaves (**Figure 1B**). This activity is assumed to originate from subtilases belonging to the P69 family. P69 activity depletion upon detachment is a surprising observation, as subtilases accumulate upon stresses of different nature in other species[17]. For example, in the Solanaceae family several members of P69 family (PR-7) are induced upon infection of different pathogens such as *Ralstonia solanacearum*[18], citrus exocortis viroids[19], *Pseudomonas syringae*[20] or *P. infestans*[21]. Moreover, plant pathogens such as *P. infestans* secrete subtilase inhibitors that can target members of P69 family[21,22]. The fact that the apoplast undergoes P69 subtilase depletion upon detachment suggests that immune responses could be compromised in detached leaves, and this served as a ground to further experiments.

Mass spectrometry revealed major changes in protein accumulation upon detachment in AF and TE of *N. benthamiana* leaves (**Figure 2**). We identified three protein families with significant changes upon detachment in AF that can play a role in immunity: five thaumatin-like proteins (PR-5), four subtilases and two GDSL lipases/esterases (**Figure 2C**). Thaumatin-like proteins or PR-5 are named after a protein from *Thaumatococcus daniellii*, and have been found in several plant species, commonly induced by biotic and osmotic stress[23]. PR-5 in tobacco showed antifungal activity[24], and tea plant *Camellia sinensis* PR-5 expressed in potato increases resistance against *P. infestans*[25]. Interestingly, a recent study showed that a PR-5 induced in tomato fruits upon osmotic stress enhances resistance against fungal infection[26]. In our proteomics data set, four PR-5 proteins were up-regulated upon detachment in the apoplast and one with a relative low abundance was depleted. It is expected that leaf detachment generates osmotic stress due to the interrupted supply of fluids from the roots to the aerial parts of the plant and this might be the cause of PR-5 accumulation. This accumulation could also impact immunity as thaumatins play roles in the common ground between biotic and abiotic stress responses.

Three highly abundant apoplastic subtilases were down-regulated (a P69F homolog, a SBT1.7 and a SBT1.2) and one up-regulated (a SBT1.4) in detached leaves compared to intact plants. Apoplastic subtilases have a important role in plant immune responses. Members of the P69 family in Arabidopsis promote salicylic acid immune priming improving host resistance against pathogens[20]. As commented before, P69F homolog reduction in *N. benthamiana* contrasts with the induction and post-translational activation of P69F previously reported in tomato upon *Ralstonia solanacearum* infection[18]. We hypothesise that P69F homolog NbD038072.1 decreased upon detachment could be responsible for the activity depletion seen in ABPP experiment. Moreover, P69 subtilase dependent immunity might be negatively affected in *N. benthamiana* apoplast of detached leaves. It would be interesting to confirm this hypothesis with transient expression of tagged NbD038072.1 under a native promoter, that would allow us to monitor the endogenous accumulation of NbD038072.1 subtilase in detached leaves and confirm that NbD038072.1 is responsible for the subtilase activity depletion observed in protein gels. SBT1.2 subtilases have been related to stomata development processes in Arabidopsis[27], and SBT1.7 with mucilage release during seed germination[28]. It is also known that subtilases of the SBT1.4 group are induced during senescence[29]. Therefore, the accumulation of SBT1.4 in apoplast in our experiment might be a response to an enhanced senescence upon detachment.

GDSL lipases are important element of stress responses and plant immunity. A soybean GDSL lipase confers higher tolerance to osmotic stress to Arabidopsis mutants in genomic complementation assays[30]. Another GSDL lipase in Arabidopsis enhances resistance to *Alternaria brassicicola* throughout modulation of ethylene and salicylic acid responses[31]. Our data show a strong reduction in two apoplastic GDSL lipases and provide more evidence of a significant impact in immunity upon detachment.

In TE samples, a total of 827 proteins showed significant changes upon detachment. GO analysis revealed a general decrease in protein translation (**Figure 2D**). Translation regulation upon different stresses has been widely studied in plants since ribosome profiling techniques were implemented[32]. Abiotic stress such as water deficit or starvation inhibit initiation of general mRNA translation in favour of translation of key survival proteins[33]. The fact that photosynthesis is down-regulated in detached leaves could be causing a sucrose starvation that might trigger a general translation depletion and consequently, protein folding reduction as these processes are closely interconnected. By contrast, signal transduction, vesicle transport, and carbohydrate metabolic processes are enriched biological processes in TE proteomes upon detachment. Biotic and abiotic stresses in plants activate kinases that can lead to signal transduction[34] and vesicle transport[35].

Altogether, our data shows protein accumulation changes in leaves upon detachment that could be driven by stress responses that may significantly impact elements of immunity.

This would have major consequences for infection and phenotyping assays in *N. benthamiana* detached leaves.

Detachment impacts responses triggered by *P. syringae*

Our results showed a significantly delayed ROS burst peak in detached leaves upon flg22 sensing and PTI activation (**Figure 3A**). However, the magnitude of the ROS burst measured as the area under the curve over time did not show significant differences (**Figure 3B**). PTI constitutes the first basal immunity in plants, and it is usually enough to counteract colonisation by non-adapted pathogens. Flg22 is sensed by the receptor FLS2 in Arabidopsis[36]. FLS2 transduces a signalling cascade that results in a RBOH-dependent ROS burst in the apoplast[37] and PTI activation. It is unclear whether a delayed ROS burst might have consequences in PTI activation. However, proteins implicated in the release of pathogen-associated molecular patterns (PAMPs) such as chitinases, are induced earlier in resistant than in susceptible potato cultivars upon *P. infestans* infection[8,38].

In addition, we investigated if detachment could also impact in ETI assessing the infection phenotype of WT and *ΔhopQ P. syringae* DC3000 strain. Fluorescent scans as readout were not sufficiently robust to show differences in WT and *ΔhopQ* symptom development in intact plants. Nonetheless, we observed a trend of a stronger fluorescence in intact plants infected with WT *P. syringae* compared to the *ΔhopQ* mutant (**Figure 4B**). This trend is not observed in detached leaves that showed strong cell death lesions compared to intact plants (**Figure 4A** and **B**). The HopQ effector is recognised by the immune receptor Roq1[39] triggering a strong ETI response that results in incompatible interaction and bacteria avirulence. However, bacteria lacking this effector evade immunity recognition and cause disease in the non-host *N. benthamiana*[12]. This observation could indicate a possible ETI impairment upon detachment, but our experiment needs to be repeated including more biological replicates and bacterial growth measurement to confirm the observed trend in intact plants. If confirmed, it would demonstrate that ETI responses are impacted by leaf detachment in *N. benthamiana.*

PAMP Sensing and immunity against *P. infestans* are compromised upon detachment.

Our results demonstrate that cell death triggered by *P. infestans* secretome in *N. benthamiana* leaves is diminished upon detachment, and we showed that *sobir1* mutants exhibit similar lack of response to *P. infestans* secretome (**Figure 5A** and **B**). The *P. infestans* secretome is a mixture of PAMPs in which HR-triggering effectors such as INF1 can be found[15,40]. It has been reported that INF1 is sensed by ELR receptor in potato[41]. This receptor not only associates with BAK1/SERK3 upon INF1 recognition but also requires the SOBIR1 coreceptor to activate the signalling cascade that ultimately results in programmed cell death (PCD)[15]. The fact that we observed a similarly impaired *P. infestans* secretome-triggered cell-death in detached leaves compared to *sobir1* mutant plants, made us hypothesise that leaf detachment could have some impact in SOBIR1 signalling cascade.

To test that hypothesis, we infected WT and *sobir1* mutant *N. benthamiana* intact plants and detached leaves with *P. infestans* spores. We measured *P. infestans* genomic DNA as a proxy of the pathogen biomass and compared it across the different genotypes and treatments (**Figure 6B**). Strikingly, our results showed a higher *P. infestans* growth in intact WT plants than in *sobir1* mutants. These results alone contradict the claim made by Domazakis *et al.* (2018)[15] where the authors state that "SOBIR1 contribute to resistance against *P. infestans*" based on a detached leaf assay. If we have a closer look at the methods used by Domazakis *et al.*, we can see that they used detached leaves of *TRV:sobir1* plants for their infection assays and gDNA quantification. This can partially explain the incompatibility with our results in intact plants. However, our data also clearly show no differences in detached leaves infection among WT and *sobir1* genotypes supported by leaf fluorescent scans. These observations are very similar to the ones made by Guosheng *et al.* (2007)[7] in intact plants and detached leaves of two different Arabidopsis ecotypes (one resistant and other susceptible) infected with *Colletotricum higginsianum*. Domazakis *et al.* might have had unfortunate data stochasticity combined with low statistical power derived from calculating the standard deviation of biomass quantification from only two technical replicates. Our data shows considerable data point dispersion in detached leaves for the six biological replicates. The authors state that the experiment was repeated three times with similar results, but they do not specify how many biological replicates they used for each experiment in the main figure or in the Supplementary figure S2, nor they show the data from those additional experiments. Nevertheless, our results support the SOBIR1-dependency of *P. infestans* triggered PCD in *N. benthamiana*. It is tempting to hypothesise that the lack of cell death in intact *sobir1* plants might create an incompatible interaction between *P. infestans* and *N. benthamiana* in intact plants and thus, impair *P.*

infestans growth compared to WT plants. A possible explanation is that PCD developed by intact WT plants upon *P. infestans* infection might dismantle surface protection that is usually sufficient to counteract non-adapted pathogen attacks[42,43]. From its side, *P. infestans* might switch almost directly to a necrotrophic phase and colonise dead tissues. Conversely, the lack of PCD in *sobir1* mutants might contribute to maintain leaf surface integrity and consequently be sufficient for repelling *P. infestans* colonisation.

Comparison of intact plants with detached leaves revealed an increased susceptibility in detached leaves both in WT and *sobir1* mutants (**Figure 6B**, third panel). Accumulation of SBT1.4 in the apoplast upon detachment points towards an enhanced leaf senescence upon detachment and we showed that detached leaves *P. infestans* secretome triggered PCD decreases compared to intact plants. Senescence has been correlated with delayed programmed cell death (PCD) that reduces resistance against hemibiothrophic pathogens[10] and higher pathogenicity in Arabidopsis detached leaves infected with *Colletotricum* spp[7]. These independent studies support our findings and highlight the complex network of responses following leaf detachment in *N. benthamiana*.

Overall, our data demonstrate radical differences of *P. syringae* and *P. infestans* infection phenotype in detached leaves of *N. benthamiana* compared to intact plants that has not been reported before. We also deepened in the impact of leaf detachment over SOBIR1 dependent responses. Moreover, we provide a complete analysis of protein and enzymatic changes occurring in the apoplast in total extracts of detached leaves that can partially explain our observations. Altogether our study indicates that conclusions made in pathogenicity assays on detached leaves of *N. benthamiana* cannot be extrapolated to whole plants.

Materials and methods

N. benthamiana and *P. infestans* growth conditions

Four weeks old *N. benthamiana* plants were grown in a greenhouse at a temperature of 21°C with a 18h light regime.

Isolates of *P. infestans* 88069 and 90128 were grown in Rye A agar for 10 days. Rye agar A was prepared with supernatant from 60g of rye soaked overnight. Grains were blended for 2 minutes and heated at 68°C in a glass beaker for 1 hour. Blended grain was filtered through 4 layers of cheese cloth and the filtrate was combined with the supernatant prior to add 20g of sucrose and

15g of agar. Mixture volume was topped up with water up to 1 litre of volume and autoclaved before use.

Apoplastic fluid extraction and fluorescent ABPP and SDS-PAGE

To isolate apoplastic fluid, *N. benthamiana* leaves were vacuum infiltrated with cold MiliQ water using a 50 ml syringe. The leaf surface was dried using a tissue and placed inside a 20 ml syringe without plunger. Syringes were put inside a 50 ml falcon tube and centrifuged at 1500X g for 25 minutes at 4°C. Apoplastic fluid was transferred into 2 ml tubes and snap frozen until further analysis.

Labelling of serine hydrolases was done in reducing conditions (5 mM DTT) and buffered with 50 mM NaAc pH 5 for one hour in total darkness using FP-TAMRA fluorescent probe (Thermo 88318). 43 µl of apoplastic fluid was used in each reaction. Five volumes of cold acetone were used to precipitate the proteins. After 2 minutes of centrifugation at maximum speed, the acetone was removed and the protein pellet was airdried completely. Proteins were resuspended in 20 µl of PBS-SDS loading buffer (phosphate-buffered saline (PBS) pH 7.4, 1% (w/v) sodium dodecyl sulphate (SDS) and denatured for 5 minutes at 90°C. Up to 10 µl of sample was loaded in 12% SDS- PAGE acrylamide gels and proteins were separated by electrophoresis at 180V. Gels were scanned in an Amersham Typhoon 5 (GE Healthcare Life Sciences) at a 575 nm. Loading controls were obtained after gel staining with Coomassie Brilliant Blue G-250.

FASP sample preparation for mass spectrometry analysis

Micron centrifugal filters YM-10 (Millipore) were washed prior to sample loading with 200 µl of 0.1% trifluoroacetic acid (TFA) in 50% acetonitrile (ACN) and centrifuged at maximum speed for 15 minutes (room temperature). Then, equilibration of filters was done with 200 µl of 8 M urea in 100 mM triethylammonium bicarbonate (TEAB) pH 8.5 and centrifuged at 15,000 g for 15 minutes. 200 µl of AF samples or the equivalent of 200 µg for TE samples were loaded on the filters mixed with 200 µl of 8 M urea in 100 mM TEAB pH 8.5. Filters were centrifuged at 15,000 g for 40 minutes and retained proteins were washed four times with 200 µl of 8 M urea in 100 mM TEAB pH 8.5. Reduction step was performed adding 200 µl of 8 M urea and TCEP (tris(2-carboxyethyl) phosphine hydrochloride, 10 mM final concentration) in 100 mM TEAB pH 8.5 for 30 minutes at room temperature. Reduction buffer was removed by centrifugation at 15,000 g for

15 minutes. Alkylation was done adding 200 µl of 8 M urea and 2-chloroacetamide (50 mM final concentration) in 100 mM TEAB pH 8.5 for 30 minutes at room temperature in total darkness. Alkylation buffer was removed by centrifugation at 15,000 g for 15 minutes. Reduced/alkylated proteins on the filter were washed twice using 6 M urea in 50 mM TEAB. Enzymatic digestion was performed in two steps. First, with 2.5 µl of lysin endopeptidase (Lys-C from FUJIFILM Wako, in 50 mM Tris-HCL pH 8) for 4 hours incubation at 37 °C. Secondly, 5 µl of trypsin (Trypsin Gold from Promega, in 50 mM TEAB pH 8.5) were used for overnight digestion at 37 °C. Peptides from the digestion were eluted by centrifugation. Filters were washed with 150 µl 0.1% TFA and 150 µl 0.1% TFA in 50% ACN to collect any remaining peptide. Elutes were combined and vacuum dried prior to samples submission for MS analysis.

Proteomic analysis

Peptides found in MaxQuant[43] were removed when matched to contaminants or reverse database were or did not belong to a unique protein group. In tensity values equal to 0 were substituted for missing value (NA). Peptides with more than 80% of missing values in their assigned intensities were not considered robust and were removed. Intensity distributions were normalised using variance stabilisation method[44]. Only peptides not missed at random were imputed with a minimum deterministic value. Peptidic intensities were aggregated to protein group intensities with a statistical method based on the median. From unique protein groups, only the leading razor protein was considered. Fold changes and BH adjusted p-values were calculated fitting a linear model using Limma R package.

Oxidative burst luminol assay

N. benthamiana leaf discs of 0.125 cm^2 were incubated in MilliQ water overnight. Next day, they were placed in a white 96 COSTAR well plate. 100 µl solution containing luminol 1X (Sigma-Aldrich), 0.25 µg/µl horse radish peroxidase (Pierce™ Horseradish Peroxidase) and 100 nM of flg22 were added immediately before the assay. Fluorescence was measured using a Tecan infinite 200 plate reader every minute for one hour.

WT and ΔhopQ *P. syringae* DC3000 spot infiltrations

P. syringae DC300 WT and ΔhopQ cells were grown overnight in 3 ml of LB media at 28°C. OD600 was adjusted by dilution with MilliQ water to 0.001. *N. benthamiana*s leaves were spot

infiltrated using a syringe and plants and detached leaves were kept in sealed boxes until sample collection. Leaves were then scanned with a Amersham Typhoon 5 (GE Healthcare Life Sciences) and 665 nm wavelength (Cy5 laser).

P. infestans secretome collection

P. infestans 88069 mycelia plugs were collected from 10-12 days old Rye A agar plates and placed in petri dishes containing 5 ml of autoclaved V8 juice diluted 4 times. Cultures were kept at 18°C in darkness for 10 days. Mycelia was carefully collected and filtered through 4 layers of miracloth. Liquid secretome was then filtered with Whatman Puradisc syringe filters of 0.45 μm prote size (Thermo Fisher WHA10462100) and placed in 15 ml Eppendorf tubes. Secretome was then centrifugated at 5000g for 30 minutes, and supernatant was collected prior to be snap frozen in liquid nitrogen and storaged.

P. infestans infection biomass analysis

P. infestans spores were harvested from 10-12 days old rye A agar plates grown at 18°C in darkness. To stimulate the sporulation, plates were flooded with cold MilliQ water and kept at 4 in the dark for 4 hours. Supernatant containing the spores was collected and spores were counted using an haematocytometer under the microscope. *N. benthamiana* whole plants or detached leaves were spray inoculated with 10^5 zoospores/ml. Plants were kept in sealed plastic boxes and leaves were placed in square flat boxed over two layers of wet tissue to retain the humidity until sample collection. Two leaf discs from 3 different leaves on each plant/detached leaf were collected and combined. gDNA was extracted using DNeasy Plant kit (Qiagen 69104) following manufacture's instructions. gDNA for each sample was measured and adjusted to a concentration of 70 ng/μl approximately when possible. qPCR plates were loaded with SYBR green master mix (Fisher 4309155) in each well and 70ng of gDNA were loaded of each sample for amplification (Thermo 4376357). Two technical replicates for each reaction were included. Reaction was monitored using a qPCR over the time (Thermo using default parameters for calculating ΔCt values. Primers published by Domazakis *et al.* (2018)[14] were used for specific gDNA amplification (Supplementary table S1). Values were compared using a pairwise Wilcox statistical test for non-parametric data.

Bibliography

1. Goodin, M. M *et al. Nicotiana benthamiana*: its history and future as a model for plant–pathogen interactions. *Mol. Plant Microbe Interact.* **12**. (2008)

2. Kourelis, J. *et al.* Evolution of a guarded decoy protease and its receptor in solanaceous plants. *Nat. Commun.* **11**, 4393 (2020).

3. Yu, J. *et al.* A *Nicotiana benthamiana* AP2/ERF transcription factor confers resistance to Phytophthora parasitica. *Phytopathol. Res.* **2**, 4 (2020).

4. Bozkurt, T. O. *et al. Phytophthora infestans* effector AVRblb2 prevents secretion of a plant immune protease at the haustorial interface. *Proc. Natl. Acad. Sci.* **108**, 20832–20837 (2011).

5. Miller-Butler, M. A *et al.* Comparison of whole plant and detached leaf screening techniques for identifying anthracnose resistance in strawberry plants. *Plant Dis.* **102**, 2112–2119 (2018).

6. Bos, J. I. B. *et al. Phytophthora infestans* effector AVR3a is essential for virulence and manipulates plant immunity by stabilizing host E3 ligase CMPG1. *Proc. Natl. Acad. Sci. U. S. A.* **107**, 9909–9914 (2010).

7. Liu, G. *et al.* Detached and attached *Arabidopsis* leaf assays reveal distinctive defense responses against hemibiotrophic *Colletotrichum* spp. *Mol. Plant-Microbe Interactions®* **20**, 1308–1319 (2007).

8. Orłowska, E. *et al.* Revealing the importance of meristems and roots for the development of hypersensitive responses and full foliar resistance to *Phytophthora infestans* in the resistant potato cultivar Sarpo Mira. *J. Exp. Bot.* **63**, 4765–4779 (2012).

9. Hou, S., *et al.* Damage-associated molecular pattern-triggered immunity in plants. *Front. Plant Sci.* **10**, (2019).

10. Zhang, Y *et al.* Genetic network between leaf senescence and plant ommunity: crucial regulatory nodes and new insights. *Plants* **9**, 495 (2020).

11. Smith, J. M. & Heese, A. Rapid bioassay to measure early reactive oxygen species production in Arabidopsis leave tissue in response to living *Pseudomonas syringae*. *Plant Methods* **10**, 6 (2014).

12. Wei, C.-F. *et al.* A *Pseudomonas syringae* pv. tomato DC3000 mutant lacking the type III effector HopQ1-1 is able to cause disease in the model plant *Nicotiana benthamiana*. *Plant J. Cell Mol. Biol.* **51**, 32–46 (2007).

13. Xi, Y., Chochois *et al.* A novel robust and high-throughput method to measure cell death in *Nicotiana benthamiana* leaves by fluorescence imaging. *Mol. Plant Pathol.* **22**, 1688–1696 (2021).

14. Huang, W. R. H., Schol, C., Villanueva, S. L., Heidstra, R., & Joosten, M. H. A. J. Knocking out SOBIR1 in *Nicotiana benthamiana* abolishes functionality of transgenic receptor- like protein Cf-4. *Plant physiology*, *185*(2), 290–294 (2021).

15. Domazakis, E. *et al.* The ELR-SOBIR1 complex functions as a two-component receptor-like kinase to mount defense against *Phytophthora infestans*. *Mol. Plant-Microbe Interactions* **31**, 795–802 (2018).

16. Meijer, H. J. G. *et al.* Profiling the secretome and extracellular proteome of the potato late blight pathogen *Phytophthora infestans*. *Mol. Cell. Proteomics MCP* **13**, 2101–2113 (2014).

17. Schaller, A. *et al.* From structure to function - a family portrait of plant subtilases. *New Phytol.* **218**, 901–915 (2018).

18. Planas-Marquès, M. *et al.* Protease activities triggered by *Ralstonia solanacearum* infection in susceptible and tolerant tomato lines. *Mol. Cell. Proteomics MCP* **17**, 1112–1125 (2018).

19. Vera, P. & Conejero, V. The induction and accumulation of the pathogenesis-related P69 proteinase in tomato during citrus exocortis viroid infection and in response to chemical treatments. *Physiol. Mol. Plant Pathol.* **34**, 323–334 (1989).

20. Jordá, L. & Vera, P. Local and systemic induction of two defense-related subtilisin-like protease promoters in transgenic Arabidopsis plants. Luciferin induction of PR gene expression. *Plant Physiol.* **124**, 1049–1058 (2000).

21. Tian, M., *et al.* A Kazal-like extracellular serine protease inhibitor *from Phytophthora infestans* targets the tomato pathogenesis-related protease P69B. *J. Biol. Chem.* **279**, 26370–26377 (2004).

22. Tian, M., *et al.* A second Kazal-Like protease inhibitor from *Phytophthora infestans* inhibits and interacts with the apoplastic pathogenesis-related protease P69B of tomato. *Plant Physiol.* **138**, 1785–1793 (2005).

23. Breiteneder, H. Thaumatin-like proteins – a new family of pollen and fruit allergens. *Allergy* **59**, 479–481 (2004).

24. Vigers, A. J. *et al.* Thaumatin-like pathogenesis-related proteins are antifungal. *Plant Sci.* **83**, 155–161 (1992).

25. Acharya, K. *et al.* Overexpression of *Camellia sinensis* thaumatin-like protein, CsTLP in potato confers enhanced resistance to *Macrophomina phaseolina* and *Phytophthora infestans* infection. *Mol. Biotechnol.* **54**, 609–622 (2013).

26. An, M. *et al.* Molecular characterization of the thaumatin-like protein PR-NP24 in tomato fruits. *J. Agric. Food Chem.* **67**, 13001–13009 (2019).

27. Groll, U. von, *et al.* The subtilisin-like serine protease SDD1 mediates cell-to-cell signaling during Arabidopsis stomatal development. *Plant Cell* **14**, 1527–1539 (2002).

28. Rautengarten, C. *et al.* A subtilisin-like serine protease essential for mucilage release from Arabidopsis seed coats. *Plant J.* **54**, 466–480 (2008).

29. Martinez, D. E. *et al.* SASP, a senescence-associated subtilisin protease, is involved in reproductive development and determination of silique number in Arabidopsis. *J. Exp. Bot.* **66**, 161–174 (2015).

30. Su, H.-G. *et al.* Genome-side identification, evolution, and expression of GDSL-type esterase/lipase gene family in soybean. *Front. Plant Sci.* **11**, (2020).

31. Oh, I. S. *et al.* Secretome analysis reveals an Arabidopsis lipase involved in defense against *Alternaria brassicicola*. *Plant Cell* **17**, 2832–2847 (2005).

32. Kage, U., *et al.* Ribosome profiling in plants: what is not lost in translation? *J. Exp. Bot.* **71**, 5323–5332 (2020).

33. Muñoz, A. & Castellano, M. M. Regulation of translation initiation under abiotic stress conditions in plants: is it a conserved or not so conserved process among Eukaryotes? *Comp. Funct. Genomics* **2012**, e406357 (2012).

34. Fujii, H. & Zhu, J.-K. Osmotic stress signaling via protein kinases. *Cell. Mol. Life Sci.* **69**, 3165–3173 (2012).

35. Gu, X., *et al.* Vesicle transport in plants: a revised phylogeny of SNARE proteins. *Evol. Bioinforma. Online* **16**, (2020).

36. Chinchilla, D., *et al.* The Arabidopsis receptor kinase FLS2 binds flg22 and determines the specificity of flagellin perception. *Plant Cell* **18**, 465–476 (2006).

37. Lee, D. *et al.* Regulation of reactive oxygen species during plant immunity through phosphorylation and ubiquitination of RBOHD. *Nat. Commun.* **11**, 1838 (2020).

38. Orłowska, E., *et al.* Plant integrity: an important factor in plant-pathogen interactions. *Plant Signal. Behav.* **8**, e22513 (2013).

39. Schultink, A., *et al.* Roq1 mediates recognition of the *Xanthomona*s and *Pseudomonas* effector proteins XopQ and HopQ1. *Plant J.* **92**, 787–795 (2017).

40. Du, J., *et al.* Proteomic analysis of differentially expressed proteins of *Nicotiana benthamiana* triggered by INF1 elicitin from *Phytophthora infestans*. *J. Gen. Plant Pathol.* **83**, 66–77 (2017).

41. Du, J. *et al.* Elicitin recognition confers enhanced resistance to *Phytophthora infestans* in potato. *Nat. Plants* **1**, 1–5 (2015).

42. Yu, Shen, *et al.* Leaf cuticle can contribute to non-host resistance to poplar leaf rust. *Forests* **10**, 870 (2019).

43. Naveed, Z. A., *et al.* . The PTI to ETI continuum in *Phytophthora*-plant interactions. *Front. Plant Sci.* **11**, (2020).

44. Cox, J. & Mann, M. MaxQuant enables high peptide identification rates, individualized p.p.b.-range mass accuracies and proteome-wide protein quantification. *Nat. Biotechnol.* **26**, 1367–1372 (2008).

45. Huber, W., *et al.* Variance stabilization applied to microarray data calibration and to the quantification of differential expression. *Bioinformatics* **18**, S96–S104 (2002).

Supplementary materials

Supplemental table S1. Nucleotide sequences used for qPCR amplification of *P. infestans* and *N. benthamiana* gDNA.

Lab ID	**Name**	**Sequence**
LOCPrim_37_Pinf_gDNA_For	Piβ-tubulin for	GGTCGTGGAGCCCTATAACG
LOCPrim_38_Pinf_gDNA_Rev	Piβ-tubulin rev	GTCACCATAAGTGGGGGTGG
LOCPrim_39_benthy_gDNA_For	St/NbEF1α for	TGACCAAGATTGACAGGCGT
LOCPrim_40_benthy_gDNA_Rev	St/NbEF1α rev	GCAAAACGACCCAATGGTGG

Supplemental files S1: protein levels in intact plants and detached leaves (AF and TE samples).

Supplemental files S2: MaxQuant files and scripts used for proteomic quantitative analysis and GO clustering.

Supplemental files S3: Raw files of luminiscence measurements and scripts used to analyse ROS burst over time in *N. benthamiana* intact plants ot detached leaves upon incubation with elicitor flg22.

Supplemental files S4: Leaf scans of *N. benthamiana* infiltrated leaves with *P. syringae* DC3000.

Supplemental files S5: Raw files of fluorescence measurements of *N. benthamiana* infiltrated leaves with *P. syringae* DC3000 and scripts used for analysis.

Supplemental files S6: Leaf scans of *N. benthamiana* infiltrated leaves with *P. infestans* 88069 secretome.

Supplemental files S7: Leaf scans of WT, *sobir1-1* and *sobir 1-2 N. benthamiana* leaves infected with *P. infestans* 90128 secretome.

Supplemental files S8: Raw files of gDNA amplification ΔCt values and script used for analysis.

Chapter 3: Large-scale activity-based protein profiling of apoplast reveals hydrolase manipulation upon infection by *Phytophthora infestans*.

Laura Ossorio Carballo[1], Felix Homma[1], Maria Font Farré[1], Farnusch Kaschani[2], Markus Kaiser[2], Renier A. L. van der Hoorn[1].

[1] The Plant Chemetics Laboratory, Department of Plant Sciences, University of Oxford, Oxford, UK.

[2] University of Kaiserslautern, Department of Biology, Germany.

Introduction

Hydrolases catalyse fundamental and diverse chemical reactions in living organisms. These chemical reactions can be part of developmental processes, metabolism or defensive responses against pathogens[1–7]. In plants, the extracellular space is guarded by defence-related hydrolases that counteract pathogen colonisation[8]. These plant hydrolases can process structures of pathogens; release elicitors that act as receptor agonists; or activate other immunity elements in proteolytic cascades[9–11]. Subtilases are a well-known example of immunity-related hydrolases. In tomato leaves, subtilases from the P69 family are actively secreted in response to the attack by different pathogens[12]. The subtilase P69B is known to activate the immune-protease Rcr3 as well as to process *Phytophthora infestans* secreted protein PC2, triggering a strong immune reaction[10,11]. Other prominent examples of hydrolases involved in plant immunity are Papain-like Cysteine proteases (PLCPs)[2], GDSL-like lipases[13] and carboxypeptidases[14]. On the other side, pathogens may have evolved different strategies to manipulate plant hydrolytic activity. Inhibitor secretion to suppress plant hydrolases is widely spread among plant pathogens, such as *Pseudomonas syringae, Cladosporium fulvum*, *Phytophthora palmivora* or *P. infestans*[9,15–17]. Moreover, pathogens can also secrete hydrolases themselves that inactivate immune elements of the host[18].

In recent years, mass spectrometry (MS) has become a powerful tool to study antagonistic interactions between plant and pathogens at protein level[19,20]. Abundance changes of thousands of proteins can be monitored using shot-gun proteomics, providing meaningful insights into the dynamic changes occurring during pathogen colonisation[21]. Moreover, MS can be coupled with activity-based protein profiling (ABPP) to investigate the hydrolytic activity landscape (activome). ABPP is based on the covalent labelling of hydrolase active sites by a probe attached to an affinity tag or a fluorophore. This technique monitors active hydrolases in a complex protein sample and

can be used in plant pathology to examine how active hydrolases change upon infection (comparative ABPP)[22]. Additionally, ABPP can be used to investigate the specificity of pathogen derived inhibitors (competitive ABPP). A protocol based on the combination of comparative and competitive ABPP can be employed to detect novel inhibited hydrolases (convolution ABPP)[23].

Planas *et al.* have successfully coupled ABPP with MS to study pathogen-derived hydrolase manipulation in tomato (*Solanum lycopersicum*) upon *Ralstonia solanacearum* infection[24]. This study exemplifies the power of ABPP-MS, in which the activity of 80 hydrolases could be monitored in a single experiment.

In the present chapter, we studied hydrolytic activity and proteome changes occurring in the apoplast of tomato upon infection with *P. infestans*. *P. infestans* is a major food security threat causing yield loses in tomato and potato every year[25]. We followed a quantitative and qualitative approach to investigate tomato proteome changes in the apoplast and provide a list of *P. infestans* proteins robustly identified in the apoplast of infected tissue. Moreover, we profiled the activome in tomato apoplast upon *P. infestans* infection providing activity evidence for over 80 hydrolases. Ultimately, we combined abundance, activity and inhibition data to generate a list of putative hydrolases whose activity could be post-translationally regulated upon infection. Altogether, the current chapter is the first-to-date wide-ranging study of the hydrolytic landscape in tomato apoplast infected by *P. infestans*, providing a set of putative manipulated hydrolases and generating significant opportunities for future studies and crop protection strategies.

Results

Tomato apoplastic proteome changes upon *P. infestans* infection

To address changes in protein abundance and hydrolytic activity in tomato apoplast, we performed shot-gun proteomics and ABPP coupled with mass spectrometry (ABPP-MS). Detached leaflets of Money Maker tomato plants were spray infected with zoospores of *P. infestans* isolate 90128 and apoplastic fluid was collected three days post inoculation (**Figure 1A**). To analyse total apoplastic proteomes, we purified apoplastic proteins with the SP3 method (Supplementary file 1) prior to in-solution digestion (ISD) with LysC and trypsin. To analyse the active apoplastic proteome (activome) serine hydrolases (SHs) and cysteine proteases (CPs) were labelled with activity-based probes, enriched, and purified prior to on-bead digestion (OBD) with LysC and trypsin. We considered protein group intensity values as a proxy for relative abundance (**Figure 1B**).

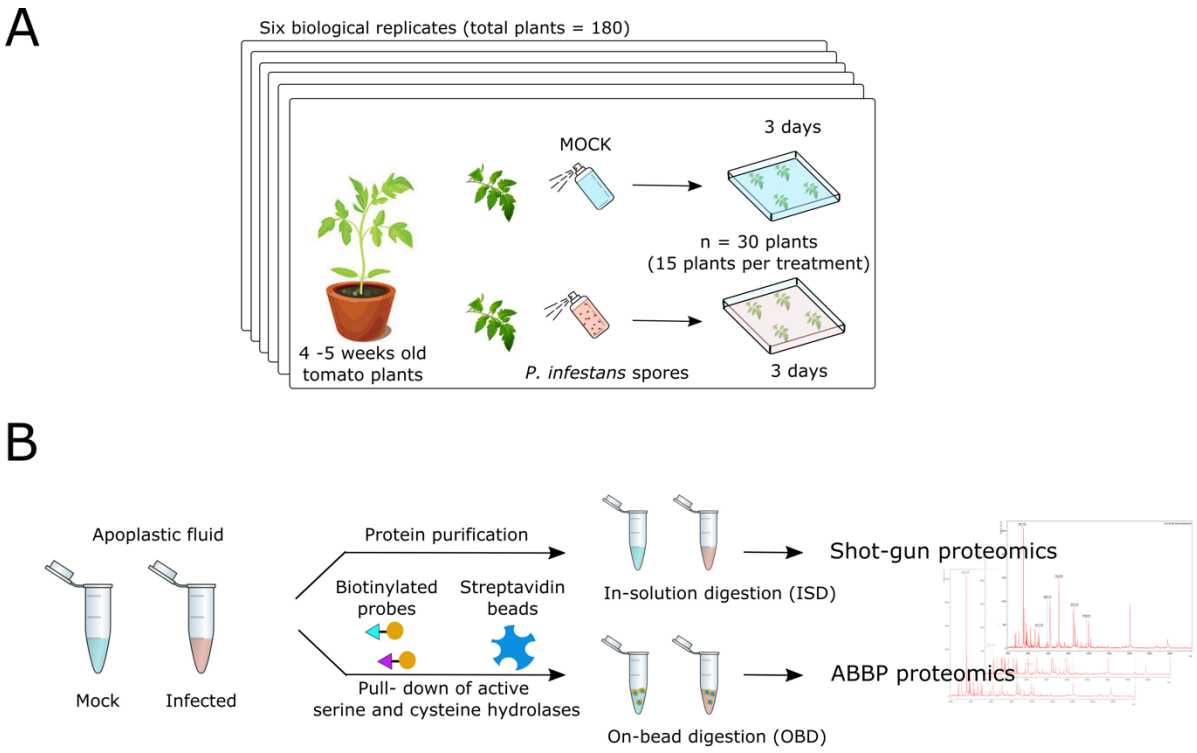


Figure 1. Experimental design. **A, Infections set up of six biological replicate**s. Leaflets from 15 plants of tomato var. Money Maker were sprayed with zoospores of *P. infestans* isolate 90128 (50 zoospores per µl) or with water (a total of 30 plants per replicate). Leaves were kept in sealed petri dishes over two layers of wet tissue for three days. Apoplastic fluid was isolated at 3 days post infection following procedures detailed in materials and methods and stored at -80° C until further analysis. **B, Mass spectrometry workflow diagram**. Apoplastic proteomes and enzymatic activity were analysed using mass spectrometry protocols after ISD and OBD, respectively.

Prior to statistical comparisons, we addressed the quality of the experimental procedures and protein quantification using unsupervised clustering of the samples, or principal component analysis of each of the three protocols: ISD, comparative ABPP and convolution ABPP (**Figure 2A, B** and **C**). Clustering using the 6 available replicates for ISD and comparative ABPP revealed replicate 1 (R1) infected samples clustering close together with water treated (mock) samples (**Figure 2A** and **B**). This replicate was removed for further analysis. Convolution ABPP was performed using replicates R1, R3, R4, R5 and R6 due to a shortage of apoplastic fluid in R2. Principal component analysis revealed that replicate R3 M&L sample clustered together with L&M samples (**Figure 2C**) and was removed prior to quantitative analysis.

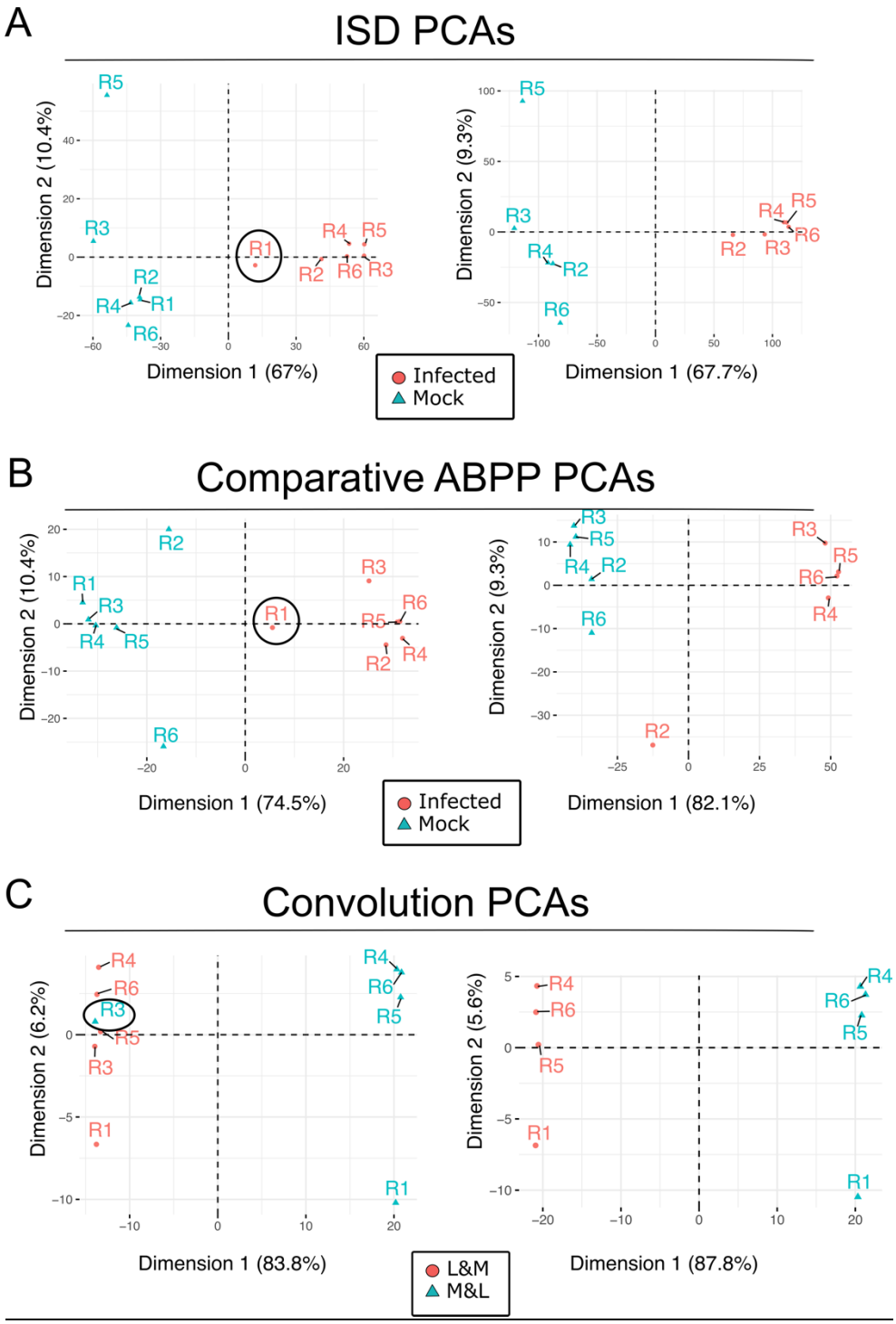


Figure 2. Unsupervised clustering or principal component analysis of experimental procedures. **A, ISD PCA.** Left panel indicates the PCA of all the replicates. Highlighted R1 was considered an outlier and removed in the second PCA (right panel). **B, comparative ABPP PCA.** R1 was also considered an outlier and removed from the analysis. **C, convolution ABPP PCA.** Indicated R3 was removed from the analysis.

To investigate tomato protein changes during *P. infestans* infection, we analysed differential protein abundances in tomato apoplastic total proteome. Protein concentration was measured and a total of 15µg of protein was used for sample preparation (**Figure 2A**).

After filtering non robust peptide identifications, normalisation, imputation and peptide intensities aggregation, we confidently identified a total of 2153 protein groups of tomato and 17 of *P.infestans*.

Quantitative data revealed significant changes in 132 tomato protein groups of which 32 were predicted to contain a SignalP-predicted signal peptide. Five protein groups lacking such signal peptide were annotated as apoplastic protein groups by ApoplastP. 94 protein groups were up-regulated and 38 down-regulated upon *P. infestans* infection (**Figure 2B**). Among up-regulated protein groups with possible role in immunity and signal peptide or predicted apoplastic location, we found five glycosyl hydrolases (Solyc11g044910.2.1, Solyc02g091920.3.1, Solyc05g049980.3.1 and Solyc01g008610.4.1), two peroxidases (Solyc01g105070.3.1-Solyc02g064970.4.1 and Solyc01g105070.3.1), two chitinases (Solyc02g061770.4.1 and Solyc04g072000.4.1) and two Kunitz-type trypsin inhibitors (Solyc03g098670.1.1 and Solyc03g098740.1.1). Remarkably, among those without signal peptide and no predicted apoplastic location by ApoplastP we observed three up-regulated PR-10/Bet v1-like proteins (Solyc05g054380.2.1, Solyc09g090980.3.1 and Solyc09g090990.2.1).

Down-regulated secreted proteins that had the strongest depletion were a GDSL lipase (Solyc01g079160.4.1), the S-locus receptor kinase protein (Solyc07g063820.3.1) and a NAD-dependent epimerase (Solyc09g091970.4.1) (**Figure2B**).

Focusing on predicted hydrolases, we found among up-regulated proteins a carboxylesterase and a prolyl oligopeptidase of the MEROPS S9 family (Solyc07g040890.1.1 and Solyc08g068400.4.1, respectively) with the highest fold change. Two subtilisin-like proteases of subfamily SBT 1.9 were also up-regulated, with Solyc01g087850.2.1 showing the strongest fold change and Solyc10g084320.3.1 displaying the highest protein intensity. Among induced proteins we also identified one carboxypeptidase C (Solyc02g014830.4.1) and one patatin-like phospholipase (Solyc02g090490.3.1). Conversely, accumulation of two hydrolases with lipase and carboxylesterase activity (Solyc01g079160.4.1 and Solyc11g012070.3.1, respectively) was strongly reduced in AF from infected plants (**Figure 2C**).

Altogether, our results show that tomato apoplastic proteome undergoes significant changes upon *P. infestans* infection. Those changes are mainly caused by protein up-regulation. The complete list of differential protein groups can be found in Supplementary table 1.



Figure 3. Apoplastic total proteome analysis reveals changes in abundance of tomato protein groups. **A, Averaged total protein concentrations from six biological replicates of tomato apoplastic fluid from mock treated or *P. infestans* infected leaflets.** Total protein concentration was measured using Bradford protein assay (Biorad 5000001) following manufacturer's instructions. **B, Tomato apoplastic proteome changes upon *P. infestans* infection**. A total of 132 protein groups has significant abundance changes upon infection: 38 are down-regulated (red) and 94 are significantly more abundant (green) and the rest is not significantly changed (grey). Six down-regulated protein groups have a signal peptide and one is predicted to be apoplastic by ApoplastP despite the lack of signal peptide (left hand-side pie chart). 24 up-regulated protein groups have signal peptide and four are predicted to be apoplastic by ApoplastP (right hand-side pie chart). **C, Tomato SHs showing significant changes upon *P. infestans* infection.** Functional classification of differentially abundant tomato apoplastic hydrolases. Left hand-side bar plot shows the log 2 averaged ion intensity for each protein group. More intensively coloured bars indicate a higher ion intensity. Panel on the right hand-side shows the log2 fold change of each of the protein groups. Green bars represent up-regulation and red bars indicate depletion.

In addition to tomato proteins, the proteomes of infected plants also contain 17 consistently identified *P. infestans* protein groups that either had a signal peptide or were predicted to be apoplastic (**Figure 3**). These proteins were absent from the mock control samples. Among these protein found in all five replicates, we observed ribonuclease protein group (PITG_01495 and PITG_16015), berberine-like protein PITG_02930, secreted cysteine-rich protein PITG_11060, a highly abundant uncharacterised protein (PITG_12205) and an S33 serine protease (PITG_15239). Among the five protein groups that were observed in four of the five biological replicates. We find the carbohydrate binding protein PITG_07303 and a protein group containing two endoglucanases (PITG_08944 and PITG_16985) having the highest intensities. Carbohydrate binding proteins and endoglucanases are overrepresented in the predicted *P. infestans* secretome described by Raffaele *et al.* (2010)[26]. We also robustly identified a protein group containing three secreted Hsp70-like proteins (PITG_11252, PITG_15370 and PITG_05721) but there is no evidence for a possible role of Hsp70-like proteins in *P. infestans* infection. Moreover, we found another uncharacterised protein (PITG_11450) and a transglutaminase elicitor protein group (PITG_16958 and PITG_16956).

Among *P. infestans* secreted protein groups present in three of the five biological replicates, we detected dehydrogenases, two more berberine-like protein groups, an uncharacterised protein, an endoglucanase, a glycoside hydrolase and a chitinase (**Figure 4**).

Altogether, we provide a data set with robust proteomic evidence for 17 apoplastic *P. infestans* secreted protein groups during tomato infection. Details of the qualitative analysis pipeline can be found in Supplementary file 2.

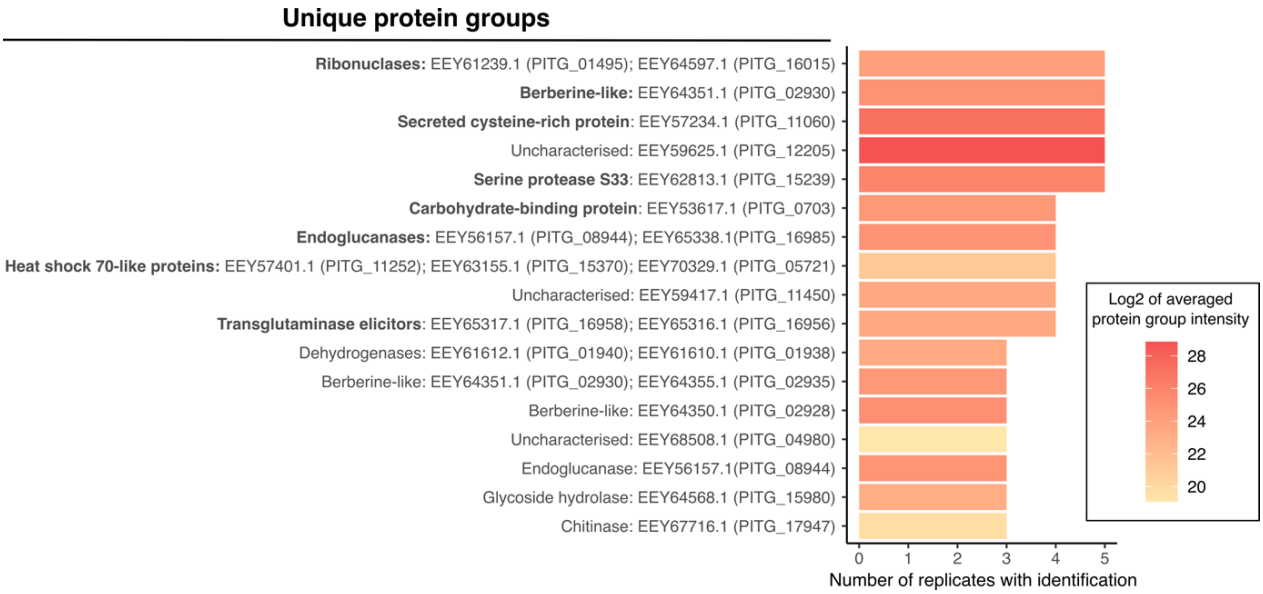


***Figure 4. P. infestans* secreted proteins robustly identified in apoplastic proteomes.** These proteins found in at least 3 biological replicates and contain a predicted signal peptide or have predicted apoplastic location by ApoplastP. Family classification is based on domain functional annotation.

ABPP-MS unveils *P. infestans* and tomato apoplastic activome during infection.

We performed ABPP-MS to generate the first activome data set from the apoplast of tomato upon *P. infestans* infection. Apoplastic samples were incubated with a cocktail of FP-biotin (for SH labelling) and DCG04 (for CP labelling) or DMSO (no-probe controls, NPCs) prior to enrichment on avidin beads, on-bead digest (OBD) and MS analysis. A customised R pipeline used for quantitative analysis can be found in Supplementary file 4.

A total of 3004 unique protein groups were identified in the analysis of the same 5 biological replicates considered in analysis of ISD of total proteomes. After removing contaminants and peptides detected in only one sample, protein groups present in NPCs as well as in labelled samples were considered avidin bead contaminants. These proteins can be endogenously biotinylated and generate false positives in avidin/streptavidin-based protein purifications[27]. The full list of 161 bead contaminants can be found in Supplementary table 4.

Statistical comparisons returned a total of 350 proteins enriched upon labelling, of which 266 were probe off-targets. Probe off-targets are commonly detected in activity-based pull downs[28]. Despite being considered a technical artifact, these off-target proteins might be a source of possible SH and CP interactors. However, we cannot exclude that these proteins are not labelled and might be prone to stick to other (labelled) proteins in an unspecific way.

From the 350 enriched proteins, 84 proteins (24% of the total enriched proteins) were predicted to be probe targets (**Figure 5A**). The percentage of detected serine hydrolases (SHs) and cysteine proteases (CPs) is considerably higher than observed in ISD samples, where SHs and CPs only represent the 6.92% of the total protein identifications.

Subtilases with or without fibronectin domain were the most numerous in the activome (17 proteins). Among them, we can find phytaspase 1 and four members of the PR-P69 family including P69B, known to play important roles in pathogen defence[12,24,29,30]. Following in number of enriched proteins are carboxypeptidase C proteases from the family S10 (15 proteins) and GDSL lipases (10 proteins) (**Figure 4B**).

Interestingly, two enriched proteins of *P. infestans* belonged to the PLCP family: PIGT_03020 (containing a ML lipid recognition domain) and PITG_06927.

Moreover, 63 probe targets enriched in ABPP-MS are also confidently identified in the ISD data-set.

Overall, our ABPP-MS dataset delivers a comprehensive record of apoplastic activome in *P. infestans* infection of tomato. A full table containing enriched SH and CP can be found in Supplementary table 2.

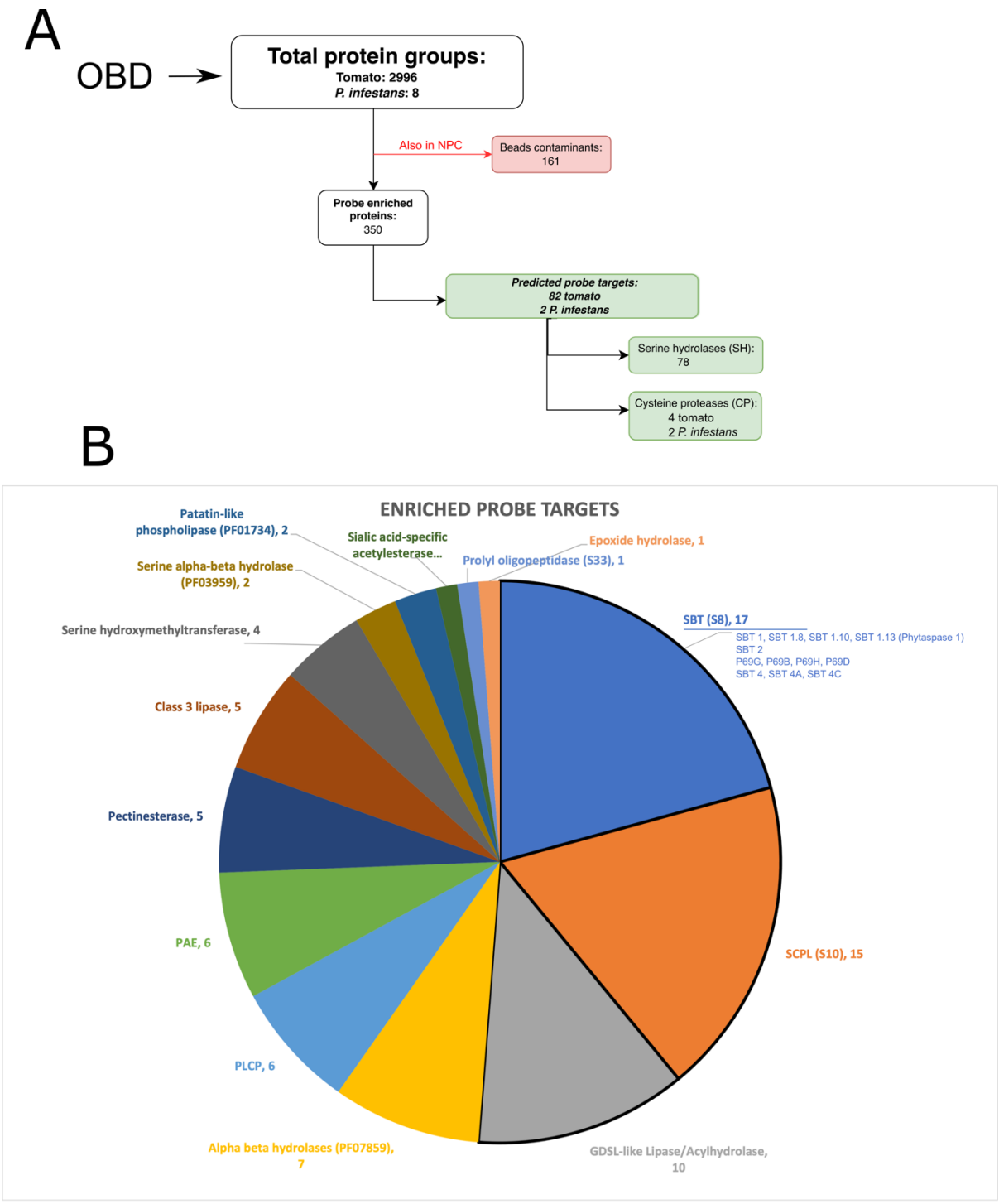


***Figure 5. Activity-based enriched cysteine and serine hydrolases in tomato apoplast during P. infestans infection*. A, Flowchart of activome bioinformatic pipeline used to generate list of enriched labelled serine hydrolases (SH) and cysteine proteases (CP)**. Apoplastic fluid was incubated with 4 µM biotinylated probes (FP-biotin and DCG04) or equivalent volume of DMSO for four hours. After labelling, samples were incubated with streptavidin beads, and labelled proteins were enriched and purified prior to LysC and Trypsin on-beads digestion. Tryptic peptides were analysed by LC-MS/MS. Labelled proteins were annotated based on their predicted protein domains. Statistical analyses were performed separately in each sample type. Biological replicates n = 5. **B, SH and CP families found in analysed activome**. Protein family annotation is based in functional domain predictions. Most abundant families are highlighted. Analysis files can be found in Supplementary File 4.

Seven tomato hydrolase protein groups might be subject of post-translational regulation during infection.

To investigate possible post-translational regulation of tomato SH and CP activity in *P. infestans* infection, we compared abundance data from our total proteome analysis and activity data from ABPP-MS analysis in mock versus infected samples (n = 5). Nine hydrolases showed significant activity changes (**Figure 5A**) while other predicted probe targets did not show significant activity changes. Differential abundance and activity data were obtained for seven hydrolase protein groups. A complete list of the hydrolase protein groups exhibiting dynamic fluctuations in activity upon infection is in Supplementary table 3.

We classified protein groups in three different groups depending on their activity and abundance trends. Group 1 contains protein groups with significant increase in activity and in abundance. Group 2 contains protein groups with significant increase in activity but no changes in abundance and Group 3 contains proteins that have a similar activity but show activity changes or activity depletion (**Figure 5B**).

In group 1, the patatin-like Solyc02g090490.3.1 and the SCPL Solyc02g014830.4.1 in group 1 had a significantly increased abundance and activity in infected tissue, showing a strong induction at both levels.

In group 2, the pectin esterase Solyc06g009190.4.1 has a significant strong activity induction, whereas its abundance remains unaltered. SBT Solyc08a079900.3.1 and the SCPL Solyc01g108490.3.1 also show a significant increase in activity not correlated with a significant increase in abundance. These data suggest a post-translational activation.

In group 3, subtilase SBT 1.9 Solyc10g084320.3.1 exhibits a significant increase in abundance that is not accompanied by a significant increase in activity. Subtilase SBT 5.2 Solyc049081810.4.1 have a significantly decreased activity upon infection while their abundance do not change significantly. Group 3 trends indicate a possible inhibition.

Taken together, these results suggest a post-translational regulation in groups 2 to and 3 of five hydrolases in tomato apoplast during *P. infestans* infection. However, for 4 of these proteins, trends are similar between activity and abundance, despite showing a different level of significance in

statistical tests for abundance and activity. Despite these differences in significance, the fact that trends are similar highlights the need for further confirmation experiments.

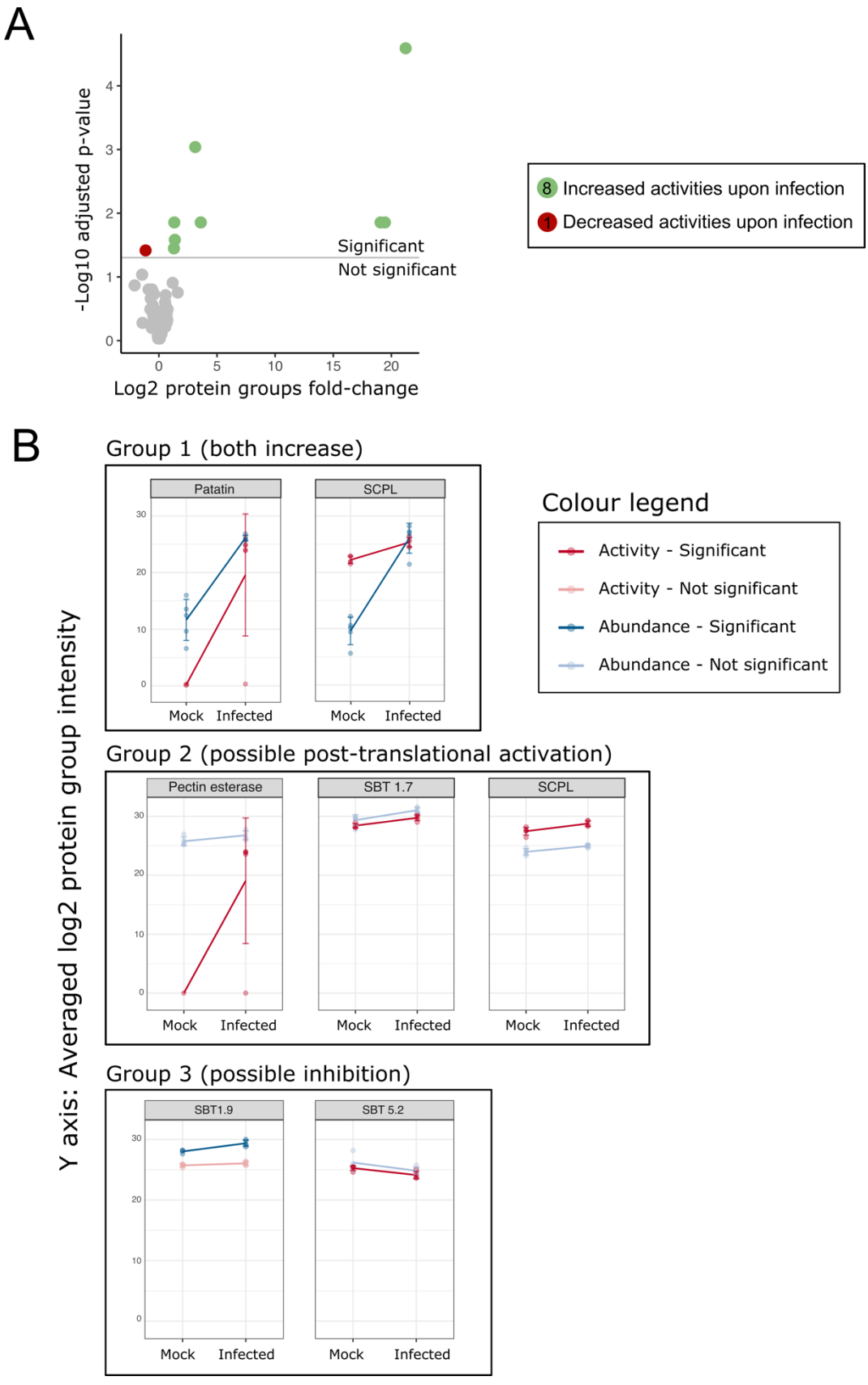


Figure 6. Comparative analysis o activome and proteomic upon P. infestans infection. **A, volcano plot of differentially active enriched hydrolases. B, Dynamic changes of abundance and activity of enriched hydrolase protein groups**. Three clustering groups were considered depending on the trends observed for each protein group. Left-hand side panel shows the log2 fold change for activity and abundance and right-hand side panels plots the averaged log2 protein group intensity for each protein group in the four biological replicates (mock and infected samples). Bars represent standard deviation of the samples. The R script and files used for the analysis can be found in Supplementary File 5.

Convolution ABPP-MS reveals a tomato SCPL as a possible inhibited hydrolase upon infection.

We performed the first large-scale convolution ABPP on apoplast of tomato infected with *P. infestans* to discover novel inhibited host hydrolases. Mock treated and infected samples of five biological replicates were labelled separately with a probe cocktail containing FP-biotin and DCG04 prior to be mixed in a 1:1 proportion (Label&Mix [L&M]). Independently, infected and mock treated samples were first mixed in a 1:1 proportion and incubated for 30 minutes. The mixture was then labelled with the probe cocktail containing FP-biotin and DCG04 (Mix&label [M&L]). We monitored the activity changes between L&M and M&L of 82 probe targets enriched upon labelling. Full R pipeline used for quantitative analysis can be found in Supplementary file 6.

Statistical analysis of labelling intensity revealed a significantly less active SCPL (Solyc06g074850.3.1) in M&L samples compared to L&M (**Figure 6A**), pointing towards the presence of a carboxypeptidase inhibitor in infected samples. We named Solyc06g074850.3.1 Serine CarboxyPeptidase Inhibited by *P. infestans* 1 (SCPIP1). Ranking of all protein group intensities in ISD and in comparative ABPP revealed that SCPIP1 is highly abundant in ISD. However, SCPIP1 activity ranks in the middle of the 82 probe targets monitored in the ABPP-MS analysis (**Figure 6B**), supporting the notion that it is inhibited.

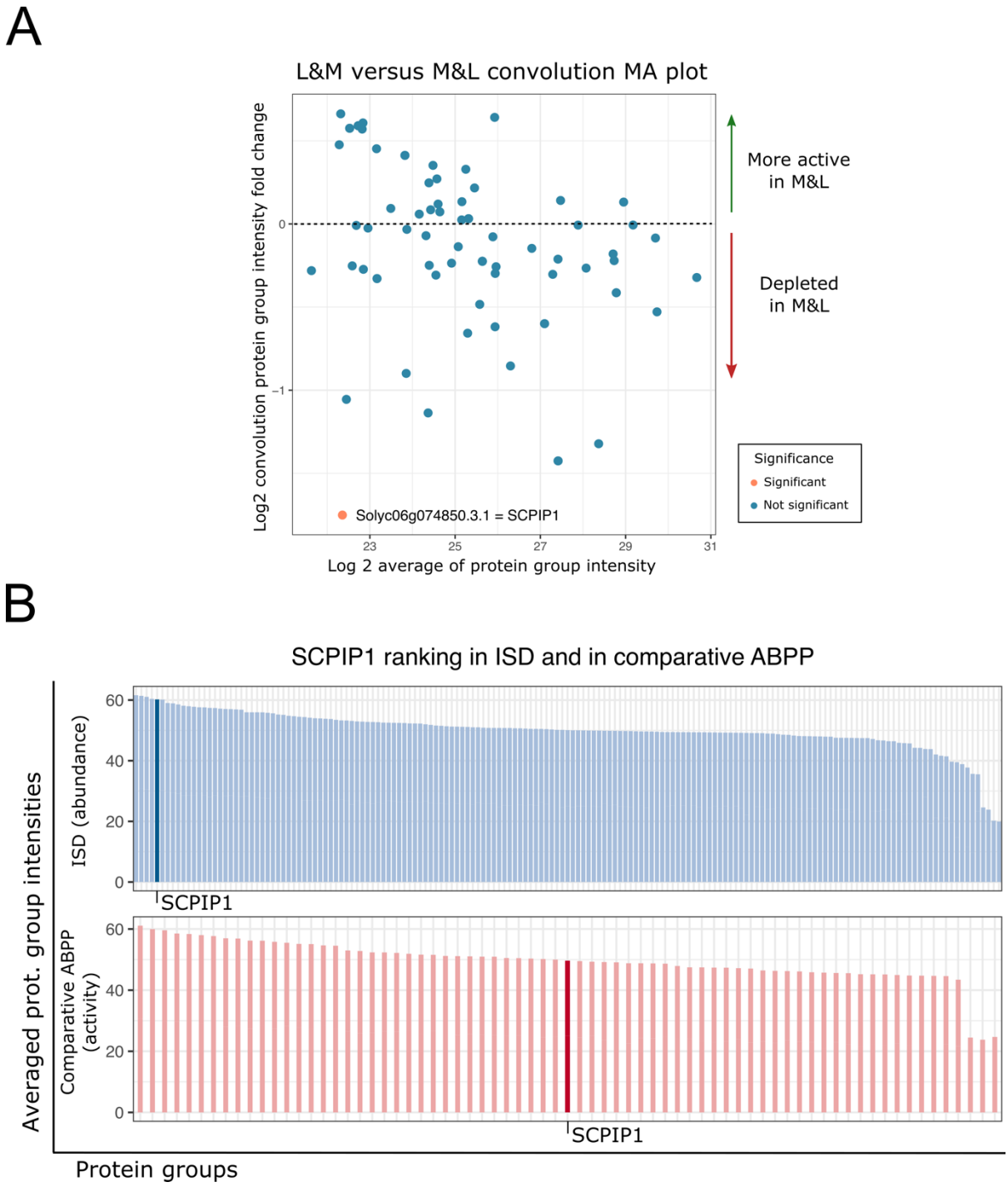


Figure 7. Convolution ABPP reveals one possible inhibited tomato serine carboxypeptidase. **A, MA plot of L&M versus M&L samples.** Each dot corresponds to a probe target enriched in ABPP-MS pull-down. Y axis represents the log fold change of the intensities and the X axis represents the log2 averaged protein group intensities. Protein groups were considered significantly differential when a BH corrected p-value below 0.05 was observed. **B, Ranking of the protein group intensities in ISD and comparative ABPP-MS experiments.** Averaged protein group intensities were ordered from highest to lowest in each of the experiments. Putative inhibited SCPIP1 position in the ranking is highlighted.

To obtain additional evidence for SCPIP1 inhibition, we performed fluorescent convolution ABPP in the same samples with FP-TAMRA probe, scanned fluorescent gels (**Figure 7A**) and

measured fluorescent intensity with ImageJ of the protein band at the predicted molecular weight of mature SCPIP1: 53 kDa (**Figure 7B**). In all replicates (n = 4), intensities of the 53 kDa protein band were significantly weaker in infected samples compared to mock treated samples. Furthermore, this 53 kDa band was significantly less intense in M&L samples compared to L&M (**Figure 7C**). SCIPIP1 is not the only protein within the range of 50-60 kDa identified in convolution ABPP-MS. However, it was the only protein presenting significant inhibition in M&L compared to L&M. Gel fluorescent measurements support the predicted inhibition of SCPIP1 detected in convolution ABPP-MS. Moreover, SCIP1 showed a log2 fold change of 0.77 in ISD that indicated an increased apoplastic accumulation upon infection. SCPIP1 did not show significant changes in activity in comparative ABPP-MS, but it presented a log2 fold-change of -0.34 upon infection pointing towards a reduction of SCPIP1 activity in infected samples.

In conclusion, our convolution ABPP-MS results and fluorescent convolution ABPP analysis support a putative inhibition of SCPIP1 upon infection and these results are not contradicted by the trends observed for SCPIP1 in ISD and comparative ABPP.

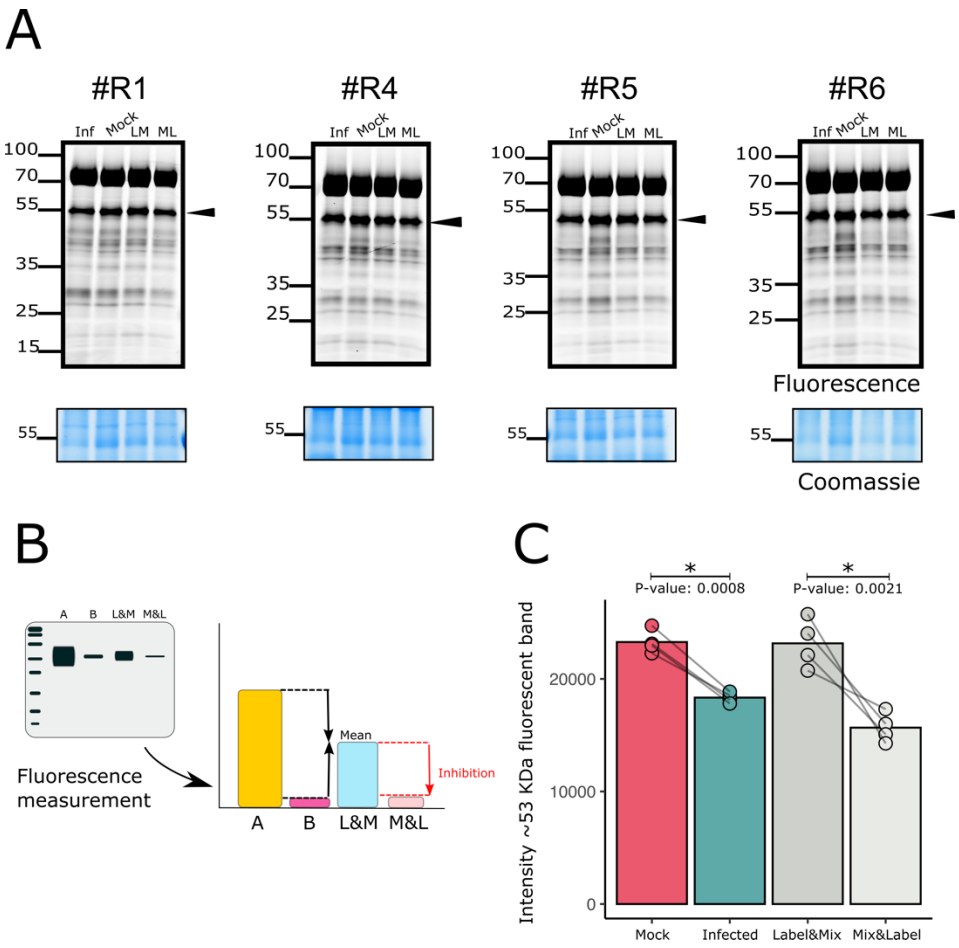


Figure 8. Fluorescent convolution ABPP results support SCPIP1 inhibition upon infection. **A, Fluorescent comparative and convolution ABPP of tomato AF infected with *P. infestans*.** Same samples used for the ABPP LC-MS/MS analysis were labelled for one hour with FP-TAMRA. Proteins were precipitated using five volumes of cold acetone prior to separation in acrylamide gel and scanned with Fpr-10 Cy3 laser. Arrows point to the approximately 53 kDa band which fluorescence was measured and analysed. **B, Diagram of fluorescent convolution experimental design.** ABPP fluorescent labelling is measured in control and treatment samples. Labelling would be prevented in M&L samples if there is a hydrolase inhibitor in excess in one of the samples. That will be reflected in a lower fluorescence in M&L samples compared to L&M samples. L&M samples usually show values close to the average of control and treatment samples. **C, Fluorescent intensity of 53 kDa band acrylamide protein gels.** Fluorescence intensity was measured using ImageJ tool (U.S. National Institutes of Health). Significant reduction 53kDa band was observed upon infection and in M&L samples compared to L&M, pointing towards a possible inhibition of SCPIP1 observed in convolution ABPP-MS. P-values < 0.05 are considered significant. R scripts for convolution coupled with LC-MS/MS, input files, script for fluorescence analysis and raw data can be found in Supplementary File 6 and 7.

Discussion

In this chapter, we show dynamic fluctuations of apoplastic proteome and activome of tomato upon *P. infestans* infection. We also compare abundance and activity values and performed convolution ABPP-MS to provide a list of possible hydrolases with post translationally regulated activity.

Tomato subtilases are prominent and widely studied apoplastic serine proteases with a crucial function in plant immunity[1,10,11]. Total proteome analysis revealed a significant increase of two tomato SBT1.9 subtilases (Solyc01g087850.2.1 and Solyc10g084320.3.1, **Figure 3C**) however, we could only detect activity of Solyc10g084320.3.1. *Arabidopsis thaliana* SBT1.9 family comprises secreted subtilases expressed during flowering stage and has four orthologs in potato[1,31]. Nonetheless, we lack studies that clarify their specific function and substrates. Our finds suggest that tomato SBT1.9 proteins could have a role in plant immunity. More specifically, Solyc08a079900.3.1 shows significant accumulation upon infection but its activity levels remain unaltered (**Figure 6B**, group 3). *P. infestans* secretes kazal-like EPI1 and EPI10 inhibitors to suppress subtilase P69B activity in early stages of infection[16,32,33]. This observation suggests a post-translational inactivation of SBT1.9 Solyc08a079900.3.1 activity during infection, possibly caused by *P. infestans* secreted subtilase inhibitors of the EPI family. Activity of tomato SBT1.7 Solyc08a079900.3.1 is significantly up-regulated upon infection whereas its abundance does not show significant changes, suggesting an infection-induced activation (**Figure 6B**, group 2). Arabidopsis SBT1.7/ARA12 (At5g67360) play a role in the seed germination process and ara12 mutants exhibit impaired seed mucilage release and low germination rate[34]. Also, a possible role in immunity has been suggested due to an induction of *ARA12* expression following jasmonate treatment[35]. Our study implicates SBT1.7 in defence against pathogens in tomato. Moreover, our data suggests an infection-induced zymogen maturation and an activity-dependent function of SBT1.7 Solyc08a079900.3.1.

Tomato phytaspase 1 SlPhyt1 (Solyc12g088760) and four members of P69 subtilase family (P69B, D, G and H) were among the enriched activome (**Figure 5B**). Tomato phytaspases are extracellular subtilases involved in programmed cell death (PCD) and systemin hormone maturation. They are often compared with animal caspases due to their specificity, that require internalisation within the cell to be functional. Phytaspases also increase resistance to tobacco mosaic virus. Differing from other members of phytaspase family, SlPhyt1 is constitutively expressed and it is the only phytaspase found in roots[30,36,37]. The identification of Phyt1 in our

activome serves as experimental validation of the ABPP-MS technique. P69 family has six members (P69A to P69F)[38] and owns its name to the molecular weight of the first cloned member of the family: 69 kDa[12]. Some members are associated to developmental processes such as P69D[39] and others are pathogenesis related (PR) proteins, such P69B and P69G, identified in our activome. P69B is induced during infection in tomato leaf apoplast and it confers resistance against *Pseudomonas syryngae* and *P. infestans*[16,40]. PR-P69G is expressed in leaves and roots and its accumulation can be induced by gibberellic acid and infection with tomato Torrado virus[41,42]. Altogether these results serve as benchmark of our experimental procedures and consolidate ABPP-MS as a reliable technique for the discovery of active hydrolases.

Serine Carboxypeptidases-like (SCPLs) are S10 proteases that may release residues from the C-termini of proteins. In our datasets, we could monitor accumulation and activity of three SCPLs and one SCPL protein group (Solyc02g014830.4.1, Solyc01g108490.3.1 and Solyc06g9083040.3.1-Solyc06g083050.3.1, **Figures 6B** and **7**). Remarkably, Solyc02g014830.4.1 activity and abundance were increased upon infection whereas Solyc01g108490.3.1 only showed a significant increase in activity, suggesting a possible post-translational activation (**Figure 6B**, groups 1 and 2). Convolution ABPP-MS returned SCPIP1 (Solyc06g074850) as a strong, highly accumulated candidate for being inhibited (**Figure 7C**). These opposed dynamics observed in SCPLs could result from a fined-tuned post-translational regulation. For instance, plants can secrete serine carboxypeptidase inhibitors (SCI) that suppress digestive enzymes in insects[43] and a potato SCI confers resistance against fungal pathogens such as *Magnaporthe oryzae* in rice[14]. Accumulation or reduction of a putative tomato SCI during infection could explain the dynamics we observed in SCP family. However, we could not exclude that *P. infestans* could also secrete SCPL inhibitors during tissue colonisation. Altogether these results provide rationale for experiments focused on investigating a possible role of a SCI during *P. infestans* infection of tomato apoplast, and an inhibited candidate SCPL (SCPIP1).

Carbohydrate active enzymes are another numerous group in our data sets. Four tomato glycoside hydrolases (GH) (Solyc11g044910.2.1, Solyc02g091920.3.1, Solyc05g049980.3 and Solyc01g008610.4.1) are up-regulated in the apoplast upon infection (**Figure 3B**). Plant glycoside hydrolases play an role in cell wall integrity maintenance during development an also during biotic stress[44]. Arabidopsis MORE1 GH and a close homolog from rice both confer resistance to a necrotrophic fungus whist it benefits hemibiotrophic pathogens[45]. *P. infestans* is an hemibiotroph and these four up-regulated GH could be promoting susceptibility to *P. infestans* in tomato in our experiments. This hypothesis makes Solyc11g044910.2.1, Solyc02g091920.3.1, Solyc05g049980.3

and Solyc01g008610.4.1 interesting candidates to be tested in functional and genetic analysis in the context of tomato-pathogen interactions. Also, two tomato chitinases (Solyc02g061770.4.1, Solyc04g072000.4.1) show accumulation during infection. Chitin is a major component of fungal cell walls and chitinase activity can impair pathogenic fungus colonisation by hydrolysing the β-1,4-glycosidic chitin bonds[46] and pathogenesis-related (PR) proteins PR-3, PR-4, PR-8 and PR-11 have endochitinase activity. Accumulation of chitinases is associated with enhanced resistance against potato blight in tomato cultivars[47] however, *P. infestans* cell wall is mainly composed of cellulose and *P. infestans* chitin production has not been proved yet[48,49]. As such, the accumulation of tomato chitinases such as Solyc02g061770.4.1 and Solyc04g072000.4.1 might be part of a general immune response that might not be specifically targeting *P. infestans*.

Among *P. infestans* secreted carbohydrate active proteins we found two endoglucanases (PITG_08944 and PITG_16985) and one carbohydrate binding protein (PITG_07303). These *P. infestans* carbohydrate active enzymes might be part of hyphae growth metabolism for and could also play a role in degrading plant cell walls to promote infection[50]. Our data-set provides robust proteomic evidence of three carbohydrate active *P. infestans* proteins secreted during infection. It would be interesting to perform homologs search in *P. sojae* and assess phenotypes of knockout mutants for those candidates.

Six tomato serine hydrolases with (GSDL) lipase (Solyc01g079160.4.1 and Solyc01g079160.4.1), esterase (Solyc06g009190.4.1), carboxylesterase (Solyc11g012070.3.1 and Solyc07g040890.1.1) and phospholipase activity (Solyc02g090490.3.1) were found in our data-sets with significative activity and/or accumulation changes (**Figure 3C** and **6B**). In rice, the GSDL lipase OsGLIP1 decreases resistance against *Xantomonas oryzae* and *Magnaporthe oryzae* pathogens[13]. This observation could explain the decreased accumulation we observed for Solyc01g079160.4.1, Solyc11g012070.3.1 and Solyc01g079160.4.1 upon infection. However, further confirmation of activity dynamics would be important to understand the role of these hydrolases in tomato apoplastic immunity of tomato. Carboxylesterases involved in the synthesis of jasmonic acid hormone are induced in Arabidopsis upon *Pseudomonas syringae* infection and they control the release of volatile signalling compounds in tomato[51,52]. In our data, we observed accumulation of the carboxylesterase Solyc07g040890.1.1, possibly as a response to biotic stress. Another hormone, the lipid-derived phosphatidic acid, is key in the signalling of defence processes in tomato such as oxidative burst and its synthesis depends on phospholipase enzymes[53]. We observed an accumulation and increased activity for the tomato patatin-like phospholipase Solyc02g090490.3.1 upon infection (**Figure 6B**, group 1). Pectin esterases function is key in abiotic stress-induced cell wall remodelation[54] and a pectin

esterase inhibitor discovered in cotton promotes Verticillium wilt resistance[55]. We could monitor the abundance and activity of Solyc06g009190.4.1 pectin esterase. This enzyme does not show significant changes in abundance, but its activity is greatly increased upon infection (**Figure 6B**, group 2). These dynamics might be caused by a down-regulation of a Solyc06g009190.4.1 inhibitor. It would be very interesting to assess how pectin esterase Solyc06g009190.4.1 activity could affect cell wall remodelation during infection and if an inhibitor is playing a role in enzymatic activation.

Among accumulated protein groups in infection with a likely role in tomato immunity we find peroxidases (Solyc01g105070.3.1-Solyc02g064970.4.1 and Solyc01g105070.3.1), Kutnitz-type trypsin inhibitors (Solyc03g098670.1.1 and Solyc03g098740.1.1) and PR-10/Bet v1-like proteins (Solyc05g054380.2.1, Solyc09g090980.3.1 and Solyc09g090990.2.1). Apoplastic reactive oxygen species (ROS) burst is an important signalling process during biotic stress and it is usually followed by the activation of pathogen molecular pattern triggered immunity[56]. A well-known example is the ROS burst triggered by flg22, the immunogenic peptide of flagellin sensed in tomato[57]. Kunitz-type inhibitors have been associated with enhanced resistance against herbivores in cocoa and Arabidopsis[58,59], but a possible role against *P. infestans* infection in tomato has not been described. PR-10/Bet v1-like proteins have been extensively studied. Their activity can range from lipid-binding to PLCP inhibition or ribonuclease activity, and PR-10 proteins can act against nematodes in the case of *Crotalaria pallida* or suppressing pathogenic fungus in the case of peanut PR10[60–62]. Three tomato PR-10 proteins (Solyc05g054380.2.1, Solyc09g090980.3.1 and Solyc09g090990.2.1) accumulated upon infection and serve as interesting candidates to study further in the context on *P. infestans* infection and elucidate their function and activity.

We found two depleted apoplastic tomato proteins with a potential role in immunity: the S-locus receptor kinase Solyc07g063820.3.1 and the NAD-dependent epimerase Solyc09g091970.4.1. S-locus receptor kinase is involved in pollen self-incompatibility in Arabidopsis[63,64] and some members of the family can act as negative regulators of immunity [65]. The depletion of Solyc07g063820.3.1 the S-locus receptor kinase could potentiate tomato immune responses during infection but further investigation of Solyc07g063820.3.1 is encouraged. Secreted NAD-dependent epimerases in lentil plants are induced upon infection by *Colletotrichum lentils*[66] but little else is known about this protein family. Here we report tomato Solyc09g091970.4.1 as a down-regulated NAD-dependent epimerase upon infection, opening the possibility for further studies to characterise the role of this protein in more detail.

On the pathogen side, we find apoplastic ribonucleases PITG_01495 and PITG_16015, berberine-like oxidoreductase PITG_02930, secreted cysteine-rich protein PITG_11060 and serine hydrolase S33 PITG_15239 as the most confidently identified *P. infestans* apoplastic proteins (**Figure 4**). Raffaele *et al.* (2010)[26] also showed that ribonucleases and berberine-like oxidorreductases are highly represented in the *P. infestans* secretome and were proposed as possible virulence factors[26]. More precisely, in the same study PITG_02930 was annotated for the first time and was revealed to be induced upon infection. In our study, we provide proteomic evidence for PITG_01495 and PITG_16015 ribonucleases and for the oxidoreductase PITG_02930, complementing the transcriptomic data of Raffaele *et al. P. infestans* and demonstrating that cysteine-rich protein PITG11060 can function as an effector. A prominent example is PC2, a cysteine-rich secreted effector that can trigger PCD in *Nicotiana benthamiana* upon cleavage by tomato subtilase P69B[10]. PITG_11060 was also identified in *P. infestans* secretome of axenic culture in previous studies[67]. In our study, we provide proteomic evidence of PITG_11060 in tomato infected apoplast that highlights the possible role of this secreted protein in pathogenesis. MEROPS family of S33 serine hydrolases can be prolyl amino exopeptidases however, some S33 enzymes such as Hip1 from *Mycobacterium tuberculosis* also exhibit esterase activity[68]. We observed a robust presence of PITG_15239 in AF infected samples. However, our ABPP-MS did not indicate a labelling of this serine hydrolase, suggesting it might not be active. Further analysis of *P. infestans* PITG_15239 will shed light on the role of this hydrolase during infection.

We also found three heat shock protein 70-like (Hsp70-like) among *P. infestans* apoplastic protein collection (PITG_11252, PITG_15370 and PITG_05721, **Figure 4**). Plant-derived Hsp70 proteins act as molecular chaperones and they enhance immune responses to *P. infestans* in *N. benthamiana*[69–71] and are upregulated in *N. benthamiana* plants overexpressing a cytoplasmic effector of *P. sojae* [72]. These proteins are known to suppress cytotoxicity generated during cell over proliferation during carcinogenesis and to promote cellular survival[73]. There are no defined roles described for *P. infestans* secreted Hsp70s to date but perhaps they might contribute to the maintenance of the biothrophic phase, influencing positively plant cell survival and avoiding apoptosis. Another possible function of these proteins could be to protect *P. infestans* cells from the proteotoxic environment generated at the necrotrophic phase.

Moreover, two secreted *P. infestans* cell wall transglutaminases (PITG_16958 and PITG_16956, **Figure 3**) were identified robustly in AF of infected tomato. These proteins play a role in cell wall regulation of the pathogen[74]. PITG_16956 is induced during early phases of potato infection and mycelia sporulation[75,76]. Moreover, PITG_16956 contains the conserved Pep-13 immunogenic

peptide that is able to trigger an immune response in parsley and potato[77]. It is expected that these transglutaminases also generate an immune response in tomato.

Interestingly, we could detect labelling of two *P. infestans* PLCPs: PITG_03020 and PITG_06927 (**Figure 5**). This is remarkable because *P. infestans* secretes PLCP inhibitors during early stages of infection that target host PLCPs to promote virulence[17]. Remarkably, these two *P. infestans* PLCPs might be susceptible to EPIC inhibitors as we demonstrate for Pain1a in thesis chapter 3. As explained in chapter X, we could not achieve a successful heterologous expression of PITG_03020, but the fact that it has an induced expression during infection and that we successfully enriched it in ABPP-MS proving that is an active PLCP during infection, makes PITG_03020 an remarkable candidate to explore further its role in pathogenicity.

Materials and methods

Money Maker tomato plants infection with *P. infestans* spores.

Tomato plants of the cultivar Money Maker were grown under long day conditions at 23-26°C and 60% relative humidity.

10-12 days old rye A agar plates containing *P. infestans* isolate 90128 were flooded with 4°C mili-Q water and left at 4°C in darkness for 4 hours to induce sporulation. The supernatant containing *P. infestans* zoospores was collected and filtered through two layers of miracloth to remove micelia and sporangia. Zoospores were counted in a microscope, placing a 10 µl drop of the zoopores on a haemocytometer. Zoospores concentration was adjusted by dilution to 50 zoospores per µl.

Detached Money Maker tomato leaflets were placed over two layers of wet tissue within 20x20 cm square transparent boxes. Mock solution containing cold miliQ water or zoospores solution were sprayed over the leaflets (15 plants per treatment) uniformly. Boxes were sealed with parafilm to keep the relative humidity close to 100% and placed in a cabinet at 18°C and 16 hours of light for 3 days prior to sample collection.

Apoplastic fluid isolation

Apoplastic fluid was collected 3 days after infection or mock treatment. Leaflets were infiltrated with cold miliQ water applying vacuum and pressure using a 50 ml syringe. Then leaflets were

dried with tissue and placed inside a 20 ml syringe without plunger. The syringes containing the infiltrated leaflets were placed inside a 50 ml Falcon tube and centrifuged at 4°C, 1500Xg for 30 minutes. The apoplastic fluid was then placed in 15 ml Eppendorf screw cap tubes and snap frozen until further analysis.

In-solution trypsin digestion of total proteomes

Tryptic peptides of apoplastic total proteomes were generated using Single-Pot Solid-Phase-enhanced Sample Preparation (SP3) method by our collaborators at the Analytical Core Facility of Essen (Germany). A detailed protocol with all the steps and chemicals required can be found in Supplementary file 1. In brief, proteins are diluted with organic solvents such as ethanol and acetonitrile and then immobilised on the surface of magnetic beads. This allows to clean and purify the proteins and to easily exchange buffers for reduction and alkylation steps. After that, proteins are digested by LysC and trypsin on beads, and peptides are recovered for their mass spectrometry analysis.

Labelling of active apoplastic hydrolases and affinity purification

Three ml of tomato apoplastic fluid (AF) per treatment were labelled with 4 μM of FP-biotin and 4 μM DCG04 during 4 hours at room temperature and with rotation. Reaction was buffered using 50 mM NaAc pH 5 and 5mM of dithiothreitol (DTT). No no-probe control (NCP) samples were identical to labelled samples but instead of probes, an equal volume of DMSO was added to the 3 ml of AF. Labelling reactions were stopped by chloroform/methanol precipitation. 1:3:4 volumes of cold chloroform:water:methanol were added to the samples and mixed thoroughly. Precipitating samples were kept in the freezer at -20°C until next steps of the protocol were performed. Subsequently, samples were centrifugated at 3000xg for 30 minutes (4°C). The aqueous top phase was removed without disturbing the interphase in which the proteins were present. Then 4 volumes of cold methanol were added, and samples were centrifuged again for 45 minutes at 3000xg (4°C). The supernatant was removed without disturbing the pellet and the precipitated proteins were left drying at room temperature. Precipitated proteins were resuspended with 2 ml of 1.2% sodium dodecyl sulphate (SDS) phosphate saline buffer (PBS) (Life Technologies, 18912-014) for at least 40 minutes. Then, samples were sonicated in a sonicating bath (ASK_REF) at maximum power for 10 minutes. A further 5 ml of PBS were added to the samples and proteins were denatured in a water bath at 90°C for five minutes. A further 3 ml of PBS were added to the

samples to lower the SDS concentration below 0.2%. To enrich labelled proteins, 130 µl of PBS washed avidin beads (Sigma, A9207) were added to each sample, including the NPC. Beads were incubated with resuspended proteins for 1 hour at room temperature while rotating. Beads were then centrifugated for 1 minute at 400xg and supernatant was discarded. Avidin beads were then washed 5 times with 10 ml of 1% SDS PBS buffer to remove unspecific protein-beads interactions, and 3 times with 10 ml of ultra-pure HPLC-MS grade water. Avidin beads were transferred into 2 ml LoBind protein tubes (Eppendorf, Z666505-100EA).

Convolution

For Mix&label samples, 1.5 ml of mock and infected AF of each replicate were mixed and incubated at room temperature for 1 hour, prior to labelling and protein precipitation (detailed above). The same labelling procedure detailed above was followed for Label&Mix samples using half of volumes for 1.5 ml of AF. After 4 hours labelling, samples were mixed and immediately 1:3:4 volumes of cold chloroform:water:methanol were added to stop reactions. Protocol was followed as described before.

On-bead digestion and peptide purification

250 µl of 8M Urea in 50 mM TrisHCl pH8 were added to the beads. Proteins reduced by adding 500mM of TCEP and incubating samples at 56°C for 30 minutes while shaking. Samples were then cooled down to room temperature before the alkylation step. 30 µl of 500mM chloroacetamide was added and alkylation was performed at 36°C for 30 minutes in dark.

Samples were centrifuged at 2000 rpm for three minutes and the supernatant was removed.

A vial of 20 µg of LysC endopeptidase enzyme (Wako, 125-02543) was resuspended into 1220 µl 1M urea in 50mM Tris-HCl pH. 80 µl of this resuspended LysC were added to each sample. Tubes were sealed with parafilm and LysC disgestion was performed over night at 37°C while shaking. Next day, trypsin endopeptidase (Trypsin gold MS grade Promega V5280) was reconstituted following manufacturer's instructions in 50mM NaAc pH 5. 20 µg of reconstituted trypsin were added to 1200 µl 50 mM Tris-HCl pH8. 80 µl of the diluted trypsin was added to each sample (2 µg per sample) and incubated for at least 8 hours at 36°C.

After trypsin digestion, tryptic peptides present in the supernatant were recovered into a new Lobind protein tube. Prior to mass spectrometry analysis of the peptidic composition, tryptic peptides were purified using 100 µl Agilent Bond Elut OMIX Pipette tips for micro extractions (Agilent, A57003100) using a 1 ml syringe coupled with a 1000 µl cut filter tip to push buffers and samples through the C18 column. Manufacturer's instructions were followed in this step.

LC-MS analysis

All the analytical steps until obtaining the list of identified tryptic peptides was done by our collaborators at the Analytical Core Facility of Essen (Germany).

Samples were separated in a self-packed fused silica capillary analytical column with integrated emitter (no frit) (ESi Source Solutions, PTC3-75-50-SP) in a liquid chromatography Thermo Easy-nLC 1200 system prior to peptides ionisation. The ion source for peptides ionisation was a Thermo Nanospray Flex. Retention varied between ± 0.08 and 0.15 minutes based on average retention time shift of 4 monitored BSA internal standard peaks.

For the mass spectra analysis, a Thermo Orbitrap Fusion Lumos (Thermo) was used with a scan range (m/z) of 375-1750.

RAW spectra generated in the mass spectrometry Orbitrap was submitted to MaxQuant software (version v1.6.10.43) for a peptide search powered by Andromeda engine with default parameters. The ITAG4.0 tomato proteome from Solgenomics consortia and *P. infestans* RefSeq proteome from NCBI were used as databases for the theoretical tryptic peptides matching. Searches included a database of contaminants (built in MaxQuant software, 245 entries) and reverse hits data-base. Carbamidomethylation was set as static modification and oxidation, acetylation and demethylation of the N termini were specified as dynamic modifications. The MS-MS tolerance was set to ± 0.5 Da and peptide spectrum match FDR to 0.01. Minimum peptide length allowed was 7 amino acids.

Data analysis

Data analysis of the different experimental procedures (ISD, OBD of ABP-MS and OBS of convolution ABPP-MS) was done separately.

To determine *P. infestans* proteins identified with confidence, a qualitative filter was applied, and unique protein groups present in at least 60% of the biological replicates were considered robustly identified. Details can be found in the scripts included in Suplementary file 1.

For quantitative comparisons of in-solution digestions, peptides matching the contaminants or reverse hits data-bases or those that were not belonging to unique protein groups were removed.

Peptide intensities equal to 0 were considered a missing value (NA). Peptides with 60% or more missing values across the in-solution samples were removed. Intensities distributions were normalised against each other using variance stabilisation method. Peptides that were not found in all the samples of a given treatment (mock or infected) but had at least 40% of assigned intensities in the other treatment were considered biologically relevant (or not missed at random -NMAR-) and values in the sample where they were not found were imputed to 0. Peptides intensities were aggregated using a method based on the median to calculate unique protein groups intensities. Principal component analysis was used to assess the clustering of the biological replicates, and outlying replicates were not considered when applicable. Fold change and adjusted p-values (BH method) were calculated with Bayesian statistic methods implemented in Limma R package.

Similar analyses were also done for labelled versus NPC samples but in this case peptidic intensities were not normalised in this case to avoid artificial generation of high values in NPC. In this analysis NA filter was set to 80%.

Details can be found in Supplementary files 4, 5 and 6.

Fluorescent ABPP

For SH labelling, 5 mM DTT and 50 mM NaAc pH 5 (final concentrations) were added to 43 µl of apoplastic fluid. FP- TAMRA fluorescent probe was added to a final concentration of 0.2 µM and labelling was performed for 1 hour at room temperature. Proteins were then precipitated by adding 5 volumes of cold pure acetone and centrifuging at maximum speed for 2 minutes. Protein pellets were air dried at room temperature and resuspended in 20 µl of PBS-SDS loading buffer (phosphate-buffered saline (PBS) pH 7.4, 1% (w/v) sodium dodecyl sulphate (SDS) and denatured for 5 minutes at 90°C.

Then, up to 10 µl was loaded in 12% SDS- PAGE acrylamide gels and separated with 180V electric current. The gels were placed in a Amersham Typhoon 5 (GE Healthcare Life Sciences) and fluorescence was scanned at 647 nm wavelength. To obtain loading controls, gels were stained with Coomassie Brilliant Blue G-250.

Bibliography

1. Schaller, A. *et al.* From structure to function – a family portrait of plant subtilases. *New Phytol.* **218**, 901–915 (2018).

2. Misas-Villamil, J. C., van der Hoorn, R. A. L. & Doehlemann, G. Papain-like cysteine proteases as hubs in plant immunity. *New Phytol.* **212**, 902–907 (2016).

3. Salguero-Linares, J. & Coll, N. S. Plant proteases in the control of the hypersensitive response. *J. Exp. Bot.* **70**, 2087–2095 (2019).

4. Zhao, J. Phospholipase D and phosphatidic acid in plant defence response: from protein-protein and lipid-protein interactions to hormone signalling. *J. Exp. Bot.* **66**, 1721–1736 (2015).

5. Shimada, T., *et al.* Plant Vacuoles. *Annu. Rev. Plant Biol.* **69**, 123–145 (2018).

6. Rennie, E. A. & Scheller, H. V. Xylan biosynthesis. *Curr. Opin. Biotechnol.* **26**, 100–107 (2014).

7. D'Ippólito, S., *et al.* Role of proteases in the response of plants to drought. *Plant Physiol. Biochem. PPB* **168**, 1–9 (2021).

8. Wang, Y., Wang, Y. *et al.* Apoplastic proteases: powerful weapons against pathogen infection in plants. *Plant Commun.* **1**, 100085 (2020).

9. Buscaill, P. *et al.* Glycosidase and glycan polymorphism control hydrolytic release of immunogenic flagellin peptides. *Science* **364**, eaav0748 (2019).

10. Wang, S. *et al.* Cleavage of a pathogen apoplastic protein by plant subtilases activates immunity. *BioRxiv* (2019).

11. Paulus, J. K. *et al.* Extracellular proteolytic cascade in tomato activates immune protease Rcr3. *Proc. Natl. Acad. Sci.* **117**, 17409–17417 (2020).

12. Tornero, P., *et al.* Primary structure and expression of a pathogen-induced protease (PR-P69) in tomato plants: Similarity of functional domains to subtilisin-like endoproteases. *Proc. Natl. Acad. Sci. U. S. A.* **93**, 6332–6337 (1996).

13. Gao, M. *et al.* GDSL lipases modulate immunity through lipid homeostasis in rice. *PLoS Pathog.* **13**, e1006724 (2017).

14. Quilis, J. *et al.* A potato carboxypeptidase inhibitor gene provides pathogen resistance in transgenic rice. *Plant Biotechnol. J.* **5**, 537–553 (2007).

15. Rooney, H. C. E. *et al. Cladosporium* Avr2 inhibits tomato Rcr3 protease required for Cf-2-dependent disease resistance. *Science* **308**, 1783–1786 (2005).

16. Tian, M., *et al.* A kazal-like extracellular serine protease inhibitor from *Phytophthora infestans* targets the tomato pathogenesis-related protease P69B. *J. Biol. Chem.* **279**, 26370–26377 (2004).

17. Gumtow, R., *et al.* A *Phytophthora palmivora* extracellular cystatin-like protease inhibitor targets papain to contribute to virulence on papaya. *Mol. Plant-Microbe Interactions* **31**, 363–373 (2017).

18. Shao, F. *et al.* Cleavage of Arabidopsis PBS1 by a bacterial type III Effector. *Science* **301**, 1230–1233 (2003).

19. Jain, A., Singh, H. B. & Das, S. Deciphering plant-microbe crosstalk through proteomics studies. *Microbiol. Res.* **242**, 126590 (2021).

20. Elmore, *et al.* Advances in functional proteomics to study plant-pathogen interactions. *Curr. Opin. Plant Biol.* **63**, 102061 (2021).

21. Larsen, M. K. G., *et al.* Time-course investigation of *Phytophthora infestans* infection of potato leaf from three cultivars by quantitative proteomics. *Data Brief* **6**, 238–248 (2016).

22. Morimoto, K. & van der Hoorn, R. A. L. The increasing impact of activity-based protein profiling in plant science. *Plant Cell Physiol.* **57**, 446–461 (2016).

23. Chandrasekar, B., *et al.* Inhibitor Ddscovery by convolution ABPP. in *Activity-Based Proteomics: Methods and Protocols* **47–56** (2017).

24. Planas-Marquès, M. *et al.* Protease activities triggered by *Ralstonia solanacearum* infection in susceptible and tolerant tomato lines. *Mol. Cell. Proteomics MCP* **17**, 1112–1125 (2018).

25. Boevink, P. C., *et al.* Devastating intimacy: the cell biology of plant–*Phytophthora interactions*. *New Phytol* **445-458** (2020).

26. Raffaele, S., Win, J., Cano, L. M. & Kamoun, S. Analyses of genome architecture and gene expression reveal novel candidate virulence factors in the secretome of *Phytophthora infestans*. *BMC Genomics* **11**, 637 (2010).

27. Tytgat, H. L. P. *et al.* Endogenous biotin-binding proteins: an overlooked factor causing false positives in streptavidin-based protein detection. *Microb. Biotechnol.* **8**, 164–168 (2015).

28. Morimoto, K. *et al.* Triazine probes target ascorbate peroxidases in plants. *Plant Physiol.* **180**, 1848–1859 (2019).

29. Meichtry, J., Amrhein, N. & Schaller, A. Characterization of the subtilase gene family in tomato (*Lycopersicon esculentum* Mill.). *Plant Mol. Biol.* **12**. (1999).

30. Chichkova, N. V. *et al.* Phytaspase, a relocalisable cell death promoting plant protease with caspase specificity. *EMBO J.* **29**, 1149–1161 (2010).

31. AT5G67090(SBT1.9). https://www.arabidopsis.org/servlets/TairObject?name=AT5G67090&type=locus.

32. Tian, M. & Kamoun, S. A two disulfide bridge Kazal domain from *Phytophthora* exhibits stable inhibitory activity against serine proteases of the subtilisin family. *BMC Biochem.* **6**, 15 (2005).

33. Tian, M., Benedetti, B. & Kamoun, S. A second Kazal-Like protease inhibitor from *Phytophthora infestans* inhibits and interacts with the apoplastic pathogenesis-related protease P69B of tomato. *Plant Physiol.* **138**, 1785–1793 (2005).

34. Rautengarten, C. *et al.* A subtilisin-like serine protease essential for mucilage release from Arabidopsis seed coats. *Plant J.* **54**, 466–480 (2008).

35. Golldack, D., *et al.* Expression of subtilisin-like serine proteases in *Arabidopsis thaliana* is cell-specific and responds to jasmonic acid and heavy metals with developmental differences. *Physiol. Plant.* **118**, 64–73 (2003).

36. Beloshistov, R. E. *et al.* Phytaspase-mediated precursor processing and maturation of the wound hormone systemin. *New Phytol.* **218**, 1167–1178 (2018).

37. Reichardt, S. *et al.* The tomato subtilase family includes several cell death-related proteinases with caspase specificity. *Sci. Rep.* **8**, 10531 (2018).

38. Jordá, L., *et al.* Genomic cluster containing four differentially regulated subtilisin-like processing protease genes is in tomato plants. *J. Biol. Chem.* **274**, 2360–2365 (1999).

39. Figueiredo, J., *et al.*, A. Subtilisin-like proteases in plant defence: the past, the present and beyond. *Mol. Plant Pathol.* **19**, 1017–1028 (2018).

40. Jordá, L. & Vera, P. Local and systemic induction of two defense-related subtilisin-like protease promoters in transgenic Arabidopsis plants. Luciferin induction of PR gene expression. *Plant Physiol.* **124**, 1049–1058 (2000).

41. Wieczorek, P., *et al.* Contribution of Tomato torrado virus Vp26 coat protein subunit to systemic necrosis induction and virus infectivity in Solanum lycopersicum. *Virol. J.* **16**, 9 (2019).

42. Lisón, P. *et al.* A noncoding plant pathogen provokes both transcriptional and posttranscriptional alterations in tomato. *PROTEOMICS* **13**, 833–844 (2013).

43. Bayés, A. *et al.* Structural basis of the resistance of an insect carboxypeptidase to plant protease inhibitors. *Proc. Natl. Acad. Sci.* **102**, 16602–16607 (2005).

44. Vaahtera, L., Schulz, J. & Hamann, T. Cell wall integrity maintenance during plant development and interaction with the environment. *Nat. Plants* **5**, 924–932 (2019).

45. Kim, C.-Y. *et al.* A rice gene encoding glycosyl hydrolase plays contrasting roles in immunity depending on the type of pathogens. *Mol. Plant Pathol.* **23**, 400–416 (2022).

46. Fukamizo, T. & Shinya, S. Chitin/Chitosan-Active Enzymes Involved in Plant-Microbe Interactions. *Adv. Exp. Med. Biol.* **1142**, 253–272 (2019).

47. Laurindo, B. S. *et al.* Comparative analysis of constitutive proteome between resistant and susceptible tomato genotypes regarding to late blight. *Funct. Integr. Genomics* **18**, 11–21 (2018).

48. Grenville-Briggs, L. J. *et al.* Cellulose synthesis in *Phytophthora infestans* is required for normal appressorium formation and successful infection of potato. *Plant Cell* **20**, 720–738 (2008).

49. Hinkel, L. & Ospina-Giraldo, M. D. Structural characterization of a putative chitin synthase gene in *Phytophthora* spp. and analysis of its transcriptional activity during pathogenesis on potato and soybean plants. *Curr. Genet.* **63**, 909–921 (2017).

50. Ospina-Giraldo, M. D., *et al.* The CAZyome of *Phytophthor*a spp.: a comprehensive analysis of the gene complement coding for carbohydrate-active enzymes in species of the genus *Phytophthora. BMC Genomics* **11**, 525 (2010).

51. Vlot, A. C. *et al.* Identification of likely orthologs of tobacco salicylic acid-binding protein 2 and their role in systemic acquired resistance in *Arabidopsis thaliana. Plant J. Cell Mol. Biol.* **56**, 445–456 (2008).

52. Goulet, C. *et al.* Role of an esterase in flavor volatile variation within the tomato clade. *Proc. Natl. Acad. Sci. U. S. A.* **109**, 19009–19014 (2012).

53. Shah, J. Lipids, lipases, and lipid-modifying enzymes in plant disease resistance. *Annu. Rev. Phytopathol.* **43**, 229–260 (2005).

54. Wu, H.-C., *et al.* Pectin methylesterases: cell wall remodeling proteins are required for plant response to heat stress. *Front. Plant Sci.* **9**, (2018).

55. Liu, N. *et al.* A pectin methylesterase inhibitor enhances resistance to verticillium wilt. *Plant Physiol.* **176**, 2202–2220 (2018).

56. Qi, J., Wang, J., Gong, Z. & Zhou, J.-M. Apoplastic ROS signaling in plant immunity. *Curr. Opin. Plant Biol.* **38**, 92–100 (2017).

57. Felix, G., *et al.* Plants have a sensitive perception system for the most conserved domain of bacterial flagellin. *Plant J.* **18**, 265–276 (1999).

58. do Amaral, M. *et al.* TcTI, a Kunitz-type trypsin inhibitor from cocoa associated with defense against pathogens. *Sci. Rep.* **12**, 698 (2022).

59. Arnaiz, A. *et al.* Arabidopsis kunitz trypsin inhibitors in defense against spider mites. *Front. Plant Sci.* **9**, (2018).

60. Morris, J. S., *et al.* PR10/Bet v1-like proteins as novel contributors to plant biochemical diversity. *ChemBioChem* **22**, 264–287 (2021).

61. Andrade, L. B. da S. *et al.* Effects of a novel pathogenesis-related class 10 (PR-10) protein from *Crotalaria pallida* roots with papain inhibitory activity against root-knot nematode *Meloidogyne incognita*. *J. Agric. Food Chem.* **58**, 4145–4152 (2010).

62. Chadha, P. & Das, R. H. A pathogenesis related protein, AhPR10 from peanut: an insight of its mode of antifungal activity. *Planta* **225**, 213–222 (2006).

63. Nasrallah, J. B. & Nasrallah, M. E. S-locus receptor kinase signalling. *Biochem. Soc. Trans.* **42**, 313–319 (2014).

64. Strickler, S. R., *et al.* Regulation of the s-locus receptor kinase and self-incompatibility in *Arabidopsis thaliana*. *G3 GenesGenomesGenetics* **3**, 315–322 (2013).

65. Kim, H. S. *et al.* An S-locus receptor-like kinase plays a role as a negative regulator in plant defense responses. *Biochem. Biophys. Res. Commun.* **381**, 424–428 (2009).

66. Bhadauria, V., *et al.* Transcriptome analysis reveals a complex interplay between resistance and effector genes during the compatible lentil-*Colletotrichum lentis* interaction. *Sci. Rep.* **7**, 42338 (2017).

67. Meijer, H. J. G. *et al.* Profiling the secretome and extracellular proteome of the potato late blight pathogen *Phytophthora infestans*. *Mol. Cell. Proteomics MCP* **13**, 2101–2113 (2014).

68. Naffin-Olivos, J. L. *et al.* Structure determination of *Mycobacterium tuberculosis* serine protease Hip1 (Rv2224c). *Biochemistry* **56**, 2304–2314 (2017).

69. Berka, M., *et al.* Regulation of heat shock proteins 70 and their role in plant immunity. *J. Exp. Bot.* erab549 (2022).

70. Kanzaki, H. *et al.* Cytosolic HSP90 and HSP70 are essential components of INF1-mediated hypersensitive response and non-host resistance to *Pseudomonas cichorii* in *Nicotiana benthamiana*. *Mol. Plant Pathol.* **4**, 383–391 (2003).

71. Lee, J. H., *et al.* HSP70s Enhance a *Phytophthora infestans* effector-induced cell death via an MAPK cascade in *Nicotiana benthamiana*. *Mol. Plant-Microbe Interact. MPMI* **31**, 356–362 (2018).

72. Zhang, M. *et al.* A *Phytophthora sojae* cytoplasmic effector mediates disease resistance and abiotic stress tolerance in *Nicotiana benthamiana*. *Sci. Rep.* **5**, 10837 (2015).

73. Radons, J. The human HSP70 family of chaperones: where do we stand? *Cell Stress Chaperones* **21**, 379–404 (2016).

74. Fabritius, A.-L. & Judelson, H. S. A mating-induced protein of *Phytophthora infestans* is a member of a family of elicitors with divergent structures and stage-specific patterns of expression. *Mol. Plant-Microbe Interact. MPMI* **16**, 926–935 (2003).

75. Svante, R. *et al.* Proteomic analysis of *Phytophthora infestans* reveals the importance of cell wall proteins in pathogenicity. *Mol. Cell Proteomics* **1958-1971** (2017).

76. Grenville-Briggs, L. *et al.* Identification of appressorial and mycelial cell wall proteins and a survey of the membrane proteome of *Phytophthora infestans*. *Fungal Biol.* **702-23** (2010).

77. Brunner, F. *et al.* Pep-13, a plant defense-inducing pathogen-associated pattern from *Phytophthora* transglutaminases. *EMBO J.* **21**, 6681–6688 (2002).

Supplementary materials

Supplementary table 1: Proteins with significant differential abundance in tomato apoplast upon *P. infestans* infection.

ID	logFC	AveExpr	all.domain	diff_activity	apop_pred
Solyc00g500050.1.1	-2.0403340766288	23.4377381853871	P-loop containing nucleoside triphosphate hydrolases, ATP synthase alpha and beta subunits signature., C-terminal domain of alpha and beta subunits of F1 ATP synthase, N-terminal domain of alpha and beta subunits of F1 ATP synthase, ATP-synt_F1_alpha_N, -, -, F1_ATPase_alpha, ATP synthase subunit alpha [atpA]., F_ATPase_subunit_alpha, atpA: ATP synthase F1, alpha subunit, ATP synthase alpha/beta family, beta-barrel domain, -, ATP-synt_F1_alpha_C, ATP synthase alpha/beta chain, C terminal domain, ATP synthase alpha/beta family, nucleotide-binding domain	NA	Non-apoplastic
Solyc00g500133.1.1	-2.0403340766288	23.4377381853871	P-loop containing nucleoside triphosphate hydrolases, ATP synthase alpha and beta subunits signature., C-terminal domain of alpha and beta subunits of F1 ATP synthase, N-terminal domain of alpha and beta subunits of F1 ATP synthase, ATP-synt_F1_alpha_N, -, -, F1_ATPase_alpha, ATP synthase subunit alpha [atpA]., F_ATPase_subunit_alpha, atpA: ATP synthase F1, alpha subunit, ATP synthase alpha/beta family, beta-barrel domain, -, ATP-synt_F1_alpha_C, ATP synthase alpha/beta chain, C terminal domain, ATP synthase alpha/beta family, nucleotide-binding domain	NA	Non-apoplastic
Solyc00g500203.1.1	-2.0403340766288	23.4377381853871	P-loop containing nucleoside triphosphate hydrolases, ATP synthase alpha and beta subunits signature., C-terminal domain of alpha and beta subunits of F1 ATP synthase, N-terminal domain of alpha and beta subunits of F1 ATP synthase, ATP-synt_F1_alpha_N, -, -, F1_ATPase_alpha, ATP synthase subunit alpha [atpA]., F_ATPase_subunit_alpha, atpA: ATP synthase F1, alpha subunit, ATP synthase alpha/beta family, beta-barrel domain, -, ATP-synt_F1_alpha_C, ATP synthase alpha/beta chain, C terminal domain, ATP synthase alpha/beta family, nucleotide-binding domain	NA	Non-apoplastic
Solyc00g500292.1.1	-2.0403340766288	23.4377381853871	P-loop containing nucleoside triphosphate hydrolases, ATP synthase alpha and beta subunits signature., C-terminal domain of alpha and beta subunits of F1 ATP synthase, N-terminal domain of alpha and beta subunits of F1 ATP synthase, ATP-synt_F1_alpha_N, -, -, F1_ATPase_alpha, ATP synthase subunit alpha [atpA]., F_ATPase_subunit_alpha, atpA: ATP synthase F1, alpha subunit, ATP synthase alpha/beta family, beta-barrel domain, -, ATP-synt_F1_alpha_C, ATP synthase alpha/beta chain, C terminal domain, ATP synthase alpha/beta family, nucleotide-binding domain	NA	Non-apoplastic
Solyc00g500323.1.1	-2.0403340766288	23.4377381853871	P-loop containing nucleoside triphosphate hydrolases, ATP synthase alpha and beta subunits signature., C-terminal domain of alpha and beta subunits of F1 ATP synthase, N-terminal domain of alpha and beta subunits of F1 ATP synthase, ATP-synt_F1_alpha_N, -, -, F1_ATPase_alpha, ATP synthase subunit alpha [atpA]., F_ATPase_subunit_alpha, atpA: ATP synthase F1, alpha subunit, ATP synthase alpha/beta family, beta-barrel domain, -, ATP-synt_F1_alpha_C, ATP synthase alpha/beta chain, C terminal domain, ATP synthase alpha/beta family, nucleotide-binding domain	NA	Non-apoplastic
Solyc00g500332.1.1	-2.0403340766288	23.4377381853871	P-loop containing nucleoside triphosphate hydrolases, ATP synthase alpha and beta subunits signature., C-terminal domain of alpha and beta subunits of F1 ATP synthase, N-terminal domain of alpha and beta subunits of F1 ATP synthase, ATP-synt_F1_alpha_N, -, -, F1_ATPase_alpha, ATP synthase subunit alpha [atpA]., F_ATPase_subunit_alpha, atpA: ATP synthase F1, alpha subunit, ATP synthase alpha/beta family, beta-barrel domain, -, ATP-synt_F1_alpha_C, ATP synthase alpha/beta chain, C terminal domain, ATP synthase alpha/beta family, nucleotide-binding domain	NA	Non-apoplastic
Solyc01g008610.4.1	2.3437828098705	22.102899309466	Glycosyl hydrolases family 17 signature., Glycosyl hydrolases family 17, Glycosidases, (Trans)glycosidases	NA	Apoplastic
Solyc01g079160.4.1	-12.1925113829679	17.246288714031	SGNH_plant_lipase_like, GDSL-like Lipase/Acylhydrolase, SGNH hydrolase, Coil, SGNH hydrolase	NA	Non-apoplastic

Solyc01g080560.1.1	20.5265659366542	10.2632829683271	Nucleoside hydrolase, Inosine-uridine preferring nucleoside hydrolase	NA	Apoplastic
Solyc01g080570.4.1	20.5265659366542	10.2632829683271	Nucleoside hydrolase, -, -, Nucleoside hydrolase, Inosine-uridine preferring nucleoside hydrolase, Inosine-uridine preferring nucleoside hydrolase	NA	Non-apoplastic
Solyc01g087850.2.1	20.2307815372516	10.1153907686258	Peptidases_S8_3, -, Serine proteases, subtilase family, serine active site., Serine proteases, subtilase domain profile., Peptidase S8/S53 domain, PA_subtilisin_like, Subtilisin serine protease family (S8) signature, Subtilisin serine protease family (S8) signature, Subtilisin serine protease family (S8) signature, Peptidase inhibitor I9, consensus disorder prediction, SignalP-noTM, -, Subtilase family, Subtilisin-like, Fibronectin type-III domain, Peptidase S8 propeptide/proteinase inhibitor I9	NA	Apoplastic
Solyc01g088560.3.1	13.9732830099215	15.202735491887	ran_sub_2, small_GTP: small GTP-binding protein domain, small GTPase Ras family profile., small GTPase Rho family profile., rho_sub_3, Rab6, rab_sub_5, Transforming protein P21 ras signature, Transforming protein P21 ras signature, Transforming protein P21 ras signature, Transforming protein P21 ras signature, Transforming protein P21 ras signature, Ras family, P-loop containing nucleoside triphosphate hydrolases, ras_sub_4, -, small GTPase Rab1 family profile.	NA	Non-apoplastic
Solyc01g090190.3.1	-19.7003694053087	9.85018470265437	-, HABP4_PAI_RBP1_2, consensus disorder prediction, Hyaluronan / mRNA binding family, Coil, consensus disorder prediction, Stm1, consensus disorder prediction, consensus disorder prediction	NA	Non-apoplastic
Solyc01g091660.3.1	-11.1445092060156	22.1403456092552	Enoyl-(Acyl carrier protein) reductase, NAD(P)-binding Rossmann-fold domains, Glucose/ribitol dehydrogenase family signature, Glucose/ribitol dehydrogenase family signature, Glucose/ribitol dehydrogenase family signature, Glucose/ribitol dehydrogenase family signature, Glucose/ribitol dehydrogenase family signature, Glucose/ribitol dehydrogenase family signature, -, Short-chain dehydrogenase/reductase (SDR) superfamily signature, Short-chain dehydrogenase/reductase (SDR) superfamily signature, Short-chain dehydrogenase/reductase (SDR) superfamily signature	NA	Non-apoplastic
Solyc01g097810.3.1	-19.9353758298847	9.96768791494235	Flavin containing amine oxidoreductase, Adrenodoxin reductase family signature, Adrenodoxin reductase family signature, FAD/NAD(P)-binding domain, -, zeta_caro_desat: 9,9'-di-cis-zeta-carotene desaturase	NA	Non-apoplastic
Solyc01g098640.3.1	-16.9157001205299	17.5848305712101	TPM domain, consensus disorder prediction, consensus disorder prediction, -	NA	Non-apoplastic
Solyc01g099110.4.1	-1.25527913296382	24.6274548961095	Metallopeptidase family M24, C-terminal region of peptidase_M24, Creatinase/methionine aminopeptidase superfamily, Creatinase/Prolidase N-terminal domain, APP, -, -, Creatinase/Prolidase N-terminal domain, Creatinase/prolidase N-terminal domain, Creatinase/aminopeptidase	NA	Non-apoplastic
Solyc01g100050.3.1	16.3010989271892	8.15054946359462	WD domain, G-beta repeat, WD domain, G-beta repeat, Trp-Asp (WD) repeats circular profile., Trp-Asp (WD) repeats profile., Quinoprotein alcohol dehydrogenase-like, Trp-Asp (WD) repeats signature., Trp-Asp (WD) repeats profile., ctlh, Trp-Asp (WD) repeats profile., consensus disorder prediction, -, -, -, -, -, consensus disorder prediction, WD40 repeat-like, Trp-Asp (WD) repeats profile., consensus disorder prediction, C-terminal to LisH (CTLH) motif profile., WD40_4, WD40_4, WD40_4, WD40_4, WD40_4, WD40_4, WD40_4, WD40_4, WD40_4, WD40_4, WD40_4, WD40_4, WD40_4, Lish, LIS1 homology (LisH) motif profile., consensus disorder prediction	NA	Non-apoplastic
Solyc01g101060.4.1	15.3310007105646	18.1429680836388	-, S-adenosylmethionine synthetase, central domain, S-adenosylmethionine synthase [metK]., metK: methionine adenosyltransferase, MAT, -, S-adenosylmethionine synthetase, C-terminal domain, S-adenosylmethionine synthetase, S-adenosylmethionine synthetase, N-terminal domain, S-adenosylmethionine synthetase, S-AdoMet_synt, S-adenosylmethionine synthase signature 2., S-adenosylmethionine synthetase, S-adenosylmethionine synthase signature 1., -	NA	Non-apoplastic
Solyc01g104880.3.1	-19.6890109755752	9.84450548778762	EF-hand, consensus disorder prediction, EF-hand calcium-binding domain., PS_decarb: phosphatidylserine decarboxylase, C2 domain, EF-hand calcium-binding domain profile., C2, -, EF-hand calcium-binding domain., consensus disorder prediction, C2 domain (Calcium/lipid-binding domain, CaLB), EFh, Phosphatidylserine decarboxylase proenzyme [psd]., Phosphatidylserine decarboxylase, EF-hand calcium-binding domain profile., EF-hand domain pair, C2 domain, efh_1, efh_1, C2 domain profile.	NA	Non-apoplastic

Solyc01g105070.3.1	2.93540203232575	28.5944862760863	Haem peroxidase superfamily signature, Haem peroxidase superfamily signature, Haem peroxidase superfamily signature, Haem peroxidase superfamily signature, Haem peroxidase superfamily signature, Peroxidase, domain 2, Plant peroxidase signature, Plant peroxidase signature, Plant peroxidase signature, Plant peroxidase signature, Plant peroxidase signature, Plant peroxidase signature, Plant peroxidase signature, Plant peroxidase signature, Peroxidases active site signature., Plant heme peroxidase family profile., secretory_peroxidase, Peroxidase, -, Peroxidases proximal heme-ligand signature., Heme-dependent peroxidases	NA	Apoplastic
Solyc01g105070.3.1	3.5189704034664	28.7286017731751	Haem peroxidase superfamily signature, Haem peroxidase superfamily signature, Haem peroxidase superfamily signature, Haem peroxidase superfamily signature, Haem peroxidase superfamily signature, Peroxidase, domain 2, Plant peroxidase signature, Plant peroxidase signature, Plant peroxidase signature, Plant peroxidase signature, Plant peroxidase signature, Plant peroxidase signature, Plant peroxidase signature, Plant peroxidase signature, Peroxidases active site signature., Plant heme peroxidase family profile., secretory_peroxidase, Peroxidase, -, Peroxidases proximal heme-ligand signature., Heme-dependent peroxidases	NA	Apoplastic
Solyc01g109140.3.1	22.2467992087368	11.3693486585197	Cytochrome P450, E-class P450 group IV signature, E-class P450 group IV signature, E-class P450 group IV signature, Cytochrome P450, Cytochrome P450	NA	Non-apoplastic
Solyc01g109300.3.1	-1.38789869400663	25.7851700510219	ispH_lytB: 4-hydroxy-3-methylbut-2-enyl diphosphate reductase, LytB protein, 4-hydroxy-3-methylbut-2-enyl diphosphate reductase [ispH]., -, -, lytB_ispH	NA	Non-apoplastic
Solyc01g109790.3.1	-20.1412309405767	10.0706154702884	ADP-glucose pyrophosphorylase signature 3., ADP-glucose pyrophosphorylase signature 1., Spore Coat Polysaccharide Biosynthesis Protein SpsA; Chain A, ADP-glucose pyrophosphorylase signature 2., ADP_Glucose_PP, Nucleotidyl transferase, Trimeric LpxA-like enzymes, Hexapeptide repeat proteins, glgC: glucose-1-phosphate adenylyltransferase, LbH_G1P_AT_C, Nucleotide-diphospho-sugar transferases	NA	Non-apoplastic
Solyc01g111940.4.1	-19.7548831773042	9.87744158865208	consensus disorder prediction, consensus disorder prediction, Coiled-coil domain-containing protein 124 /Oxs1, Coil, Coil, consensus disorder prediction	NA	Non-apoplastic
Solyc02g014830.4.1	16.4771663374666	17.8234796159131	-, Serine carboxypeptidases, serine active site., -, Carboxypeptidase C serine protease (S10) family signature, Carboxypeptidase C serine protease (S10) family signature, Carboxypeptidase C serine protease (S10) family signature, Carboxypeptidase C serine protease (S10) family signature, alpha/beta hydrolase, Serine carboxypeptidase, Serine carboxypeptidases, histidine active site., alpha/beta-Hydrolases	yes	Apoplastic
Solyc02g061770.4.1	1.72221038591833	26.3889343069133	Chitinase class I, Lysozyme-like, -, chitinase_GH19, Chitinases family 19 signature 2., Endochitinase, domain 2, Chitinases family 19 signature 1., Endochitinase	NA	Apoplastic
Solyc02g062300.3.1	19.9878194172648	10.7434285789184	BURP domain, BURP_2, SignalP-noTM, BURP domain profile.	NA	Non-apoplastic
Solyc02g064970.4.1	3.5189704034664	28.7286017731751	consensus disorder prediction, Peroxidase, domain 2, Haem peroxidase superfamily signature, Haem peroxidase superfamily signature, Haem peroxidase superfamily signature, Haem peroxidase superfamily signature, Haem peroxidase superfamily signature, -, Heme-dependent peroxidases, Peroxidases proximal heme-ligand signature., Peroxidases active site signature., secretory_peroxidase, Peroxidase, Plant heme peroxidase family profile., consensus disorder prediction, Plant peroxidase signature, Plant peroxidase signature, Plant peroxidase signature, Plant peroxidase signature, Plant peroxidase signature, Plant peroxidase signature, Plant peroxidase signature, Plant peroxidase signature	NA	Non-apoplastic
Solyc02g070110.1.1	20.4327893361925	10.2163946680963	FAD binding domain, SignalP-noTM, SignalP-TM, -, PCMH-type FAD-binding domain profile., Berberine and berberine like, FAD-binding/transporter-associated domain-like, SignalP-noTM, -, -	NA	Non-apoplastic
Solyc02g070110.1.1	21.7237904253313	10.8618952126656	FAD binding domain, SignalP-noTM, SignalP-TM, -, PCMH-type FAD-binding domain profile., Berberine and berberine like, FAD-binding/transporter-associated domain-like, SignalP-noTM, -, -	NA	Non-apoplastic
Solyc02g070130.1.1	20.4327893361925	10.2163946680963	-, -, FAD binding domain, -, SignalP-noTM, PCMH-type FAD-binding domain profile., Berberine and berberine like, SignalP-noTM, FAD-binding/transporter-associated domain-like, SignalP-TM	NA	Non-apoplastic

Solyc02g070180.3.1	21.7237904253313	10.8618952126656	-, FAD-binding/transporter-associated domain-like, Berberine and berberine like, -, FAD binding domain, -, PCMH-type FAD-binding domain profile.	NA	Apoplastic
Solyc02g086680.4.1	-18.6286273837167	9.31431369185837	Coil, Peptide deformylase [def]., Polypeptide deformylase, Peptide deformylase, Peptide deformylase, Peptide deformylase signature, Peptide deformylase signature, Peptide deformylase signature, Peptide deformylase signature, Pep_deformylase, pept_deformyl: peptide deformylase	NA	Non-apoplastic
Solyc02g086880.4.1	1.57383372136003	22.8608540131448	-, D-isomer specific 2-hydroxyacid dehydrogenases signature 3., -, Formate/glycerate dehydrogenase catalytic domain-like, NAD(P)-binding Rossmann-fold domains, D-isomer specific 2-hydroxyacid dehydrogenase, NAD binding domain, D-isomer specific 2-hydroxyacid dehydrogenases signature 2., FDH, D-isomer specific 2-hydroxyacid dehydrogenase, catalytic domain, Formate dehydrogenase, mitochondrial., D-isomer specific 2-hydroxyacid dehydrogenases NAD-binding signature.	NA	Non-apoplastic
Solyc02g087070.4.1	18.2121990800906	11.6351212749945	Animal haem peroxidase signature, Animal haem peroxidase signature, Animal haem peroxidase signature, Animal heme peroxidase superfamily profile., Coil, Haem peroxidase domain superfamily, animal type, Animal haem peroxidase, Heme-dependent peroxidases	NA	Non-apoplastic
Solyc02g087070.4.1	21.3289203701795	10.6644601850898	Animal haem peroxidase signature, Animal haem peroxidase signature, Animal haem peroxidase signature, Animal heme peroxidase superfamily profile., Coil, Haem peroxidase domain superfamily, animal type, Animal haem peroxidase, Heme-dependent peroxidases	NA	Non-apoplastic
Solyc02g087090.4.1	21.3289203701795	10.6644601850898	Coil, Animal haem peroxidase, Heme-dependent peroxidases, Animal heme peroxidase superfamily profile., Haem peroxidase domain superfamily, animal type	NA	Non-apoplastic
Solyc02g087300.1.1	21.0797891320188	10.5398945660094	Trp-Asp (WD) repeats profile., WD40_4, WD40_4, WD40_4, WD40_4, WD40_4, WD40_4, Trp-Asp (WD) repeats profile., WD domain, G-beta repeat, WD domain, G-beta repeat, WD domain, G-beta repeat, WD domain, G-beta repeat, WD domain, G-beta repeat, WD domain, G-beta repeat, Trp-Asp (WD) repeats circular profile., Trp-Asp (WD) repeats profile., WD40 repeat-like, -, G protein beta WD-40 repeat signature, G protein beta WD-40 repeat signature, G protein beta WD-40 repeat signature	NA	Apoplastic
Solyc02g090490.3.1	14.4736751771737	18.8769332494526	SignalP-TM, SignalP-TM, Patatin-like phospholipase, Patatin-like phospholipase, Cytosolic phospholipase A2 catalytic domain, Cytosolic phospholipase A2 catalytic domain, Patatin-like phospholipase (PNPLA) domain profile., Patatin-like phospholipase (PNPLA) domain profile., SignalP-noTM, SignalP-noTM, Pat17_isozyme_like, Pat17_isozyme_like, FabD/lysophospholipase-like, FabD/lysophospholipase-like	yes	Apoplastic
Solyc02g091920.3.1	18.9486131617179	16.7219463383241	Concanavalin A-like lectins/glucanases, GH16_XET, EndGlu_transf, Glycosyl hydrolases family 16 (GH16) domain profile., Glycosyl hydrolases family 16, -, Xyloglucan endo-transglycosylase (XET) C-terminus, Glycosyl hydrolases family 16 active sites.	NA	Non-apoplastic
Solyc03g025720.3.1	10.1573742154322	19.6586510554562	Putative AMP-binding domain signature., FACL_fum10p_like, Acetyl-CoA synthetase-like, -, AMP-binding enzyme C-terminal domain, AMP-binding enzyme, -	NA	Non-apoplastic
Solyc03g044160.3.1	17.6162717658975	17.8329249150535	Transferase(Phosphotransferase) domain 1, STKc_IRAK, SignalP-noTM, Protein tyrosine and serine/threonine kinase, Protein kinases ATP-binding region signature., Protein kinase domain profile., SignalP-TM, Phosphorylase Kinase; domain 1, Malectin-like domain, -, -, Protein kinase-like (PK-like), serkin_6	NA	Non-apoplastic
Solyc03g082600.4.1	19.6686059306813	15.4770005527712	Cytochrome b5 family, heme-binding domain signature., Cytochrome b5 family, heme-binding domain profile., Cytochrome b5-like heme/steroid binding domain, Cyt_b5_2, Cytochrome b5-like Heme/Steroid binding domain, -, Cytochrome B5 signature, Cytochrome B5 signature, Cytochrome B5 signature, Cytochrome B5 signature	NA	Non-apoplastic
Solyc03g096360.4.1	-3.41916359515569	24.3243202720782	50S ribosomal protein L35Ae [rpl35ae]., Ribosomal protein L35Ae signature., translation elongation factor selb, chain A, domain 4, Translation proteins, Ribosomal protein L35Ae	NA	Non-apoplastic
Solyc03g097470.3.1	-18.5310799467499	9.26553997337495	3-oxoacyl-[acyl-carrier-protein] synthase 3 [fabH]., -, 3-Oxoacyl-[acyl-carrier-protein (ACP)] synthase III, fabH: 3-oxoacyl-[acyl-carrier-protein] synthase III, Thiolase-like, 3-Oxoacyl-[acyl-carrier-protein (ACP)] synthase III C terminal, KAS_III	NA	Apoplastic
Solyc03g098670.1.1	15.6452957660833	17.8500996559073	Soybean trypsin inhibitor (Kunitz-type) signature, Soybean trypsin inhibitor (Kunitz-type) signature, Soybean trypsin inhibitor (Kunitz-type) signature, STI, -, SignalP-TM, Trypsin and protease inhibitor, SignalP-noTM, STI-like, SignalP-noTM, kul_2	NA	Non-apoplastic

Solyc03g098740.1.1	4.1050859911362	23.4970705499001	STI, -, STI-like, Soybean trypsin inhibitor (Kunitz-type) signature, Soybean trypsin inhibitor (Kunitz-type) signature, Trypsin and protease inhibitor, kul_2, SignalP-noTM	NA	Apoplastic
Solyc03g117950.3.1	19.3587018715181	18.2236115100431	Chaperonins clpA/B signature 2., consensus disorder prediction, C-terminal, D2-small domain, of ClpB protein, ATP-dependent Clp protease ATP-binding subunit signature, ATP-dependent Clp protease ATP-binding subunit signature, ATP-dependent Clp protease ATP-binding subunit signature, ATP-dependent Clp protease ATP-binding subunit signature, Double Clp-N motif, -, Clp amino terminal domain, pathogenicity island component, Clp amino terminal domain, pathogenicity island component, ClpB_D2_small_2, AAA, -, AAA_5, AAA_5, AAA lid domain, Chaperonins clpA/B signature 1., Clp repeat (R) domain profile., -, -, -, P-loop containing nucleoside triphosphate hydrolases, AAA, AAA domain (Cdc48 subfamily), consensus disorder prediction, P-loop containing nucleoside triphosphate hydrolases, ATPase family associated with various cellular activities (AAA)	NA	Non-apoplastic
Solyc03g118340.3.1	20.6935717252991	10.3467858626496	Double Clp-N motif, AAA_5, AAA_5, C-terminal, D2-small domain, of ClpB protein, AAA domain (Cdc48 subfamily), -, Coil, AAA, -, Chaperonins clpA/B signature 1., AAA lid domain, P-loop containing nucleoside triphosphate hydrolases, UVR domain profile., Coil, ATPase family associated with various cellular activities (AAA), ATP-dependent Clp protease ATP-binding subunit signature, ATP-dependent Clp protease ATP-binding subunit signature, ATP-dependent Clp protease ATP-binding subunit signature, ATP-dependent Clp protease ATP-binding subunit signature, ClpB_D2_small_2, -, Chaperonins clpA/B signature 2., Clp repeat (R) domain profile., -, P-loop containing nucleoside triphosphate hydrolases, AAA, Clp amino terminal domain, pathogenicity island component, Clp amino terminal domain, pathogenicity island component, -, UVR domain	NA	Non-apoplastic
Solyc04g025530.3.1	20.2517829233174	10.0207592928932	Glu-decarb-GAD: glutamate decarboxylase, -, -, -, Pyridoxal-dependent decarboxylase conserved domain, PLP-dependent transferases	NA	Non-apoplastic
Solyc04g054980.3.1	19.6164356524345	9.80821782621723	PLAT domain profile., Lipase/lipooxygenase domain (PLAT/LH2 domain), PLAT/LH2 domain, PLAT_plant_stress, SignalP-noTM, PLAT/LH2 domain	NA	Non-apoplastic
Solyc04g064870.3.1	23.7342344701837	11.803065770491	-, NTF2-like	NA	Non-apoplastic
Solyc04g071900.4.1	9.40854627308565	19.2487063608477	Peroxidases proximal heme-ligand signature., Peroxidases active site signature., Peroxidase, domain 2, -, Plant peroxidase signature, Plant peroxidase signature, Plant peroxidase signature, Plant peroxidase signature, Plant peroxidase signature, Plant peroxidase signature, Plant peroxidase signature, Plant peroxidase signature, Plant peroxidase signature, Plant heme peroxidase family profile., Heme-dependent peroxidases, Haem peroxidase superfamily signature, Haem peroxidase superfamily signature, Haem peroxidase superfamily signature, Haem peroxidase superfamily signature, Haem peroxidase superfamily signature, secretory_peroxidase, Peroxidase	NA	Non-apoplastic
Solyc04g072000.4.1	1.27022798782091	22.5968160682622	Lysozyme-like, Chitinase class I, Chitinases family 19 signature 1., -, chitinase_GH19, Endochitinase, Chitin recognition or binding domain signature., Chitin-binding type-1 domain profile., ChitinBD_3, -, Chitinases family 19 signature 2., ChtBD1, Chitin recognition protein, Plant lectins/antimicrobial peptides, Endochitinase, domain 2	NA	Apoplastic
Solyc04g074480.3.1	11.4161389265078	19.9737514609606	DAHP_synth_II: 3-deoxy-7-phosphoheptulonate synthase, Aldolase class I, Class-II DAHP synthetase family, Aldolase, consensus disorder prediction	NA	Non-apoplastic
Solyc04g077270.4.1	18.2864300920911	9.14321504604557	SignalP-noTM, Protein tyrosine and serine/threonine kinase, Phosphorylase Kinase; domain 1, serkin_6, STKc_IRAK, S-locus glycoprotein domain, PAN-like domain, Bulb-type lectin domain profile., Protein kinase domain profile., ntp_6, Protein kinase-like (PK-like), D-mannose binding lectin, Domain of unknown function (DUF3403), consensus disorder prediction, -, B_lectin, Hepatocyte Growth Factor, consensus disorder prediction, blect_4, PAN/Apple domain profile., Transferase(Phosphotransferase) domain 1, alpha-D-mannose-specific plant lectins, SRK, Serine/Threonine protein kinases active-site signature., PAN_AP_plant	NA	Non-apoplastic

Solyc04g077280.3.1	18.2864300920911	9.14321504604557	blect_4, Phosphorylase Kinase; domain 1, SignalP-noTM, Hepatocyte Growth Factor, PAN_AP_plant, Protein tyrosine and serine/threonine kinase, PAN-like domain, Serine/Threonine protein kinases active-site signature., Bulb-type lectin domain profile., Protein kinase-like (PK-like), alpha-D-mannose-specific plant lectins, S-locus glycoprotein domain, D-mannose binding lectin, -, STKc_IRAK, Transferase(Phosphotransferase) domain 1, B_lectin, SRK, serkin_6, Protein kinase domain profile., ntp_6, PAN/Apple domain profile.	NA	Non-apoplastic
Solyc04g077310.3.1	18.2864300920911	9.14321504604557	Protein kinase-like (PK-like), S-locus glycoprotein domain, D-mannose binding lectin, Serine/Threonine protein kinases active-site signature., Transferase(Phosphotransferase) domain 1, serkin_6, alpha-D-mannose-specific plant lectins, Protein tyrosine and serine/threonine kinase, Bulb-type lectin domain profile., blect_4, B_lectin, -, Protein kinase domain profile.	NA	Non-apoplastic
Solyc04g078660.2.1	11.870543932088	17.118323883705	Transferase family, -, -	NA	Non-apoplastic
Solyc05g049980.3.1	18.7906049386207	17.6909230934703	Glycosyl hydrolases family 28, -, Pectin lyase-like	NA	Non-apoplastic
Solyc05g052100.3.1	25.503706913525	12.7518534567625	-, Glutamate/Leucine/Phenylalanine/Valine dehydrogenase, NAD(P)-binding Rossmann-fold domains, Glu_DH, Glutamate/leucine/phenylalanine/valine dehydrogenase signature, Glutamate/leucine/phenylalanine/valine dehydrogenase signature, Glutamate/leucine/phenylalanine/valine dehydrogenase signature, Glutamate/leucine/phenylalanine/valine dehydrogenase signature, Leucine Dehydrogenase, chain A, domain 1, NAD_bind_1_Glu_DH, ELFV_dehydrog_3, Aminoacid dehydrogenase-like, N-terminal domain, Glu/Leu/Phe/Val dehydrogenase, dimerisation domain	NA	Non-apoplastic
Solyc05g054380.2.1	3.32867373745202	22.485686775088	Pathogenesis-related protein Bet v 1 family, Major pollen allergen Bet V1 signature, Major pollen allergen Bet V1 signature, Major pollen allergen Bet V1 signature, Major pollen allergen Bet V1 signature, Major pollen allergen Bet V1 signature, Major pollen allergen Bet V1 signature, -, Bet v1-like, Bet_v1-like	NA	Non-apoplastic
Solyc05g054600.3.1	-20.0721229498818	10.0360614749409	MetRS_core, metG: methionine--tRNA ligase, Anticodon_Ia_Met, Methionyl-tRNA synthetase signature, Methionyl-tRNA synthetase signature, Methionyl-tRNA synthetase signature, Methionyl-tRNA synthetase signature, Methionyl-tRNA synthetase signature, Methionyl-tRNA synthetase signature, Nucleotidylyl transferase, tRNA synthetases class I (M), consensus disorder prediction, HUPs, -, tRNA synthetases class I (I, L, M and V), Anticodon-binding domain of a subclass of class I aminoacyl-tRNA synthetases, -, Methionine--tRNA ligase [metG].	NA	Non-apoplastic
Solyc05g056170.3.1	15.5043332003414	14.8391163385947	L-aspartase-like, PAL-HAL, Aromatic amino acid lyase, -, Phenylalanine and histidine ammonia-lyases signature., phe_am_lyase: phenylalanine ammonia-lyase, Fumarase/aspartase (Central domain), -	NA	Non-apoplastic
Solyc05g056580.3.1	23.5851944732967	11.7925972366483	consensus disorder prediction, consensus disorder prediction, consensus disorder prediction, Vaccinia Virus protein VP39, consensus disorder prediction, S-adenosyl-L-methionine-dependent methyltransferases, consensus disorder prediction, S-adenosyl-L-methionine-dependent methyltransferases, consensus disorder prediction, consensus disorder prediction, Coil, AdoMet_MTases, Putative S-adenosyl-L-methionine-dependent methyltransferase, Vaccinia Virus protein VP39	NA	Non-apoplastic
Solyc06g007670.4.1	-21.2011229725061	10.600561486253	Coil, Ribosomal large subunit proteins 60S L5, and 50S L18, -, Ribosomal_L18_L5e, Ribosomal L18 C-terminal region, Translational machinery components, 50S ribosomal protein L18 [rplR]., consensus disorder prediction, Ribosomal protein L5 signature, Ribosomal protein L5 signature, Ribosomal protein L5 signature, Ribosomal protein L5 signature, Ribosomal protein L5 signature, Ribosomal protein L5 signature	NA	Non-apoplastic
Solyc06g035960.3.1	22.4080599496341	11.0938381840602	FACL_fum10p_like, AMP-binding enzyme C-terminal domain, -, -, Putative AMP-binding domain signature., Acetyl-CoA synthetase-like, AMP-binding enzyme	NA	Non-apoplastic
Solyc06g059930.4.1	-1.03122118670936	25.8351758546761	-, Terpene synthase family, metal binding domain, Farnesyl Diphosphate Synthase, Terpene_cyclase_plant_C1, Terpene synthase, N-terminal domain, Terpenoid synthases, Terpenoid cyclases/Protein prenyltransferases	NA	Non-apoplastic
Solyc06g063240.3.1	19.8078375381635	9.90391876908174	O-FucT_plant, GDP-fucose protein O-fucosyltransferase, UCP009360, UCP009360	NA	Non-apoplastic

Solyc06g065270.4.1	9.46370478961257	18.0014087633479	ADK, Adenylate kinase, -, Adenylate kinase signature., Adenylate kinase [adk]., P-loop containing nucleoside triphosphate hydrolases, Adenylate kinase signature, Adenylate kinase signature, Adenylate kinase signature, Adenylate kinase signature, adk: adenylate kinase	NA	Non-apoplastic
Solyc06g068950.4.1	-3.37983036536672	25.7569931145168	Coil, AdoMet_MTases, Methyltransferase domain, Vaccinia Virus protein VP39, S-adenosyl-L-methionine-dependent methyltransferases, Vaccinia Virus protein VP39	NA	Non-apoplastic
Solyc06g071000.3.1	-3.69818758146068	22.6649716679221	Aldehyde dehydrogenase family, Aldehyde Dehydrogenase; Chain A, domain 2, Aldehyde Dehydrogenase; Chain A, domain 1, ALDH-like	NA	Non-apoplastic
Solyc07g008340.4.1	20.3100714532278	10.1550357266139	4Fe-4S ferredoxin-type iron-sulfur binding region signature., P-loop containing nucleoside triphosphate hydrolases, 4Fe-4S ferredoxin-type iron-sulfur binding domain profile., AAA_5, AAA_5, 4Fe-4S ferredoxins, Possible Fer4-like domain in RNase L inhibitor, RLI, ABC transporter family E signature, ABC transporter family E signature, ABC transporter family E signature, ABC transporter family E signature, ABC transporter family E signature, ATP-binding cassette, ABC transporter-type domain profile., ABC transporter, ABC transporter, -, ABC transporters family signature., ABC transporters family signature., -, ATP-binding cassette, ABC transporter-type domain profile., ABC_RNaseL_inhibitor_domain1, P-loop containing nucleoside triphosphate hydrolases, 4Fe-4S binding domain	NA	Non-apoplastic
Solyc07g008560.3.1	19.4362392037378	9.71811960186889	Purple acid phosphatase, N-terminal domain, Calcineurin-like phosphoesterase, Iron/zinc purple acid phosphatase-like protein C, Purple acid Phosphatase, N-terminal domain, -, Fn3-like domain from Purple Acid Phosphatase, Metallo-dependent phosphatases, MPP_PAPs, -, SignalP-noTM	NA	Apoplastic
Solyc07g014730.3.1	-1.56350901603852	27.2122175806751	Phospholipase A2 domain, SignalP-noTM, Phospholipase A2 histidine active site., SignalP-TM, Phospholipase A2, PLA2, PLA2_plant	NA	Apoplastic
Solyc07g019670.4.1	19.8329447160979	9.91647235804894	-, -, NAD(P)-binding Rossmann-fold domains, 6-phosphogluconate dehydrogenase C-terminal domain-like, 3-hydroxyacyl-CoA dehydrogenase, C-terminal domain, Enoyl-CoA hydratase/isomerase, ClpP/crotonase, 6-phosphogluconate dehydrogenase C-terminal domain-like, crotonase-like, 3-hydroxyacyl-CoA dehydrogenase, NAD binding domain, Enoyl-CoA hydratase/isomerase signature., -, 3-hydroxyacyl-CoA dehydrogenase signature.	NA	Non-apoplastic
Solyc07g040890.1.1	24.5813981998234	12.2906990999117	alpha/beta hydrolase fold, alpha/beta-Hydrolases, alpha/beta hydrolase	NA	Non-apoplastic
Solyc07g042550.3.1	1.36112281885072	23.5075909956934	Glycosyl transferases group 1, -, Coil, -, Glycogen Phosphorylase B;, Sucrose synthase, Glycogen Phosphorylase B;, UDP-Glycosyltransferase/glycogen phosphorylase, sucr_synth: sucrose synthase	NA	Non-apoplastic
Solyc07g043310.3.1	11.8704951540126	18.4888975900284	PLP-dependent transferases, -, Aminotransferase class-III, Coil, OAT_like, Aminotransferases class-III pyridoxal-phosphate attachment site., Aspartate Aminotransferase, domain 1	NA	Non-apoplastic
Solyc07g043500.1.1	-1.28610271035743	25.2771032350346	GT1_Gtf-like, UDP-glycosyltransferases signature., Glycogen Phosphorylase B;, UDP-glucoronosyl and UDP-glucosyl transferase, Glycogen Phosphorylase B;, Coil, UDP-Glycosyltransferase/glycogen phosphorylase	NA	Non-apoplastic
Solyc07g052980.3.1	-1.952769498599	25.8042875552069	Glycosyl hydrolase family 16 signature, Glycosyl hydrolase family 16 signature, Glycosyl hydrolase family 16 signature, Glycosyl hydrolases family 16, Concanavalin A-like lectins/glucanases, GH16_XET, -, Glycosyl hydrolases family 16 (GH16) domain profile., Xyloglucan endo-transglycosylase (XET) C-terminus, SignalP-noTM, EndGlu_transf	NA	Non-apoplastic
Solyc07g055690.1.1	27.5319351127034	13.7659675563517	D-mannose binding lectin, blect_4, alpha-D-mannose-specific plant lectins, Bulb-type lectin domain profile., SignalP-noTM, B_lectin, -, S-locus glycoprotein domain	NA	Apoplastic
Solyc07g062610.4.1	-1.3189134218041	25.0643331026891	not_thiJ: DJ-1 family protein, not_thiJ: DJ-1 family protein, GATase1_DJ-1, -, -, GATase1_DJ-1, DJ-1/Pfpl family, DJ-1/Pfpl family, Class I glutamine amidotransferase-like, Class I glutamine amidotransferase-like	NA	Non-apoplastic

Solyc07g063820.3.1	-19.315867895393	9.6579339476965	SRK, blect_4, Transferase(Phosphotransferase) domain 1, Hepatocyte Growth Factor, PAN/Apple domain profile., Protein kinase-like (PK-like), Serine/Threonine protein kinases active-site signature., ntp_6, Bulb-type lectin domain profile., S-locus glycoprotein domain, Domain of unknown function (DUF3403), PAN_AP_plant, PAN-like domain, serkin_6, Protein tyrosine and serine/threonine kinase, SignalP-noTM, Protein kinases ATP-binding region signature., alpha-D-mannose-specific plant lectins, B_lectin, -, Protein kinase domain profile., consensus disorder prediction, STKc_IRAK, Phosphorylase Kinase; domain 1, D-mannose binding lectin	NA	Non-apoplastic
Solyc07g064160.3.1	-20.2043493757646	10.1021746878823	-, TIGR00292: thiazole biosynthesis enzyme, FAD/NAD(P)-binding domain, Thiamine thiazole synthase, chloroplastic [THI4]., Thi4 family, Adrenodoxin reductase family signature, Adrenodoxin reductase family signature, Adrenodoxin reductase family signature, -	NA	Non-apoplastic
Solyc07g066470.3.1	-1.32067024944764	26.4788746102406	PBGD, -, Porphobilinogen deaminase (hydroxymethylbilane synthase), C-terminal domain, PBP2_PBGD_1, Porphobilinogen deaminase, dipyromethane cofactor binding domain, Porphobilinogen deaminase, C-terminal domain, Porphobilinogen deaminase cofactor-binding site., hemC: hydroxymethylbilane synthase, Periplasmic binding protein-like II, Porphobilinogen deaminase [hemC]., -, -, Porphobilinogen deaminase signature, Porphobilinogen deaminase signature, Porphobilinogen deaminase signature, Porphobilinogen deaminase signature, Porphobilinogen deaminase signature	NA	Non-apoplastic
Solyc07g066610.3.1	1.1186572584775	28.3482185630286	Phosphoglycerate kinase signature., Pgk, Phosphoglycerate kinase [pgk]., -, -, -, SignalP-TM, Phosphoglycerate kinase, Phosphoglycerate kinase family signature, Phosphoglycerate kinase family signature, Phosphoglycerate kinase family signature, Phosphoglycerate kinase family signature, Phosphoglycerate kinase family signature, Phosphoglycerate kinase family signature, Phosphoglycerate kinase family signature, Phosphoglycerate kinase family signature, Phosphoglycerate kinase, Phosphoglycerate_kinase, consensus disorder prediction	NA	Non-apoplastic
Solyc08g014060.4.1	22.5052578523964	11.2526289261982	consensus disorder prediction, Transl_init_eIF2A, consensus disorder prediction, Eukaryotic translation initiation factor eIF2A, DPP6 N-terminal domain-like, -, -	NA	Non-apoplastic
Solyc08g016510.3.1	-20.3080081772682	10.1540040886341	Proteasome_A_N_2, Proteasome subunit, Proteasome subunit A N-terminal signature, Glutamine Phosphoribosylpyrophosphate, subunit 1, domain 1, proteasome_alpha_type_5, N-terminal nucleophile aminohydrolases (Ntn hydrolases), Proteasome alpha-type subunit profile., Proteasome alpha-type subunits signature.	NA	Non-apoplastic
Solyc08g029000.3.1	11.0957289244383	21.1035789320384	-, Lipoxygenase iron-binding catalytic domain profile., Lipoxigenase, Plant lipoxygenase signature, Plant lipoxygenase signature, Plant lipoxygenase signature, Plant lipoxygenase signature, Plant lipoxygenase signature, Plant lipoxygenase signature, Plant lipoxygenase signature, Plant lipoxygenase signature, Plant lipoxygenase signature, LH2_4, PLAT/LH2 domain, PLAT_LH2, PLAT domain profile., -, Lipoxygenases iron-binding region signature 2., Lipoxygenase, Lipoxygenase signature, Lipoxygenase signature, Lipoxygenase signature, -, PLAT/LH2 domain, Lipoxygenases iron-binding region signature 1., -, Lipase/lipooxygenase domain (PLAT/LH2 domain)	NA	Non-apoplastic
Solyc08g043170.4.1	22.9105863306224	11.4552931653112	Aldehyde Dehydrogenase; Chain A, domain 2, AAK_P5CS_ProBA, Aldehyde Dehydrogenase; Chain A, domain 1, P5CS: delta l-pyrroline-5-carboxylate synthetase, Aldehyde dehydrogenase family, Glutamate 5-kinase signature., ALDH-like, Gamma-glutamyl phosphate reductase [proA]., ALDH_F18-19_ProA-GPR, Glutamate 5-kinase [proB]., -, proB: glutamate 5-kinase, Amino acid kinase family, Glutamate 5-kinase family signature, Glutamate 5-kinase family signature, Glutamate 5-kinase family signature, Glutamate 5-kinase family signature, Glutamate 5-kinase family signature, proA: glutamate-5-semialdehyde dehydrogenase, Carbamate kinase-like, P5C_synthetase	NA	Non-apoplastic
Solyc08g062660.3.1	18.2603483344618	9.13017416723088	consensus disorder prediction, RanBP1 domain, PH domain-like, Ran binding domain type 1 profile., ranbd_3, Coil, consensus disorder prediction, consensus disorder prediction, RanBD_RanBP1, -	NA	Non-apoplastic
Solyc08g067800.3.1	12.2104089069662	20.6192627266776	Acyl-CoA N-acyltransferases (Nat), GCN5-related N-acetyl-transferase, Yjdj-type Gcn5-related N-acetyltransferase (GNAT) domain profile., -	NA	Non-apoplastic
Solyc08g068400.4.1	23.8725680657757	11.9362840328879	Prolyl oligopeptidase family, alpha/beta hydrolase, alpha/beta-Hydrolases	NA	Non-apoplastic

Solyc08g068690.1.1	2.5223613298894	26.7363040299569	Gcn5-related N-acetyltransferase (GNAT) domain profile., Acyl-CoA N-acyltransferases (Nat), Acetyltransferase (GNAT) family	NA	Non-apoplastic
Solyc08g068730.1.1	2.5223613298894	26.7363040299569	Acetyltransferase (GNAT) family, Gcn5-related N-acetyltransferase (GNAT) domain profile., Acyl-CoA N-acyltransferases (Nat)	NA	Non-apoplastic
Solyc08g075360.3.1	20.3100714532278	10.1550357266139	AAA_5, AAA_5, Possible Fer4-like domain in RNase L inhibitor, RLI, ABC transporter family E signature, ABC transporter family E signature, ABC transporter family E signature, ABC transporter family E signature, ABC transporter family E signature, ABC transporter family E signature, 4Fe-4S ferredoxin-type iron-sulfur binding domain profile., -, ATP-binding cassette, ABC transporter-type domain profile., P-loop containing nucleoside triphosphate hydrolases, 4Fe-4S ferredoxins, P-loop containing nucleoside triphosphate hydrolases, ABC_RNaseL_inhibitor_domain1, ABC_RNaseL_inhibitor_domain2, ABC transporter, ABC transporter, 4Fe-4S binding domain, 4Fe-4S ferredoxin-type iron-sulfur binding region signature., ABC transporters family signature., ATP-binding cassette, ABC transporter-type domain profile., -	NA	Non-apoplastic
Solyc08g076470.4.1	16.6405110870575	22.5597027004409	G3POAT, plsc_2, LPLAT_GPAT, -, Acyltransferase, Glycerol-3-phosphate acyltransferase N-terminal, -, Glycerol-3-phosphate (1)-acyltransferase	NA	Non-apoplastic
Solyc08g082830.3.1	15.7100930729739	16.0675892423395	Carbon-nitrogen hydrolase, NADS_GAT, NAD_synthase, Carbon-nitrogen hydrolase, Adenine nucleotide alpha hydrolases-like, GAT_Gln-NAD-synth, Carbon-nitrogen hydrolase domain profile., HUPs, nadE: NAD+ synthetase, Glutamine-dependent NAD(+) synthetase [nadE]., NAD synthase, -	NA	Non-apoplastic
Solyc08g082850.3.1	19.6742516841962	9.83712584209809	ABC transporter, ABCF_EF-3, ATP-binding cassette, ABC transporter-type domain profile., ABCF_EF-3, Coil, P-loop containing nucleoside triphosphate hydrolases, AAA_5, AAA_5, ATP-binding cassette, ABC transporter-type domain profile., consensus disorder prediction, P-loop containing nucleoside triphosphate hydrolases, ABC transporters family signature., -, -, ABC transporter, ABC transporter, ABC transporters family signature.	NA	Non-apoplastic
Solyc09g008280.2.1	13.5270062560109	17.4418094097407	S-adenosylmethionine synthetase, central domain, -, MAT, S-adenosylmethionine synthetase, -, metK: methionine adenosyltransferase, -, S-adenosylmethionine synthase [metK]., S-AdoMet_synt, S-adenosylmethionine synthetase, N-terminal domain, S-adenosylmethionine synthetase, S-adenosylmethionine synthetase, C-terminal domain, S-adenosylmethionine synthase signature 2., S-adenosylmethionine synthase signature 1., S-adenosylmethionine synthetase	NA	Non-apoplastic
Solyc09g009690.3.1	18.6731925070588	9.33659625352941	Inosine-uridine preferring nucleoside hydrolase, Nucleoside hydrolase, nuc_hydro_CaPnhB, -	NA	Non-apoplastic
Solyc09g010370.3.1	15.5742977708356	7.78714888541782	consensus disorder prediction, Rab8_Rab10_Rab13_like, small GTPase Rab1 family profile., Ras family, P-loop containing nucleoside triphosphate hydrolases, consensus disorder prediction, -, Transforming protein P21 ras signature, Transforming protein P21 ras signature, Transforming protein P21 ras signature, Transforming protein P21 ras signature, Transforming protein P21 ras signature, small_GTP: small GTP-binding protein domain, rho_sub_3, small GTPase Rho family profile., ran_sub_2, ras_sub_4, small GTPase Ras family profile., arf_sub_2, rab_sub_5	NA	Non-apoplastic
Solyc09g011630.3.1	18.7749705896329	14.5695362735114	GST C-terminal domain-like, Thioredoxin-like, Glutathione S-transferase, C-terminal domain, GST_N_Tau, Glutaredoxin, Glutathione S-transferase, N-terminal domain, Soluble glutathione S-transferase C-terminal domain profile., -, GST_C_Tau, Soluble glutathione S-transferase N-terminal domain profile.	NA	Non-apoplastic
Solyc09g031780.3.1	17.9397546891112	8.96987734455561	Chloroplast envelope transporter	NA	Non-apoplastic
Solyc09g057670.3.1	14.7403026938954	16.5221917846816	FKBP-type peptidyl-prolyl cis-trans isomerase domain profile., -, SignalP-noTM, FKBP-type peptidyl-prolyl cis-trans isomerase, FKBP-like	NA	Non-apoplastic
Solyc09g075130.3.1	-18.4150526656893	9.20752633284466	-, consensus disorder prediction, Sm3, Sm_D2, LSM domain, Sm-like ribonucleoproteins	NA	Non-apoplastic
Solyc09g090840.3.1	-16.1961075297131	12.5796966698019	-, GatB/YqeY motif, Glutamine synthetase/guanido kinase, GatB/GatE catalytic domain, gatb_yqey_2, Glutamyl-tRNA(Gln) amidotransferase subunit B signature., -, Aspartyl/glutamyl-tRNA(Asn/Gln) amidotransferase subunit B [gatB]., gatB: aspartyl/glutamyl-tRNA(Asn/Gln) amidotransferase, B subunit, GatB domain	NA	Non-apoplastic

Solyc09g090960.4.1	-26.3446842033494	13.1723421016747	Eukaryotic RNA Recognition Motif (RRM) profile., Eukaryotic RNA Recognition Motif (RRM) profile., RNA-binding domain, RBD, RNA recognition motif. (a.k.a. RRM, RBD, or RNP domain), RNA recognition motif. (a.k.a. RRM, RBD, or RNP domain), -, -, Coil, RNA-binding domain, RBD, rrm1_1, rrm1_1, consensus disorder prediction	NA	Non-apoplastic
Solyc09g090980.3.1	3.23317392355363	28.8510943011043	Bet_v1-like, Bet v1-like, Bet_v_1_2, -, Pathogenesis-related proteins Bet v I family signature., Major pollen allergen Bet V1 signature, Major pollen allergen Bet V1 signature, Major pollen allergen Bet V1 signature, Major pollen allergen Bet V1 signature, Major pollen allergen Bet V1 signature, Major pollen allergen Bet V1 signature, Major pollen allergen Bet V1 signature, Pathogenesis-related protein Bet v 1 family	NA	Non-apoplastic
Solyc09g090990.2.1	1.70006840900935	26.2080062423241	Bet_v1-like, Pathogenesis-related protein Bet v 1 family, -, Bet_v_1_2, Bet v1-like, Pathogenesis-related proteins Bet v I family signature., Major pollen allergen Bet V1 signature, Major pollen allergen Bet V1 signature, Major pollen allergen Bet V1 signature, Major pollen allergen Bet V1 signature, Major pollen allergen Bet V1 signature, Major pollen allergen Bet V1 signature	NA	Non-apoplastic
Solyc09g091970.4.1	-19.7623396053151	9.88116980265757	NAD dependent epimerase/dehydratase family, NAD(P)-binding Rossmann-fold domains, SDR_a8, -, Domain of unknown function (DUF1731), yfcH: TIGR01777 family protein	NA	Non-apoplastic
Solyc10g007180.2.1	-24.3488553654695	12.1744276827348	consensus disorder prediction, SignalP-TM, consensus disorder prediction, consensus disorder prediction, consensus disorder prediction, consensus disorder prediction	NA	Non-apoplastic
Solyc10g007320.3.1	10.5231099807916	18.5800796821836	Uroporphyrinogen decarboxylase [hemE]., -, URO-D, UROD/MetE-like, Uroporphyrinogen decarboxylase (URO-D), Uroporphyrinogen decarboxylase signature 2., Uroporphyrinogen decarboxylase signature 1., hemE: uroporphyrinogen decarboxylase	NA	Non-apoplastic
Solyc10g049970.2.1	8.83314664535446	20.4539950756258	Putative cyclase, SignalP-TM, SignalP-noTM, Putative cyclase, Putative cyclase, SignalP-noTM	NA	Non-apoplastic
Solyc10g074820.1.1	-1.64711990023235	24.6036656399321	consensus disorder prediction, -, SignalP-noTM, Protein of unknown function (DUF1191)	NA	Non-apoplastic
Solyc10g078550.4.1	25.503706913525	12.7518534567625	Glu/Leu/Phe/Val dehydrogenase, dimerisation domain, Glu / Leu / Phe / Val dehydrogenases active site., NAD(P)-binding Rossmann-fold domains, Glutamate/Leucine/Phenylalanine/Valine dehydrogenase, ELFV_dehydrog_3, Aminoacid dehydrogenase-like, N-terminal domain, NAD_bind_1_Glu_DH, Glutamate/leucine/phenylalanine/valine dehydrogenase signature, Glutamate/leucine/phenylalanine/valine dehydrogenase signature, Glutamate/leucine/phenylalanine/valine dehydrogenase signature, Glutamate/leucine/phenylalanine/valine dehydrogenase signature, -, Glu_DH, Leucine Dehydrogenase, chain A, domain 1	NA	Non-apoplastic
Solyc10g079720.2.1	11.7751901814772	20.4065792267666	Aspartate Aminotransferase, domain 1, CGS_like, Cys/Met metabolism enzymes pyridoxal-phosphate attachment site., -, Cys/Met metabolism PLP-dependent enzyme, cysta_beta_ly_E: cystathionine beta-lyase, CGS, PLP-dependent transferases	NA	Non-apoplastic
Solyc10g084320.3.1	1.35683932912685	28.7752051445655	PA_subtilisin_like, Serine proteases, subtilase domain profile., Subtilisin serine protease family (S8) signature, Subtilisin serine protease family (S8) signature, Subtilisin serine protease family (S8) signature, -, Peptidase S8/S53 domain, Peptidases_S8_3, Peptidase inhibitor I9, Fibronectin type-III domain, -, Peptidase S8 propeptide/proteinase inhibitor I9, Serine proteases, subtilase family, serine active site., SignalP-noTM, Subtilase family, Serine proteases, subtilase family, histidine active site., Subtilisin-like	NA	Apoplastic
Solyc11g010200.3.1	-19.8220409398339	9.91102046991693	-, 14-3-3 proteins signature 1., 1433_4, 14-3-3 proteins signature 2., 14-3-3, 14-3-3 protein zeta signature, 14-3-3 protein zeta signature, 14-3-3 protein zeta signature, 14-3-3 protein zeta signature, 14-3-3 protein zeta signature, 14-3-3 protein zeta signature, 14-3-3 protein, Coil, 14-3-3 protein, Coil	NA	Non-apoplastic
Solyc11g012070.3.1	-19.9646856554629	9.98234282773144	alpha/beta hydrolase, alpha/beta-Hydrolases, Phospholipase/Carboxylesterase	NA	Non-apoplastic
Solyc11g013460.2.1	-2.48463538471227	25.6286339575897	P-loop containing nucleoside triphosphate hydrolases, TIGR00152: dephospho-CoA kinase, DPCK, Dephospho-CoA kinase (DPCK) domain profile., -, Dephospho-CoA kinase [coaE]., Dephospho-CoA kinase	NA	Non-apoplastic

Solyc11g017070.2.1	19.2648927919394	9.63244639596969	Trp-Asp (WD) repeats profile., WD40 repeat-like, -, Trp-Asp (WD) repeats signature., Trp-Asp (WD) repeats circular profile., Trp-Asp (WD) repeats profile., Trp-Asp (WD) repeats circular profile., Trp-Asp (WD) repeats circular profile., Trp-Asp (WD) repeats profile., WD40_4, WD40_4, WD40_4, WD40_4, WD40_4, Trp-Asp (WD) repeats signature., WD domain, G-beta repeat, WD domain, G-beta repeat, WD domain, G-beta repeat, WD domain, G-beta repeat, Trp-Asp (WD) repeats circular profile., G protein beta WD-40 repeat signature, G protein beta WD-40 repeat signature, G protein beta WD-40 repeat signature, Trp-Asp (WD) repeats profile., WD40, Eukaryotic translation initiation factor 3 subunit I [EIF3I]., Trp-Asp (WD) repeats circular profile., Trp-Asp (WD) repeats profile.	NA	Non-apoplastic
Solyc11g017250.2.1	-17.5875415091976	15.8549046654197	2-oxoacid dehydrogenases acyltransferase (catalytic domain), -, CoA-dependent acyltransferases, Peripheral subunit-binding domain of 2-oxo acid dehydrogenase complex, -, lipoyl_domain, 2-oxo acid dehydrogenases acyltransferase component lipoyl binding site., e3 binding domain, Biotin-requiring enzyme, Biotinyl/lipoyl domain profile., -, Peripheral subunit-binding (PSBD) domain profile., Single hybrid motif	NA	Non-apoplastic
Solyc11g044910.2.1	19.8392176837365	17.9117000457527	-, Glycosyl hydrolase family 3 C-terminal domain, (Trans)glycosidases, Glycosyl hydrolase family 3 signature, Glycosyl hydrolase family 3 signature, Glycosyl hydrolase family 3 signature, Fn3_like_2, SignalP-noTM, Immunoglobulins, Fibronectin type III-like domain, -, Glycosyl hydrolase family 3 N terminal domain, Beta-D-glucan exohydrolase, C-terminal domain	NA	Non-apoplastic
Solyc11g045110.3.1	-20.1211406011367	10.0605703005684	HAD_SPS, Sucrose-6F-phosphate phosphohydrolase, -, Glycosyl transferases group 1, Glycogen Phosphorylase B;, HAD-like, -, Glycogen Phosphorylase B;, UDP-Glycosyltransferase/glycogen phosphorylase, sucrsPsyn_pln: sucrose phosphate synthase, Glycosyltransferase Family 4, Glycogen Phosphorylase B;	NA	Non-apoplastic
Solyc11g071700.2.1	13.7221382995979	14.997519461316	Coil, Ubiquitin specific protease (USP) domain signature 1., math_3, peptidase_C19C, -, Cysteine proteinases, consensus disorder prediction, Ubiquitin specific protease (USP) domain profile., MATH/TRAF domain profile., -, Cysteine proteinases, Ubiquitin specific protease (USP) domain signature 2., ICP0-binding domain of Ubiquitin-specific protease 7, MATH, MATH domain, Ubiquitin carboxyl-terminal hydrolase, Ubiquitin-specific protease C-terminal, Apoptosis, Tumor Necrosis Factor Receptor Associated Protein 2; Chain A, TRAF domain-like	NA	Non-apoplastic
Solyc12g013830.2.1	2.25285682697007	27.0128911171534	NA	NA	Non-apoplastic
Solyc12g014440.2.1	9.18166210545152	21.5807048016359	-, Sialidase_non-viral, BNR repeat-like domain, Sialidases	NA	Non-apoplastic
Solyc12g038400.2.1	17.9708381903922	18.8737225788759	AMP-binding enzyme, -, -, Acetyl-CoA synthetase-like, Putative AMP-binding domain signature.	NA	Non-apoplastic
Solyc12g055820.3.1	14.0363886926213	16.1838524902797	HMA, -, Zinc-binding dehydrogenase, Alcohol dehydrogenase GroES-like domain, Heavy-metal-associated domain, D-isomer specific 2-hydroxyacid dehydrogenases NAD-binding signature., Zinc-containing alcohol dehydrogenases signature., GroES-like, Heavy-metal-associated domain profile., -, -, HMA, heavy metal-associated domain, PKS_ER_names_mod, CAD1, NAD(P)-binding Rossmann-fold domains	NA	Non-apoplastic
Solyc12g057060.2.1	19.0622282349909	9.53111411749545	UDP-glucoronosyl and UDP-glucosyl transferase, GT1_Gtf-like, UDP-Glycosyltransferase/glycogen phosphorylase, UDP-glycosyltransferases signature., Glycogen Phosphorylase B;, Glycogen Phosphorylase B;	NA	Non-apoplastic
Solyc12g057080.2.1	19.0622282349909	9.53111411749545	Glycogen Phosphorylase B;, Glycogen Phosphorylase B;, UDP-Glycosyltransferase/glycogen phosphorylase, GT1_Gtf-like, UDP-glycosyltransferases signature., UDP-glucoronosyl and UDP-glucosyl transferase	NA	Non-apoplastic
Solyc12g095880.2.1	14.3083696024407	20.7195748001026	ATP-dependent 6-phosphofructokinase [pfkA]., ATP_PFK_TP0108, ATP-dependent phosphofructokinase family signature, ATP-dependent phosphofructokinase family signature, ATP-dependent phosphofructokinase family signature, ATP-dependent phosphofructokinase family signature, ATP-dependent phosphofructokinase family signature, ATP-dependent phosphofructokinase family signature, consensus disorder prediction, Phosphofructokinase, -, Coil, consensus disorder prediction, Phosphofructokinase	NA	Non-apoplastic

Solyc12g096530.1.1	15.1987854566468	14.5877583093425	secretory_peroxidase, Peroxidase, domain 2, Peroxidase, Peroxidases proximal heme-ligand signature., -, consensus disorder prediction, Plant peroxidase signature, Plant peroxidase signature, Plant peroxidase signature, Plant peroxidase signature, Plant peroxidase signature, Plant peroxidase signature, Plant peroxidase signature, Plant peroxidase signature, Plant peroxidase signature, Plant heme peroxidase family profile., Heme-dependent peroxidases, Haem peroxidase superfamily signature, Haem peroxidase superfamily signature, Haem peroxidase superfamily signature, Haem peroxidase superfamily signature, Haem peroxidase superfamily signature	NA	Non-apoplastic

Supplementary table 2: List of SH and CP enriched in ABPP-MS experiment.

ID	InterProscan Protein domains descriptions
EEY53286.1	Papain family cysteine protease, Cysteine proteinases, Eukaryotic thiol (cysteine) proteases cysteine active site., pept_c1, Eukaryotic thiol (cysteine) proteases histidine active site., CYSTEINE PROTEASE FAMILY C1-RELATED, Peptidase_C1A, Papain cysteine protease (C1) family signature, Papain cysteine protease (C1) family signature, CATHEPSIN L,-LIKE-RELATED
EEY65526.1	CYSTEINE PROTEASE RDL2-RELATED, Cathepsin propeptide inhibitor domain (I29), E set domains, Papain family cysteine protease, SignalP-noTM, Inhibitor_I29_2, -, Cysteine proteinases, Eukaryotic thiol (cysteine) proteases cysteine active site., SignalP-noTM, Eukaryotic thiol (cysteine) proteases histidine active site., SignalP-TM, Peptidase_C1A, Cysteine proteinases, CYSTEINE PROTEASE FAMILY C1-RELATED, pgtp_13, ML domain, Papain cysteine protease (C1) family signature, Papain cysteine protease (C1) family signature, Papain cysteine protease (C1) family signature, pept_c1
Solyc01g010710.4.1	Serine carboxypeptidases, serine active site., alpha/beta hydrolase, Serine carboxypeptidase, -, -, Carboxypeptidase C serine protease (S10) family signature, Carboxypeptidase C serine protease (S10) family signature, Carboxypeptidase C serine protease (S10) family signature, Carboxypeptidase C serine protease (S10) family signature, alpha/beta-Hydrolases
Solyc01g010720.4.1	alpha/beta hydrolase, Carboxypeptidase C serine protease (S10) family signature, Carboxypeptidase C serine protease (S10) family signature, Carboxypeptidase C serine protease (S10) family signature, Carboxypeptidase C serine protease (S10) family signature, Serine carboxypeptidases, serine active site., Serine carboxypeptidase, -, -, alpha/beta-Hydrolases
Solyc01g079450.3.1	DPP6 N-terminal domain-like, alpha/beta-Hydrolases, alpha/beta hydrolase, Prolyl oligopeptidase family
Solyc01g087740.1.1	Peptidases_S8_3, -, Subtilase family, Serine proteases, subtilase domain profile., Subtilisin serine protease family (S8) signature, Subtilisin serine protease family (S8) signature, Subtilisin serine protease family (S8) signature, PA_subtilisin_like, Peptidase S8/S53 domain, consensus disorder prediction, Subtilisin-like, Fibronectin type-III domain, Serine proteases, subtilase family, histidine

	active site., Peptidase S8 propeptide/proteinase inhibitor I9, Peptidase inhibitor I9, Serine proteases, subtilase family, serine active site., -
Solyc01g087780.2.1	Peptidase S8/S53 domain, -, Fibronectin type-III domain, Serine proteases, subtilase domain profile., PA_subtilisin_like, Serine proteases, subtilase family, serine active site., Subtilase family, Subtilisin serine protease family (S8) signature, Subtilisin serine protease family (S8) signature, Subtilisin serine protease family (S8) signature, Subtilisin-like, -, Peptidase S8 propeptide/proteinase inhibitor I9, Peptidase inhibitor I9, Peptidases_S8_3
Solyc01g087790.2.1	Fibronectin type-III domain, Subtilase family, Peptidase inhibitor I9, Subtilisin serine protease family (S8) signature, Subtilisin serine protease family (S8) signature, Subtilisin serine protease family (S8) signature, PA_subtilisin_like, Serine proteases, subtilase family, serine active site., -, Peptidase S8 propeptide/proteinase inhibitor I9, -, Peptidase S8/S53 domain, Subtilisin-like, Serine proteases, subtilase domain profile., Serine proteases, subtilase family, histidine active site., Peptidases_S8_3
Solyc01g087970.3.1	-, SignalP-TM, Serine carboxypeptidases, serine active site., SignalP-noTM, Serine carboxypeptidase, -, alpha/beta hydrolase, SignalP-noTM, Carboxypeptidase C serine protease (S10) family signature, Carboxypeptidase C serine protease (S10) family signature, Carboxypeptidase C serine protease (S10) family signature, Carboxypeptidase C serine protease (S10) family signature, alpha/beta-Hydrolases
Solyc01g094010.3.1	alpha/beta hydrolase, consensus disorder prediction, alpha/beta hydrolase fold, alpha/beta-Hydrolases
Solyc01g099020.3.1	SGNH hydrolase, SGNH_plant_lipase_like, GDSL-like Lipase/Acylhydrolase, SignalP-noTM, SGNH hydrolase
Solyc01g100930.3.1	GDSL-like Lipase/Acylhydrolase, SGNH hydrolase, SGNH hydrolase, SignalP-TM, Coil, SGNH_plant_lipase_like
Solyc01g102330.3.1	Carbohydrate esterase, sialic acid-specific acetylesterase, SignalP-noTM, SGNH hydrolase, SGNH hydrolase
Solyc01g102350.3.1	SignalP-noTM, Pectinacetylesterase
Solyc01g108490.3.1	-, Carboxypeptidase C serine protease (S10) family signature, Carboxypeptidase C serine protease (S10) family signature, Carboxypeptidase C serine protease (S10) family signature, Carboxypeptidase C serine protease (S10) family signature, Serine carboxypeptidases, serine active site., alpha/beta-Hydrolases, -, Serine carboxypeptidase, Serine carboxypeptidases, histidine active site., alpha/beta hydrolase
Solyc01g108560.4.1	alpha/beta hydrolase fold, alpha/beta hydrolase, alpha/beta-Hydrolases

Solyc01g108570.3.1	alpha/beta hydrolase fold, alpha/beta hydrolase, alpha/beta-Hydrolases
Solyc02g014830.4.1	-, Serine carboxypeptidases, serine active site., -, Carboxypeptidase C serine protease (S10) family signature, Carboxypeptidase C serine protease (S10) family signature, Carboxypeptidase C serine protease (S10) family signature, Carboxypeptidase C serine protease (S10) family signature, alpha/beta hydrolase, Serine carboxypeptidase, Serine carboxypeptidases, histidine active site., alpha/beta-Hydrolases
Solyc02g065090.4.1	Cytosolic phospholipase A2 catalytic domain, Patatin-like phospholipase (PNPLA) domain profile., FabD/lysophospholipase-like, Patatin-like phospholipase
Solyc02g065280.3.1	alpha/beta-Hydrolases, Alpha/beta hydrolase family, alpha/beta hydrolase
Solyc02g069090.3.1	Papain cysteine protease (C1) family signature, Papain cysteine protease (C1) family signature, Papain cysteine protease (C1) family signature, Papain family cysteine protease, Eukaryotic thiol (cysteine) proteases cysteine active site., Eukaryotic thiol (cysteine) proteases histidine active site., pept_c1, Cysteine proteinases, Peptidase family C1 propeptide, Peptidase_C1A_CathepsinB, Cysteine proteinases
Solyc02g069800.1.1	alpha/beta hydrolase fold, alpha/beta hydrolase, alpha/beta-Hydrolases
Solyc02g072370.1.1	Peptidases_S8_3, SignalP-noTM, PA domain, Fibronectin type-III domain, Peptidase S8/S53 domain, SignalP-TM, PA_subtilisin_like, Peptidase S8 propeptide/proteinase inhibitor I9, Serine proteases, subtilase domain profile., PA domain, -, Subtilisin serine protease family (S8) signature, Subtilisin serine protease family (S8) signature, Subtilisin serine protease family (S8) signature, Subtilase family, Peptidase inhibitor I9, Subtilisin-like, Serine proteases, subtilase family, aspartic acid active site., -
Solyc02g077010.1.1	Lipase (class 3), Coil, Lipase_3, alpha/beta hydrolase, alpha/beta-Hydrolases
Solyc02g077020.3.1	alpha/beta-Hydrolases, Lipase (class 3), alpha/beta hydrolase, Coil, Lipase_3
Solyc02g077040.4.1	Papain family cysteine protease, pept_c1, Cathepsin propeptide inhibitor domain (I29), Cysteine proteinases, Papain cysteine protease (C1) family signature, Papain cysteine protease (C1) family signature, Papain cysteine protease (C1) family signature, Inhibitor_I29_2, Peptidase_C1A, Eukaryotic thiol (cysteine) proteases histidine active site., Cysteine proteinases, Eukaryotic thiol (cysteine) proteases asparagine active site., Eukaryotic thiol (cysteine) proteases cysteine active site.

Solyc02g077110.3.1	alpha/beta hydrolase, Lipase_3, Lipase (class 3), alpha/beta-Hydrolases
Solyc02g077420.3.1	alpha/beta-Hydrolases, Coil, Lipase_3, Lipase (class 3), alpha/beta hydrolase
Solyc02g077430.4.1	Lipase_3, Lipase (class 3), alpha/beta-Hydrolases, alpha/beta hydrolase
Solyc02g080200.4.1	Pectinesterase signature 2., PME_inhib: pectinesterase inhibitor domain, Invertase/pectin methylesterase inhibitor family protein, PMEI_2, Pectin lyase-like, PMEI-like_4, Pectinesterase signature 1., Pectinesterase, Plant invertase/pectin methylesterase inhibitor, Plant invertase/pectin methylesterase inhibitor, -
Solyc02g080220.3.1	PMEI-like_4, Pectin lyase-like, Plant invertase/pectin methylesterase inhibitor, Pectinesterase signature 2., Plant invertase/pectin methylesterase inhibitor, Pectinesterase signature 1., PME_inhib: pectinesterase inhibitor domain, -, Pectinesterase, Invertase/pectin methylesterase inhibitor family protein, PMEI_2
Solyc02g090490.3.1	SignalP-TM, Patatin-like phospholipase, Cytosolic phospholipase A2 catalytic domain, Patatin-like phospholipase (PNPLA) domain profile., SignalP-noTM, Pat17_isozyme_like, FabD/lysophospholipase-like
Solyc02g091560.3.1	Serine hydroxymethyltransferase, Serine hydroxymethyltransferase pyridoxal-phosphate attachment site., Serine hydroxymethyltransferase [glyA]., SHMT, PLP-dependent transferases, -, Aspartate Aminotransferase, domain 1, SHMT
Solyc02g092670.1.1	Serine proteases, subtilase family, serine active site., Serine proteases, subtilase domain profile., -, Subtilisin-like, SignalP-TM, Fibronectin type-III domain, Peptidase S8/S53 domain, PA domain, consensus disorder prediction, Subtilase family, Peptidases_S8_3, SignalP-noTM, Subtilisin serine protease family (S8) signature, Subtilisin serine protease family (S8) signature, Subtilisin serine protease family (S8) signature, PA domain, Peptidase inhibitor I9, consensus disorder prediction, PA_subtilisin_like, Peptidase S8 propeptide/proteinase inhibitor I9, -
Solyc03g006970.1.1	Serine proteases, subtilase domain profile., -, PA_subtilisin_like, PA domain, SignalP-noTM, Peptidase inhibitor I9, SignalP-TM, Peptidase S8 propeptide/proteinase inhibitor I9, -, Subtilase family, Peptidase S8/S53 domain, Subtilisin serine protease family (S8) signature, Subtilisin serine protease family (S8) signature, Subtilisin serine protease family (S8) signature, SignalP-noTM, PA domain, Serine proteases, subtilase family, serine active site., Subtilisin-like, Fibronectin type-III domain, Peptidases_S8_3
Solyc03g025580.1.1	Pectinacetylesterase, SignalP-noTM

Solyc03g025600.3.1	Pectinacetylesterase, SignalP-noTM
Solyc03g044150.4.1	Serine proteases, subtilase family, serine active site., Subtilisin-like, Peptidase S8/S53 domain, Subtilase family, Subtilisin serine protease family (S8) signature, Subtilisin serine protease family (S8) signature, Subtilisin serine protease family (S8) signature, Peptidase S8 propeptide/proteinase inhibitor I9, PA domain, -, -, Peptidases_S8_3, PA domain, consensus disorder prediction, Serine proteases, subtilase domain profile., Fibronectin type-III domain, PA_subtilisin_like, Peptidase inhibitor I9, SignalP-TM
Solyc04g015340.3.1	-, alpha/beta hydrolase, -, Carboxypeptidase C serine protease (S10) family signature, Carboxypeptidase C serine protease (S10) family signature, Carboxypeptidase C serine protease (S10) family signature, Carboxypeptidase C serine protease (S10) family signature, Serine carboxypeptidase, Serine carboxypeptidases, histidine active site., SignalP-noTM, alpha/beta-Hydrolases, Serine carboxypeptidases, serine active site.
Solyc04g050730.3.1	SGNH_plant_lipase_like, SignalP-noTM, SGNH hydrolase, SGNH hydrolase, GDSL-like Lipase/Acylhydrolase
Solyc04g074950.3.1	Serine hydrolase (FSH1), alpha/beta-Hydrolases, alpha/beta hydrolase
Solyc04g074960.4.1	alpha/beta-Hydrolases, Serine hydrolase (FSH1), alpha/beta hydrolase
Solyc04g076790.3.1	SHMT, SHMT, Serine hydroxymethyltransferase pyridoxal-phosphate attachment site., Aspartate Aminotransferase, domain 1, PLP-dependent transferases, Serine hydroxymethyltransferase [glyA]., Serine hydroxymethyltransferase, -
Solyc04g077670.3.1	Serine carboxypeptidase, SignalP-noTM, alpha/beta-Hydrolases, -, alpha/beta hydrolase, Carboxypeptidase C serine protease (S10) family signature, Carboxypeptidase C serine protease (S10) family signature, Carboxypeptidase C serine protease (S10) family signature, Carboxypeptidase C serine protease (S10) family signature
Solyc04g081755.2.1	SGNH_plant_lipase_like, GDSL-like Lipase/Acylhydrolase, SGNH hydrolase, SGNH hydrolase
Solyc04g081770.4.1	SGNH_plant_lipase_like, GDSL-like Lipase/Acylhydrolase, SGNH hydrolase, SGNH hydrolase
Solyc04g081810.4.1	Fibronectin type-III domain, -, Protease propeptides/inhibitors, Peptidase inhibitor I9, Serine proteases, subtilase family, histidine active site., PA_subtilisin_like, Peptidase S8 propeptide/proteinase inhibitor I9, Subtilisin serine protease family (S8) signature, Subtilisin serine protease family (S8) signature, Subtilisin serine protease family (S8) signature, Serine proteases, subtilase domain

	profile., -, Subtilisin-like, Peptidases_S8_3, Subtilase family, PA domain, Serine proteases, subtilase family, serine active site., Peptidase S8/S53 domain
Solyc05g013690.4.1	SGNH hydrolase, SGNH_plant_lipase_like, GDSL-like Lipase/Acylhydrolase, SGNH hydrolase
Solyc05g050210.4.1	GDSL-like Lipase/Acylhydrolase, SGNH hydrolase, SGNH_plant_lipase_like, SGNH hydrolase
Solyc05g053810.3.1	-, PLP-dependent transferases, Serine hydroxymethyltransferase [glyA]., SHMT, SHMT, Aspartate Aminotransferase, domain 1, Serine hydroxymethyltransferase, Serine hydroxymethyltransferase pyridoxal-phosphate attachment site.
Solyc06g009190.4.1	PME_inhib: pectinesterase inhibitor domain, Invertase/pectin methylesterase inhibitor family protein, Pectin lyase-like, Plant invertase/pectin methylesterase inhibitor, Plant invertase/pectin methylesterase inhibitor, PMEI_2, PMEI-like_3, Pectinesterase signature 2., -, Pectinesterase
Solyc06g051960.3.1	Pectin lyase-like, Pectinesterase, Pectinesterase signature 2., Plant invertase/pectin methylesterase inhibitor, -, PMEI-like_3, PME_inhib: pectinesterase inhibitor domain, Invertase/pectin methylesterase inhibitor family protein, Plant invertase/pectin methylesterase inhibitor, PMEI_2
Solyc06g068880.3.1	alpha/beta hydrolase, alpha/beta-Hydrolases, Serine carboxypeptidase, -, Carboxypeptidase C serine protease (S10) family signature, Carboxypeptidase C serine protease (S10) family signature, Carboxypeptidase C serine protease (S10) family signature, Carboxypeptidase C serine protease (S10) family signature, Serine carboxypeptidases, serine active site., -
Solyc06g074850.3.1	Carboxypeptidase C serine protease (S10) family signature, Carboxypeptidase C serine protease (S10) family signature, Carboxypeptidase C serine protease (S10) family signature, Carboxypeptidase C serine protease (S10) family signature, alpha/beta hydrolase, Serine carboxypeptidase, SignalP-noTM, Serine carboxypeptidases, serine active site., SignalP-noTM, Serine carboxypeptidases, histidine active site., alpha/beta-Hydrolases
Solyc06g083040.3.1	SignalP-noTM, alpha/beta-Hydrolases, Serine carboxypeptidases, serine active site., Serine carboxypeptidase, -, Carboxypeptidase C serine protease (S10) family signature, Carboxypeptidase C serine protease (S10) family signature, Carboxypeptidase C serine protease (S10) family signature, Carboxypeptidase C serine protease (S10) family signature, -, alpha/beta hydrolase
Solyc07g041920.4.1	Papain family cysteine protease, Eukaryotic thiol (cysteine) proteases cysteine active site., Cysteine proteinases, Eukaryotic thiol (cysteine) proteases asparagine active site., Cathepsin propeptide inhibitor domain (I29), Peptidase_C1A, Inhibitor_I29_2, pept_c1, Papain cysteine protease (C1) family signature, Papain cysteine protease (C1) family signature, Papain cysteine protease (C1) family signature, Eukaryotic thiol (cysteine) proteases histidine active site., Cysteine proteinases

Solyc07g041970.4.1	Subtilisin serine protease family (S8) signature, Subtilisin serine protease family (S8) signature, Subtilisin serine protease family (S8) signature, Serine proteases, subtilase domain profile., Serine proteases, subtilase family, serine active site., Protease propeptides/inhibitors, Peptidase S8/S53 domain, -, Subtilisin-like, Fibronectin type-III domain, Peptidase inhibitor I9, Peptidases_S8_3, Peptidase S8 propeptide/proteinase inhibitor I9, Subtilase family, PA domain, consensus disorder prediction, PA domain, PA_subtilisin_like, -
Solyc08g005800.4.1	SignalP-noTM, Pectinacetylesterase
Solyc08g007700.1.1	PA_subtilisin_like, Peptidase S8 propeptide/proteinase inhibitor I9, Serine proteases, subtilase domain profile., PA domain, Fibronectin type-III domain, Peptidase inhibitor I9, -, Subtilisin-like, Peptidase S8/S53 domain, -, Subtilase family, SignalP-noTM, Prokaryotic membrane lipoprotein lipid attachment site profile., Peptidases_S8_3, Serine proteases, subtilase family, aspartic acid active site., Subtilisin serine protease family (S8) signature, Subtilisin serine protease family (S8) signature, Subtilisin serine protease family (S8) signature
Solyc08g075060.4.1	Pectinacetylesterase
Solyc08g079850.3.1	Fibronectin type-III domain, Peptidases_S8_3, Serine proteases, subtilase domain profile., Subtilisin-like, PA_subtilisin_like, -, Subtilase family, Peptidase S8 propeptide/proteinase inhibitor I9, Peptidase S8/S53 domain, PA domain, Serine proteases, subtilase family, aspartic acid active site., Peptidase inhibitor I9, -, Subtilisin serine protease family (S8) signature, Subtilisin serine protease family (S8) signature, Subtilisin serine protease family (S8) signature
Solyc08g079870.3.1	-, Serine proteases, subtilase domain profile., Peptidase S8 propeptide/proteinase inhibitor I9, -, Subtilase family, Subtilisin serine protease family (S8) signature, Subtilisin serine protease family (S8) signature, Subtilisin serine protease family (S8) signature, Subtilisin-like, PA_subtilisin_like, Peptidases_S8_3, PA domain, Peptidase inhibitor I9, Peptidase S8/S53 domain, Fibronectin type-III domain, Serine proteases, subtilase family, aspartic acid active site., SignalP-noTM
Solyc08g079890.2.1	Fibronectin type-III domain, Peptidases_S8_3, -, PA domain, PA_subtilisin_like, -, Subtilase family, Peptidase inhibitor I9, Serine proteases, subtilase domain profile., Subtilisin-like, Peptidase S8/S53 domain, Subtilisin serine protease family (S8) signature, Subtilisin serine protease family (S8) signature, Subtilisin serine protease family (S8) signature, Peptidase S8 propeptide/proteinase inhibitor I9, SignalP-noTM, Serine proteases, subtilase family, aspartic acid active site.
Solyc08g079900.3.1	Fibronectin type-III domain, SignalP-noTM, Subtilisin serine protease family (S8) signature, Subtilisin serine protease family (S8) signature, Subtilisin serine protease family (S8) signature, PA domain, PA_subtilisin_like, Peptidases_S8_3, Peptidase inhibitor I9, Peptidase S8 propeptide/proteinase inhibitor I9, Subtilisin-like, Peptidase S8/S53 domain, -, Subtilase family, Serine proteases, subtilase domain profile., -, Serine proteases, subtilase family, aspartic acid active site.

Solyc08g079910.2.1	SignalP-noTM, Peptidase S8 propeptide/proteinase inhibitor I9, Peptidase inhibitor I9, -, PA_subtilisin_like, Subtilisin-like, Subtilisin serine protease family (S8) signature, Subtilisin serine protease family (S8) signature, Subtilisin serine protease family (S8) signature, PA domain, Fibronectin type-III domain, Subtilase family, Peptidase S8/S53 domain, Peptidases_S8_3, Serine proteases, subtilase family, aspartic acid active site., -, Serine proteases, subtilase domain profile.
Solyc09g009700.4.1	GDSL-like Lipase/Acylhydrolase, SGNH hydrolase, SGNH hydrolase, SGNH_plant_lipase_like
Solyc09g075350.4.1	Pectinesterase, Plant invertase/pectin methylesterase inhibitor, -, Pectinesterase signature 2., Plant invertase/pectin methylesterase inhibitor, PMEI_2, PME_inhib: pectinesterase inhibitor domain, Pectin lyase-like, Invertase/pectin methylesterase inhibitor family protein, PMEI-like_3
Solyc09g075700.1.1	alpha/beta-Hydrolases, alpha/beta hydrolase fold, alpha/beta hydrolase
Solyc09g075710.1.1	alpha/beta hydrolase, alpha/beta hydrolase fold, alpha/beta-Hydrolases
Solyc10g038130.3.1	Pectinacetylesterase
Solyc10g084320.3.1	PA_subtilisin_like, Serine proteases, subtilase domain profile., Subtilisin serine protease family (S8) signature, Subtilisin serine protease family (S8) signature, Subtilisin serine protease family (S8) signature, -, Peptidase S8/S53 domain, Peptidases_S8_3, Peptidase inhibitor I9, Fibronectin type-III domain, -, Peptidase S8 propeptide/proteinase inhibitor I9, Serine proteases, subtilase family, serine active site., SignalP-noTM, Subtilase family, Serine proteases, subtilase family, histidine active site., Subtilisin-like
Solyc11g006250.2.1	SGNH_plant_lipase_like, SignalP-noTM, SGNH hydrolase, GDSL-like Lipase/Acylhydrolase
Solyc11g008280.3.1	Serine carboxypeptidases, serine active site., SignalP-TM, Serine carboxypeptidases, histidine active site., alpha/beta-Hydrolases, Serine carboxypeptidase, alpha/beta hydrolase, SignalP-noTM, Carboxypeptidase C serine protease (S10) family signature, Carboxypeptidase C serine protease (S10) family signature, Carboxypeptidase C serine protease (S10) family signature, Carboxypeptidase C serine protease (S10) family signature
Solyc11g066250.2.1	Serine carboxypeptidases, serine active site., Serine carboxypeptidase, Serine carboxypeptidases, histidine active site., alpha/beta-Hydrolases, alpha/beta hydrolase, Carboxypeptidase C serine protease (S10) family signature, Carboxypeptidase C serine protease (S10) family signature, Carboxypeptidase C serine protease (S10) family signature, Carboxypeptidase C serine protease (S10) family signature, SignalP-noTM

Solyc11g066520.3.1	Serine carboxypeptidase, alpha/beta hydrolase, Carboxypeptidase C serine protease (S10) family signature, Carboxypeptidase C serine protease (S10) family signature, Carboxypeptidase C serine protease (S10) family signature, Carboxypeptidase C serine protease (S10) family signature, alpha/beta-Hydrolases, Serine carboxypeptidases, serine active site.
Solyc12g017460.1.1	SGNH hydrolase, SignalP-noTM, SGNH hydrolase, SignalP-TM, SignalP-noTM, GDSL-like Lipase/Acylhydrolase, SGNH_plant_lipase_like
Solyc12g019560.1.1	alpha/beta hydrolase, Carboxypeptidase C serine protease (S10) family signature, Carboxypeptidase C serine protease (S10) family signature, Carboxypeptidase C serine protease (S10) family signature, Serine carboxypeptidase, alpha/beta-Hydrolases
Solyc12g019570.2.1	Serine carboxypeptidase, alpha/beta-Hydrolases, alpha/beta hydrolase, Serine carboxypeptidases, histidine active site.
Solyc12g088670.2.1	Cysteine proteinases, Eukaryotic thiol (cysteine) proteases cysteine active site., Inhibitor_I29_2, Granulin repeat, SignalP-noTM, pept_c1, Eukaryotic thiol (cysteine) proteases histidine active site., Cathepsin propeptide inhibitor domain (I29), Granulin, Peptidase_C1A, Cysteine proteinases, Eukaryotic thiol (cysteine) proteases asparagine active site., Papain cysteine protease (C1) family signature, Papain cysteine protease (C1) family signature, Papain cysteine protease (C1) family signature, Papain family cysteine protease, Granulin, GRAN_2
Solyc12g088760.1.1	SignalP-noTM, Peptidases_S8_3, Peptidase inhibitor I9, Peptidase S8/S53 domain, -, -, Subtilase family, PA_subtilisin_like, Fibronectin type-III domain, Subtilisin serine protease family (S8) signature, Subtilisin serine protease family (S8) signature, Subtilisin serine protease family (S8) signature, Serine proteases, subtilase domain profile., Peptidase S8 propeptide/proteinase inhibitor I9, Subtilisin-like, Serine proteases, subtilase family, serine active site.
Solyc12g098490.2.1	Aspartate Aminotransferase, domain 1, -, PLP-dependent transferases, Serine hydroxymethyltransferase, SHMT, Serine hydroxymethyltransferase [glyA]., Serine hydroxymethyltransferase pyridoxal-phosphate attachment site., SHMT
Solyc12g099430.2.1	alpha/beta-Hydrolases, alpha/beta hydrolase, Alpha/beta hydrolase family, Alpha/beta hydrolase fold signature, Alpha/beta hydrolase fold signature, Alpha/beta hydrolase fold signature, Epoxide hydrolase signature, Epoxide hydrolase signature, Epoxide hydrolase signature, Epoxide hydrolase signature, Epoxide hydrolase signature, Epoxide hydrolase signature
XP_002904904.1	Papain family cysteine protease, Cysteine proteinases, Eukaryotic thiol (cysteine) proteases cysteine active site., pept_c1, Eukaryotic thiol (cysteine) proteases histidine active site., CYSTEINE PROTEASE FAMILY C1-RELATED, Peptidase_C1A, Papain cysteine protease (C1) family signature, Papain cysteine protease (C1) family signature, CATHEPSIN L,-LIKE-RELATED

XP_002906125.1	CYSTEINE PROTEASE RDL2-RELATED, Cathepsin propeptide inhibitor domain (I29), E set domains, Papain family cysteine protease, SignalP-noTM, Inhibitor_I29_2, -, Cysteine proteinases, Eukaryotic thiol (cysteine) proteases cysteine active site., SignalP-noTM, Eukaryotic thiol (cysteine) proteases histidine active site., SignalP-TM, Peptidase_C1A, Cysteine proteinases, CYSTEINE PROTEASE FAMILY C1-RELATED, pgtp_13, ML domain, Papain cysteine protease (C1) family signature, Papain cysteine protease (C1) family signature, Papain cysteine protease (C1) family signature, pept_c1

Supplementary table 3: SH and CP with differential relative activity upon *P. infestans* infection.

ID	logFC	InterProscan Protein domains description
Solyc01g108490.3.1	1.29440643949679	-, Carboxypeptidase C serine protease (S10) family signature, Carboxypeptidase C serine protease (S10) family signature, Carboxypeptidase C serine protease (S10) family signature, Carboxypeptidase C serine protease (S10) family signature, Serine carboxypeptidases, serine active site., alpha/beta-Hydrolases, -, Serine carboxypeptidase, Serine carboxypeptidases, histidine active site., alpha/beta hydrolase
Solyc02g014830.4.1	3.12485031858649	-, Serine carboxypeptidases, serine active site., -, Carboxypeptidase C serine protease (S10) family signature, Carboxypeptidase C serine protease (S10) family signature, Carboxypeptidase C serine protease (S10) family signature, Carboxypeptidase C serine protease (S10) family signature, alpha/beta hydrolase, Serine carboxypeptidase, Serine carboxypeptidases, histidine active site., alpha/beta-Hydrolases
Solyc02g065090.4.1	3.60172571499512	Cytosolic phospholipase A2 catalytic domain, Patatin-like phospholipase (PNPLA) domain profile., FabD/lysophospholipase-like, Patatin-like phospholipase
Solyc02g090490.3.1	3.60172571499512	SignalP-TM, Patatin-like phospholipase, Cytosolic phospholipase A2 catalytic domain, Patatin-like phospholipase (PNPLA) domain profile., SignalP-noTM, Pat17_isozyme_like, FabD/lysophospholipase-like
Solyc02g090490.3.1	19.4458202867205	SignalP-TM, Patatin-like phospholipase, Cytosolic phospholipase A2 catalytic domain, Patatin-like phospholipase (PNPLA) domain profile., SignalP-noTM, Pat17_isozyme_like, FabD/lysophospholipase-like

Solyc04g081810.4.1	-1.14487572371443	Fibronectin type-III domain, -, Protease propeptides/inhibitors, Peptidase inhibitor I9, Serine proteases, subtilase family, histidine active site., PA_subtilisin_like, Peptidase S8 propeptide/proteinase inhibitor I9, Subtilisin serine protease family (S8) signature, Subtilisin serine protease family (S8) signature, Subtilisin serine protease family (S8) signature, Serine proteases, subtilase domain profile., -, Subtilisin-like, Peptidases_S8_3, Subtilase family, PA domain, Serine proteases, subtilase family, serine active site., Peptidase S8/S53 domain
Solyc06g009190.4.1	19.0711944548732	PME_inhib: pectinesterase inhibitor domain, Invertase/pectin methylesterase inhibitor family protein, Pectin lyase-like, Plant invertase/pectin methylesterase inhibitor, Plant invertase/pectin methylesterase inhibitor, PMEI_2, PMEI-like_3, Pectinesterase signature 2., -, Pectinesterase
Solyc08g079900.3.1	1.32583060801838	Fibronectin type-III domain, SignalP-noTM, Subtilisin serine protease family (S8) signature, Subtilisin serine protease family (S8) signature, Subtilisin serine protease family (S8) signature, PA domain, PA_subtilisin_like, Peptidases_S8_3, Peptidase inhibitor I9, Peptidase S8 propeptide/proteinase inhibitor I9, Subtilisin-like, Peptidase S8/S53 domain, -, Subtilase family, Serine proteases, subtilase domain profile., -, Serine proteases, subtilase family, aspartic acid active site.
Solyc09g009700.4.1	1.37139772666882	GDSL-like Lipase/Acylhydrolase, SGNH hydrolase, SGNH hydrolase, SGNH_plant_lipase_like
Solyc09g075700.1.1	21.2293144143913	alpha/beta-Hydrolases, alpha/beta hydrolase fold, alpha/beta hydrolase

Supplementary table 4: List of streptavidin beads contaminants.

ID

Solyc02g064680.4.1, Solyc04g077870.3.1, Solyc02g092450.3.1, Solyc04g016260.3.1, Solyc10g075107.1.1,Solyc10g075100.2.1, Solyc02g085950.4.1, Solyc03g034220.3.1, Solyc09g018010.3.1, Solyc08g079880.2.1,Solyc05g054710.3.1, Solyc03g006980.4.1, Solyc02g063150.3.1, Solyc03g044100.4.1, Solyc02g062340.3.1, Solyc10g051373.1.1, Solyc01g109660.2.1, Solyc03g115990.3.1, Solyc09g091070.3.1, Solyc12g099930.2.1, Solyc03g005900.4.1, Solyc08g080650.3.1, Solyc08g080670.1.1, Solyc08g080660.1.1, Solyc03g034334.1.1, Solyc02g072370.1.1, Solyc11g072830.1.1, Solyc01g010710.4.1, Solyc02g084200.3.1, Solyc07g006570.4.1, Solyc01g102660.4.1, Solyc02g067080.4.1,

Solyc02g088690.4.1, Solyc06g069550.1.1, Solyc03g115380.3.1, Solyc01g111170.3.1, Solyc12g044600.3.1, Solyc03g083910.5.1, Solyc12g006110.3.1, Solyc10g074440.2.1, Solyc10g074390.1.1, Solyc05g013690.4.1, Solyc04g074640.4.1, Solyc02g077430.4.1, Solyc10g008720.4.1, Solyc02g077160.3.1, Solyc12g007310.3.1, Solyc08g066850.3.1, Solyc04g007980.3.1,Solyc06g060290.4.1, Solyc01g009180.4.1, Solyc07g007550.3.1, Solyc07g049530.3.1, Solyc07g049550.3.1, Solyc10g083720.3.1, Solyc09g008840.4.1, Solyc02g077420.3.1, Solyc12g099650.2.1, Solyc10g044520.3.1, Solyc01g103920.3.1, Solyc04g074960.4.1, Solyc03g114930.3.1, Solyc04g074000.3.1, Solyc08g079230.1.1, Solyc08g078920.2.1, Solyc05g053810.3.1mSolyc12g098490.2.1, Solyc02g094120.3.1, Solyc12g006470.2.1, Solyc12g006450.2.1, Solyc10g068350.1.1, Solyc10g068355.1.1, Solyc10g073353.1.1, Solyc00g500347.1.1, Solyc00g500258.1.1, Solyc07g005330.3.1, Solyc01g068530.3.1, Solyc05g005690.1.1, Solyc12g100120.2.1, Solyc11g061700.2.1, Solyc04g078950.1.1, Solyc04g074030.3.1, Solyc04g074020.2.1, Solyc03g020040.3.1, Solyc12g094620.3.1, Solyc06g072490.3.1, Solyc03g097900.3.1, Solyc04g072860.3.1, Solyc04g072870.2.1, Solyc09g082990.3.1, Solyc01g095600.4.1, Solyc04g077020.3.1, Solyc02g087880.3.1, Solyc08g006890.3.1, Solyc02g091870.3.1, Solyc11g072820.3.1, Solyc06g068010.3.1, Solyc06g073210.4.1, Solyc04g079060.3.1, Solyc12g100160.3.1, Solyc01g103220.3.1, Solyc01g094560.4.1, Solyc01g066612.1.1, Solyc05g017797.1.1, Solyc09g015140.2.1, Solyc08g062250.3.1, Solyc01g100930.3.1, Solyc10g052880.1.1, Solyc03g115740.2.1, Solyc06g048410.4.1, Solyc03g095180.3.1, Solyc05g013380.3.1, Solyc08g065610.3.1, Solyc08g065780.2.1, Solyc03g042560.3.1, Solyc00g500353.1.1, Solyc05g056170.3.1, Solyc10g086180.2.1, Solyc09g007890.1.1, Solyc09g007920.4.1, Solyc09g007910.4.1, Solyc09g007900.4.1, Solyc03g122310.4.1, Solyc03g098670.1.1, Solyc07g056490.4.1, Solyc03g114150.3.1, Solyc08g068190.3.1, Solyc02g094410.4.1, Solyc08g007690.1.1, Solyc04g011510.4.1, Solyc06g005490.3.1, Solyc02g077010.1.1, Solyc02g077020.3.1, Solyc03g111610.3.1, Solyc11g051160.2.1, Solyc10g006970.3.1, Solyc01g006510.3.1, Solyc10g050890.2.1, Solyc01g108630.3.1, Solyc08g068730.1.1, Solyc08g068710.1.1, Solyc08g068690.1.1, Solyc02g086700.4.1, Solyc01g089970.3.1, Solyc12g042060.3.1, Solyc06g064470.4.1, Solyc06g050120.3.1, Solyc06g072230.1.1, Solyc02g067180.3.1, Solyc02g090490.3.1, Solyc03g044710.4.1, Solyc02g080630.4.1, Solyc06g009970.3.1, Solyc06g005060.3.1, Solyc11g150146.1.1, Solyc06g009960.3.1, Solyc11g069700.2.1, Solyc07g065120.3.1, XP_002905012.1, EEY53394.1.

Supplementary file 1: SP3 protocol provided by Dr Farnusch Kashani (2022).

Supplementary file 2: Qualitative analysis of *P. infestans* protein groups robustly identified.

Supplementary file 3: Quantitative analysis of in-solution digestions of tomato apoplastic total proteomes upon *P. infestans* infection.

Supplementary file 4: Quantitative analysis of enriched SH and CP with biotynilated probes.

Supplementary file 5: Quantitative analysis and raw data of differential relative activity and abundance of enriched SH and CP upon infection.

Supplementary file 6: Convolution ABPP-MS quantitative analysis.

Supplementary file 7: Analysis of fluorescence intensity of 53 KDa protein band in convolution ABPP gels.

Supplementary file 8: MaxQuant peptide groups files.

Chapter 4: Characterisation of Pain1a: a Novel PaPain1-like Cysteine Protease secreted by *Phytophthora infestans*.

Laura Ossorio Carballo[1], Nattapong Sanguankiattichai[1], Sophie Eisele, Mariana Schuster[1], Renier A. L. van der Hoorn[1].

[1] The Plant Chemetics Laboratory, Department of Plant Sciences, University of Oxford, Oxford, UK.

Introduction

The oomycete *Phytophthora infestans*, causal agent of the potato blight disease, owes its name to the destruction it is causing in crops throughout last centuries. This filamentous organism is closely related to brown algae and diatoms. It was first described by Heinrich Anton de Bary[1] and is thought to originate from mid America (Mexico)[2].

P. infestans has a complex hemibiotrophic life cycle that includes host colonisation with a biotrophic and a necrotrophic phase[3,4]. During the early biotrophic phase, plant immunity is actively suppressed and host cells are kept alive by the pathogen[3]. For doing so, *P. infestans* grows exclusively intercellularly[5], forming invasive structures called haustoria. These haustoria resemble similar structures found in other species of plant symbiotic organisms[6]. Haustoria penetrate the digested cell wall and create a host cell membrane invagination through which the pathogen secretes molecules of diverse nature (such as proteins) that can suppress the plant immune system[7,8]. Effector proteins can remain in the extracellular space (apoplast) or being translocated inside the host cells. Some well described examples of *P. infestans* effectors are secreted small cysteine-rich proteins (SCP) and the host translocated RXLR effectors[9,10].

As a consequence of *P. infestans* lifestyle, the apoplast (including the extra-haustorial matrix) constitutes the first and main interphase in which antagonistic host-pathogen interactions take place. Accordingly, plants deploy immune responses upon apoplastic pathogen recognition[11]. Extracellular plant proteases play a role in this recognition by releasing pathogen-associated molecular patterns (PAMPs) during infection[12].

Among immune proteases are apoplastic cysteine proteases belonging to clan C1A, also termed papain-like cysteine proteases (PLCPs). Some well-studied cases are tomato Rcr3, Pip1 and C14[13–16] which all suppress *P. infestans* colonisation.

Pathogen-derived proteases also play a crucial role during infection. *Pseudomonas syringae* effector HopB1 is a notorious example. HopB1 cleaves and disable SERK3/BAK1 function preventing an immune response[17].

As expected, plant and pathogens secrete inhibitors to depletes each other´s proteolytic activity. A well characterised group of inhibitors are *P. infestans* secreted EPICs, that are cystatine-like inhibitors of plant PLCPs. In tomato, secreted PLCPs such as C14 play a key role in extracellular defence against *P. infestans*[18]. *P. infestans* prevent PLCPs activity by interfering in their secretion[19] or by inhibiting them with secreted EPIC1 and EPIC2B inhibitors[20,21]. From the plant side, a cysteine protease inhibitor secreted by potato (PCPI) is involved in immune defences against *P. infestans*[22].

Consequently, proteases and more precisely PLCPs, are principal elements in plant-pathogen interactions. Despite the numerous efforts dedicated to study plant and pathogen proteases and to investigate *P. infestans* effector arsenal, there are only few studies tackling the characterisation of *P. infestans* secreted proteases. Interestingly, Meijer *et al.* (2014)[23] published an exhaustive proteomic analysis of axenic *P. infestans* secretome highlighting some prominent secreted proteases. Moreover, Shoina *et al.* (2020)[24] performed a comprehensive overview of *P. infestans* secreted metallo-proteases and their possible contribution to virulence. Nevertheless, these two studies do not address if the described proteases are functional and there is a lack of correlation between protease activity and pathogen aggressiveness. To date, there are no studies tackling in depth characterisation of secreted *P. infestans* protease activity. Given the known importance of cysteine proteases in plant-pathogen interactions, we wanted to perform a functional analysis of predicted cysteine proteases secreted by *P. infestans*. For that, we made use of the secreted protein list published by Meijer *et al.* (2014) and we filtered out candidates based on expression profile and domain architecture. We successfully cloned and transiently expressed cysteine protease PITG_12041 by agroinfiltration of *N. benthamiana* and we named it as Pain1a. Moreover, we used new activity-based protein profiling probes to confirm Pain1a activity. Importantly, we showed interactions between *P. infestans* secreted EPIC inhibitors and Pain1a, and we compared the kinetics of Pain1a inhibition by EPIC2B with the apoplastic tomato PLCP C14. Finally, our results indicate that *P. infestans* regulates Pain1a activity in the apoplast by non-overlapping expression patterns of EPIC inhibitors and Pain1a during infection. The dataset in this chapter manifests the importance of PLCP activity regulation for the biology of *P. infestans* and sets the grounds for future studies such as infection phenotyping and substrate exploration.

Results

Selection of *P. infestans* secreted proteases for heterologous expression

To study secreted cysteine proteases of *P. infestans*, we applied selection criteria for candidates based on several layers (**Figure 1A**). First, we selected cysteine proteases present in the secretome of axenic *P. infestans* isolate 88069[23]. In order to determine if those proteases could have a role in *P. infestans* infection, we explored RNAseq expression data from infected tomato leaves var. Heinz[25]. After performing differential expression analysis using linear models[26,27], we found that only two cysteine proteases (PITG_12041 and PITG_03020) were significantly induced at 3dpi (**Figure 1B**).

Next, we assessed the integrity of PITG_12041 and PITG_03020 by analysing the amino acid sequences with InterproScan[28] (**Figure 1C**). Both predicted protease precursors have a signal peptide followed by an I29 autoinhibitory domain at the N-terminus. The catalytic domains belong to C1 family (also known as Papain-like Cysteine Proteases-PLCPs-[18,29,30]) and both proteases all required catalytic catalytic residues C154, H301, N321 for PITG_12041 and C126, H284, N304 for PITG_03020.

Remarkably, PITG_03020 contains an additional MD-2-related lipid-recognition domain (ML) in the C-terminal region. This domain has a immunoglobulin-like beta-sandwich fold and is typically found in arginine-specific cysteine proteases[31,32], and it is unusual in PLCPs.

Finally, successful molecular cloning using Golden Gate system[33] was achieved for PITG_12041 (pLOC001). The sequence amplified from isolate *P. infestans* 88069 cDNA contains two substitutions in codon 223 (GTT) compared to the reference genome from isolate T30-4 (GAC), resulting in a aspartic acid to valine (D223V) substitution.

We named PITG_12041 as Pain1a, from **Pa**pain-like Cysteine protease secreted by *Phytophthora **in**festans 1*.

To test if Pain1a is secreted and an active protease, we cloned Pain1a into a binary expression vector and expressed Pain1a by agroinfiltration of *Nicotiana benthamiana*. Isolation of apoplastic fluid (AF) followed by labelling with E-68 based fluorescent cysteine protease probe i912 (Schuster et al. in preparation) and detection of fluorescent labelled proteins in protein gels revealed that Pain1a is secreted and active after the autoinhibitory domain is removed (**Figure 1D**).

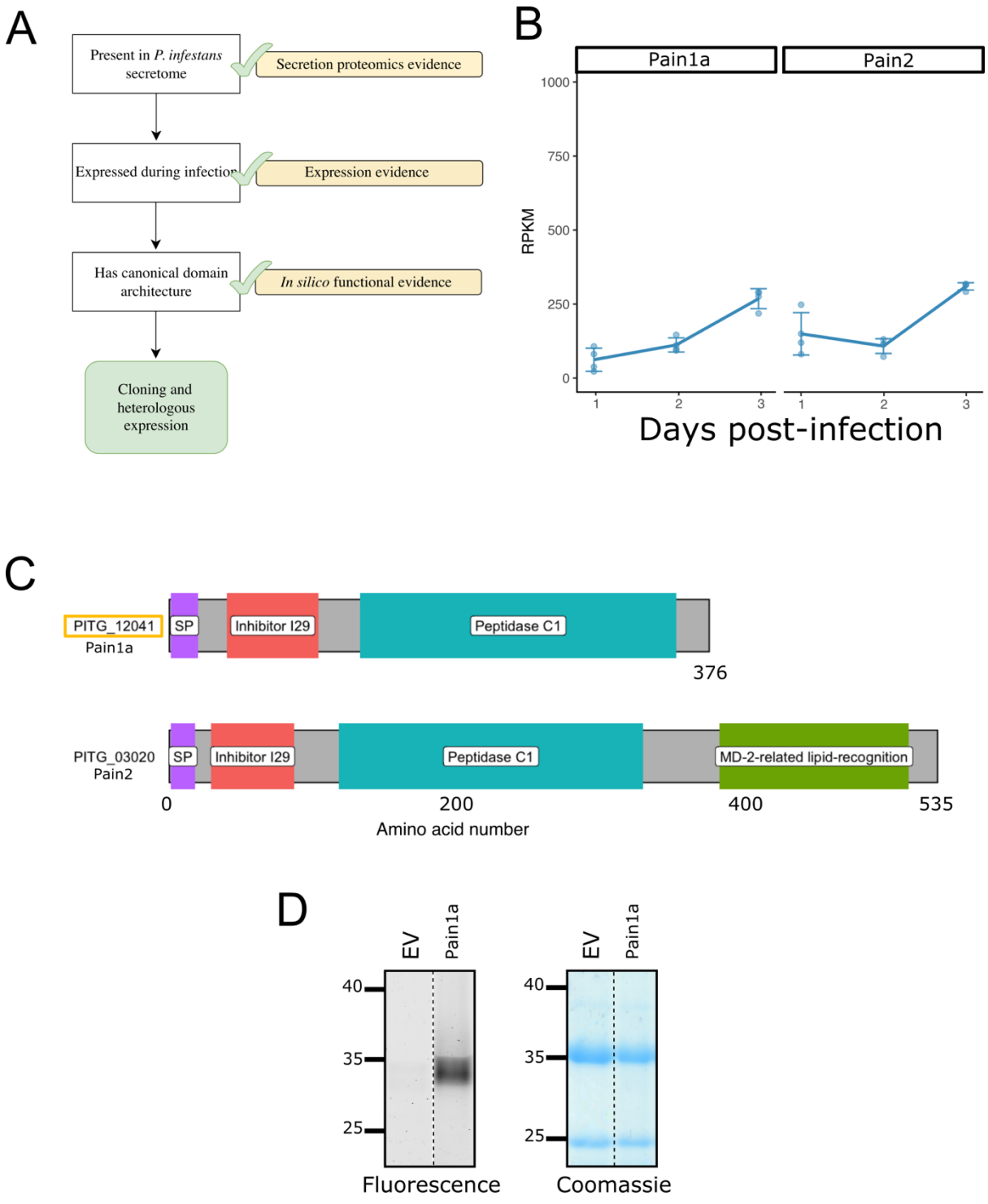


Figure 1: **Selection of *P. infestans* proteases for heterologous expression and characterisation. A, Diagram of *P. infestans* candidate secreted proteases selection for heterologous expression *in planta*. B, Expression of Pain 1a and Pain2 in tomato leaver during infection**. RNAseq data from Huang *et al.* 2020 was used to assess the expression of the candidates. **C, Pain1a (PITG_12041) and Pain2 (PITG_03020) InterproScan annotated domains.** The plot was made using drawProteins R package[34] **D, *in planta* transient overexpression of Pain1a and activity profiling**. Pain1a was transiently expressed by agroinfiltration in *N. benthamiana* leaves. Apoplastic fluid (AF) from three plants was isolated 4 days post infiltration, labelled with the E-68 based fluorescent cysteine protease probe i912 (Schuster *et al.* in preparation), run in protein gels and scanned for

fluorescence. Dotted lines indicate image cropping. The same gel was stained with Coomassie as loading control. Showing one representative biological replicate (n=3).

We also investigated if Pain1a could be a core effector by performing homology-based searches in other *Phytophthora* species. Interestingly, the search returned Pain1a as a multiple copy gene in *P. infestans*. The gene PITG_16276 shares 96.5% identity with Pain1a and we named it Pain1b. Unlike Pain1a which only has one exon, Pain1b has two exons separated by an intron. However, we did not find any expression values for Pain1b when we examined at the same RNAseq dataset used to estimate Pain1a expression[25] suggesting that Pain1b might not be relevant during infection.

Pain1a is conserved in *Phytophthora* genus.

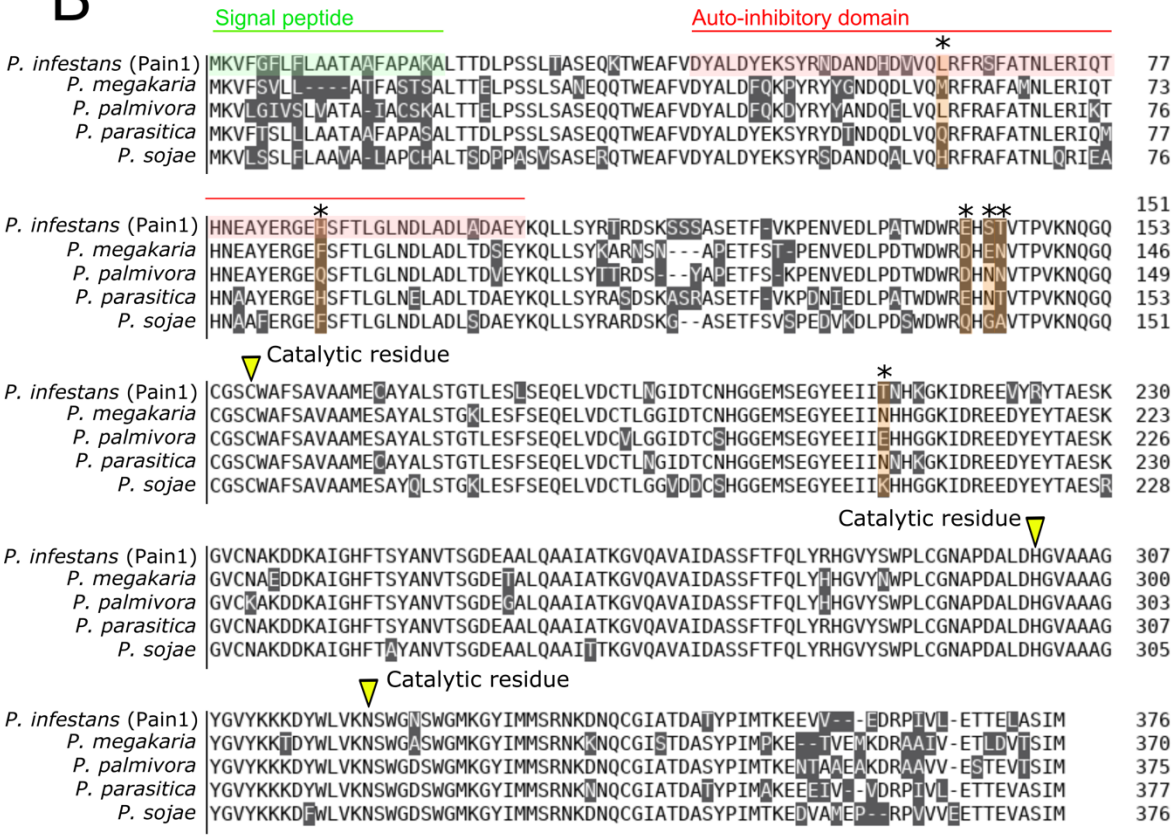
Pain1a is conserved among other *Phytophthora* species and exists in *P. megakarya*, *P. palmivora*, *P. parasitica* and *P. sojae* (**Figure 2A**). To estimate variable residues in Pain1a amino acid sequence, we made an alignment of Pain1a and its closest homologs of other *Phytophthora* species. Residues that were variable in at least three of the five Pain1a homologs were considered hypervariable residues (**Figure 2B**). Signal peptide residues (amino acids 1-20) were not considered. We found that Pain1a contains six hypervariable residues.

Pain1a hypervariable residues 63L and 87H are in the predicted I29 auto-inhibitory pro-domain. Residues 142E, 144S, 145T and 212T are in the catalytic C1 domain. To address the spatial position and the distance to the catalytic pocket of the last four hypervariable residues, we modelled mature Pain1a using AphaFold2[35,36] (**Figure 2C**). All HV residues are predicted to be surface exposed. The 3D structure revealed that hypervariable residues 142E, 144S and 145T are on the opposite side of the substrate groove. However, 212T is close to one end of the substrate groove. This indicates that Pain1a hypervariable residues 142E, 144S and 145T might not affect in substrate specificity, whereas 212T could potentially affect substrate/inhibitor binding.

A

Close homologs of Pain1 in *Phytophthora* spp		
Organism	**Entrez ID (Uniprot)**	**% amino acid identity with Pain1**
Phytophthora megakarya	PHMEG_00037267 (A0A225ULD8)	79.47%
Phytophthora palmivora var. *palmivora*	PHPALM_9950 (A0A2P4Y5Y5)	82.89%
Phytophthora parasitica	F443_13199 (V9EQN8)	90.71%
Phytophthora sojae	XP_009535435.1	80.36%

B



C

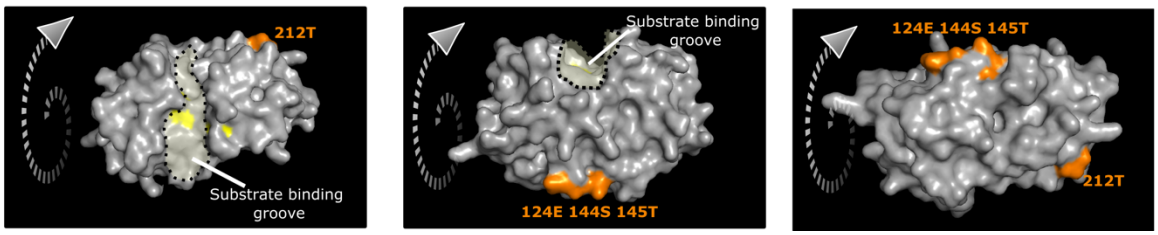


Figure 2. **Homolog genes search reveals Pain1a is conserved among several *Phytophthora* species. A, Pain1a homogs query in other Phytophthora species.** Homologs search for Pain1a using NCBI tool OrthoDB v10.1 retrieved four Pain1a genes in other *Phytophthora* species (Group 5794at4783). **B, Alignment of close Pain1a homolog genes using Geneious Global alignment.** Hypervariable residues are highlighted in orange and catalytic residues are pointed with a yellow arrow. **C, Alphafold 3D model of mature Pain1a visualised with PyMOL.** Sequence for the mature protease was based on InterproScan prediction of the C1 catalytic domain (residues 133-356). Protein was rotated in the arrow direction. Hypervariable residues (orange) and catalytic residues (yellow) are indicated.

Altogether our results show that Pain1a is a conserved gene among *Phytophthora* species and it has an un-transcribed paralog, Pain1b. Moreover, Pain1a carries six hypervariable residues that are not near the substrate groove. These results, along with Pain1a expression induction during infection suggest Pain1a is a core effector.

Pain1a does not affect flg22 signalling.

We next investigated a possible inactivation of the immunity co-receptor SERK3/BAK1 by Pain1a. SERK3/BAK1 is required for recognition of INF1, an elicitor of *P. infestans*[37]. Thus, we used flg22 induced responses as a suitable read-out to monitor the possible inactivation of SERK3/BAK1 receptor by Pain1a. To avoid the stress produced by agrobacterium infiltration, we infiltrated bacteria-free AF containing Pain1a or EV control into halves leaf of unchallenged *N. benthamiana* plants (**Figure 3A**). We measured the oxidative burst after adding flg22 to leaf discs (**Figure 2B**) and we analysed the data using the script provided in Supplementary file 2. We found that Pain1a does not alter the oxidative burst triggered by flg22, indicating that under these conditions, Pain1a does not inactivate SERK3/BAK1 receptor.

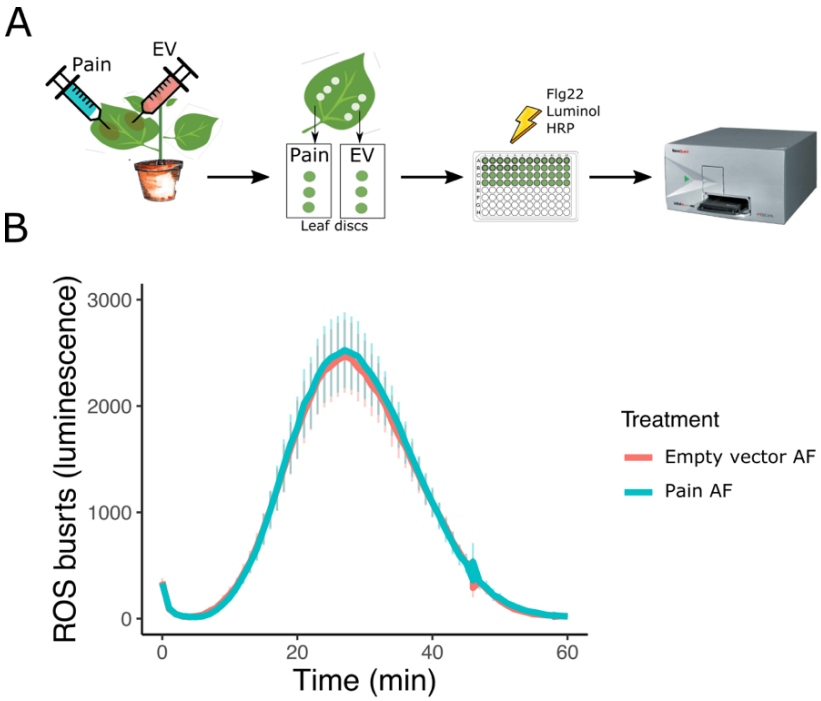


Figure 3: **Pain1a does not affect flagellin elicitor recognition. A, experimental design**. Apoplastic fluid from leaves infiltrated with Pain1a expression vector or empty vector (EV) control was infiltrated in half-leaves of four weeks old *N. benthamiana* plants and ROS burst was measured in those leaves using luminol assay. **B, ROS burst response over time as a function of chemiluminescence.** No significant changes in Flg22 response were observed between EV and Pain1a treatments. Continuous

lines indicate the mean of biological replicates (n=8) and vertical lines indicate ±SE of the mean. Three technical replicates were averaged for each biological replicate.

Pain1a activity is inhibited by EPICs of *P. infestans*.

Next, we tested whether EPIC1 and EPIC2B are able to inhibit Pain1a. Pain1a and C14 were produced by agroinfiltration and AFs isolated from these leaves were pre-incubated with either AF from EPIC1 expressing plants (EPIC1) or purified recombinant EPIC2B (rEPIC2B) and then labelled with fluorescent E-64-based probes.

Both EPIC1 and EPIC2B prevent labelling of Pain1a and C14 (**Figure 4**). Thus surprisingly, *P. infestans* secretes a protease that is sensitive to its own EPIC inhibitors.

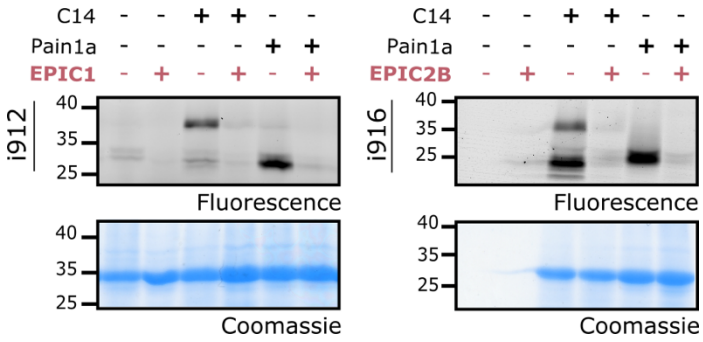


Figure 4. **EPIC1 and EPIC2B inhibit both Pain1a and C14 proteases**. *In planta* transiently expressed Pain1a and tomato C14 were labelled with fluorescent i912 and i916 probes (Schuster *et al.* in preparation) after incubation with EPIC1 and EPIC2B inhibitors and their respective controls. Then, labelled proteins were separated by SDS-PAGE and scanned with a laser using a Typhoon scanner (Amersham) (n=4). Two more experiments assessing EPIC1 and EPIC2B inhibition of Pain1a and C14 gave equivalent results.

We decided to investigate this observation further to address if Pain1a and C14 could have different affinities to EPICs using kinetic inhibition assays. First, we monitored Pain1a and C14 activity with fluorogenic peptide substrate Z-LR-AMC which is specifically cleaved by PLCPs. We measured Pain1a and C14 activity rate by detecting fluorescence over time, in the presence or absence of EPIC2B. Inhibition curves resulted in a suitable dose-response curve fit (**Figure 5B**). Statistical comparison of both curves showed significant differences between the model fits revealing a weaker EPIC2B interaction with Pain1a compared to C14. Further experimental replicates will be necessary to confirm this result.

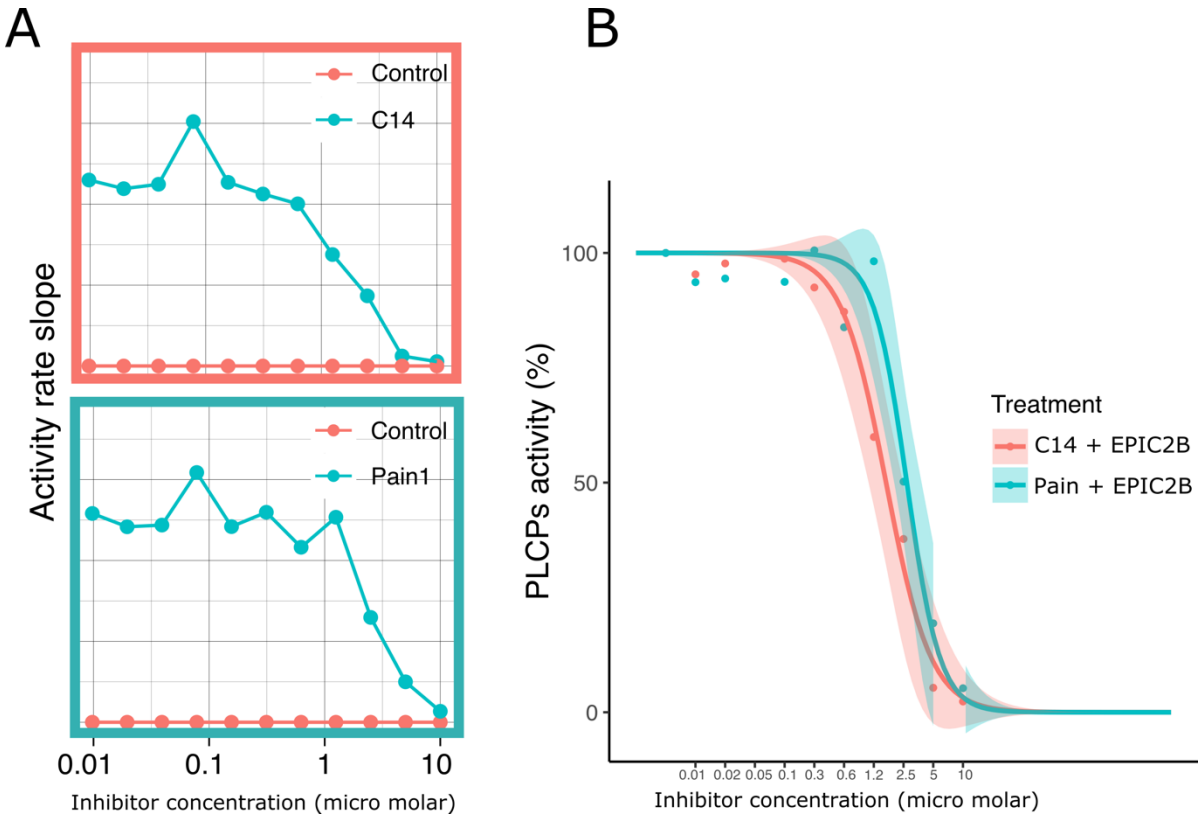


Figure 5. **EPIC2B might be a stronger inhibitor of C14 than of Pain1a. A, EPIC2B concentration course**. Initial protease activities were adjusted to similar levels prior activity assays. Slopes of substrate cleavage rates (activity rates) are plotted for *in planta* expressed Pain1a and C14 and their respective EV controls, in the presence or absence of EPIC2B 10 µM dilution series (n=4). EV control activity values were subtracted from proteases activity before statical modelling. **B, Dose-response curve of Pain1a and C14 activity inhibited by EPIC2B**. A general statistical model was fitted to the data using a four parameters non-linear function defined in "drc" R package. Shaded areas correspond to the model fitting confidence interval. Pain1a and C14 model parameters are significantly different: ANOVA p-value 0.0012.

Opposite expression pattern of Pain1a and EPICs.

Knowing that Pain1a can be inhibited *in vitro* by EPICs, we investigated the possible transcriptional regulation used by *P. infestans* to avoid inhibition of its own secreted protease during infection. *Pain1a* expression increases significantly during the late biotrophic and peaks at 3dpi (250 reads per count per million -RPKM- approximately) at the start of the necrotrophic phase (adj. p-value 0.03) (**Figure 1B**). Conversely, *EPIC2B* expression is at its highest at 1 dpi (900 RPKM approximately) and it decays significantly at 2 and 3 dpi (adj. p-value 0.01). Levels of *EPIC1* transcripts remain low during the time course (adj. p-value 0.172) (**Figure 6**).

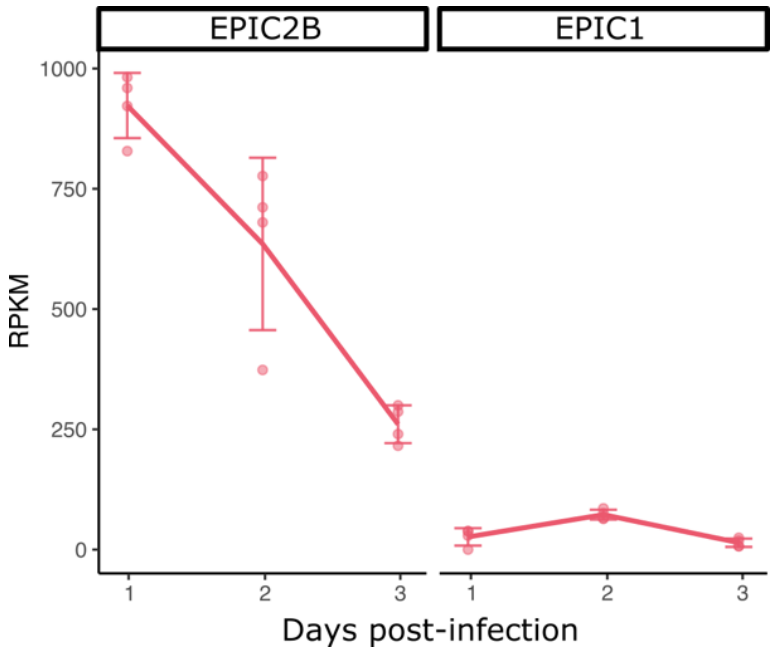


***Figure 6. EPIC2* and *EPIC1* expression levels during *P. infestans* infection.** Expression levels of *P. infestans* isolate 88069 genes during infection of tomato var. Heinz were kindly provided by Huang *et al.* 2020[25]. From left to right, reads per kilobase per million (RPKM) at 1 dpi, 2dpi and 3dpi of EPIC2B and EPIC1. Error bars indicate the standard deviation of the biological replicates mean (n=4).

These results suggest that Pain1a expression is steadily induced during the necrotrophic switch, in contrast to EPIC2B, which has an early strong expression and then reduces to 250 RPKM at 3 dpi.

Discussion

In this chapter we characterised Pain1a, a PLCP secreted by *P. infestans*. We cloned Pain1a and transiently expressed Pain1a *in planta*. We discovered that Pain1a is a conserved PLCP in *Phytophthora* and is expressed during infection, features that make Pain1a a candidate for being a core effector. We did not detect that Pain1a can inactivate SERK3/BAK1 immune receptor. Finally, we found that EPIC1 and EPIC2B of *P. infestans* can inhibit Pain1a and we observed that inhibition by EPIC2B might be weaker than C14 inhibition, and that EPICs and Pain1a have opposite expression patterns during infection. Altogether, this chapter summarises the first characterisation of a PLCP secreted by *P. infestans* to date, and it also confirms Pain1a as a new protease in the list of EPICs inhibited PLCPs. Moreover, our results suggest a coordinated and antagonistic expression between Pain1a and EPICs inhibitors.

However, Pain1a was not the only PLCP considered. Pain2 is also a PLCP, fused to a C-terminal MD-2-related lipid-recognition (ML) domain. Despite our efforts to clone Pain2, we could not achieve a successful amplification of the fragments necessary to perform the gene Golden Gate assembly. However, Pain2 appears in chapter 2 as an active protease, secreted during infection of tomato by *P. infestans*. The ML domain has a similar folding structure as immunoglobulin-like E-set (Ig-like E-set). ML or Ig-like E set domains can be present in arginine-specific cysteine proteases such as Gingipains. Gingipain is a major virulence factor of the human pathogenic bacteria *Porphyromonas gingivalis*[31,38,39]. Pain2 is strongly expressed during infection (**Figure 1**) and presents structural similarities with other unrelated pathogen virulence proteins. For these reasons, PITG_03020 might be an important PLCP for *P. infestans* pathogenicity. To overcome cloning limitations, it is suggested that Pain2 is synthesised and cloned directly into an *in planta* expression vector for further characterisation.

Pain1a has a un-transcribed paralog: Pain1b. Surprisingly, Pain1a does not have intronic regions, whereas Pain1b has an intron. Introns are usually very conserved[40]. Given the high number of transposable elements in *P. infestans* genome[41], it would be very interesting to investigate if this intron is a transposable element that inactivated Pain1b upon insertion. The resurrection of Pain1b would be a noteworthy approach gain insights in Pain1a evolution.

Pain1a is also a conserved PLCP in several *Phytophthora* species. The alignment of the Pain1a homologs revealed variable residues in the self-inhibitory domain (63L and 87H) and in the catalytic domain (142E, 144S, 145T and 212T).

Polymorphic residues in effectors can be footprints of host-pathogen arms races, and they can play an important role in effector interactions[42]. We modelled mature Pain1a using Alphafold2 and addressed where polymorphic residues are found in the protein 3D model. 142E, 144S and 145T form a cluster that locates opposite to the substrate binding groove and might not play a role in substrate processing or specificity. However, it is remarkable to have three polymorphic residues in such proximity on the Pain1a surface. This suggests that the polymorphic cluster might be a relevant area for Pain1a function. Conversely, residue 212T is located close to an edge of the substrate binding groove. This feature has been observed in residues of plant PLCPs that play a role in immunity[43]. The 212T polymorphism may play a role in substrate binding specificity or affect the interaction of Pain1a with PLCP inhibitors, such as EPIC1 and EPIC2B. It would be interesting to test Pain1a variants for altered activity and inhibition by EPICs.

Moreover, depleting Pain1a would give valuable information about its role in plant colonisation. Despite the numerous efforts invested in *P. infestans* genetic transformation, the efficiency of the procedure remains low. Nonetheless, Pain1a is conserved among *Phytophthora* species and orthologs are present in *P. palmivora* and *P. sojae*. This provides an opportunity to perform Pain1a deletion using CRISPR-Cas9 gene editing protocols established in these species[44–46]and address the role of Pain1a in *Phytophthora*.

In this chapter we also addressed how Pain1a could have an impact pathogen perception. Elicitin is a well-known *P. infestans* secreted protein that is recognised by the potato membrane receptor ELR. Upon recognition, elicitin is able to mount a strong SERK3/BAK1 and SOBIR1-dependent immune response[47,48]. These receptors and co-receptors present leucine-rich repeats (LRR) in their extracellular domains. Flg22, an elicitor from *P. syringae*, is sensed by the FLS2 receptor and the immunity response is also SERK3/BAK1-dependent. We hypothesised that Pain1a could inactive SERK3/BAK1 receptor, and we made use of the flg22 response as a read-out to test this hypothesis[49]. The fact that flg22 response is not affected by Pain1a suggests that this protease is not targeting SERK3/BAK1 receptor, hence Pain1a would not constitute an elicitin response suppressor. However, other receptors can be still targeted by Pain1a. For instance, exogenous beta-glucans (such as fungal chitins) are sensed by receptors containing LysMs domains[50–53], including CERK1, LYK4 and LYK5. Laminarin is an abundant beta-glucan present in *P. infestans* cell walls that also triggers an immune response in plants[54]. In a very similar experimental set up, we tried to address if Pain1a could be involved in the deactivation of LysM receptors. Unfortunately, due to laminarin solubilisation problems, we could not induce the reported ROS burst followed by laminarin recognition. Troubleshooting laminarin solubilisation and performing ROS burst measurements in the presence of Pain1a would be a straightforward strategy to test this possible Pain1a target.

Perhaps the most surprising observation in this chapter is the unequivocal ABPP data supporting Pain1a inhibition by both EPIC1 and EPIC2B. To fully characterise Pain1a function during infection, one should test if Pain1a is also inhibited by potato secreted PLCP inhibitor PCPI[22]. If confirmed, the interaction between Pain1a and PCPI could underly in the contribution of PCPI to resistance against *P. infestans* in potato.

Furthermore, activity assays and dose-response curve analysis suggest that EPIC2B does not inhibit Pain1a as strongly as it inhibits the tomato protease C14. If confirmed by further experiments, differential inhibition of Pain1a and C14 by EPIC2B could be the result from two

different evolutive pathways of both PLCPs. Further analysis of the C14 and Pain1a 3D model interacting with EPIC2B would shed light into which residues might be contributing to the differential inhibition and set the basis for directed mutagenesis experiments.

Gene expression profiles for *Pain1a*, *EPIC1* and *EPIC2B* (**Figure 1b**) revealed opposite expression patterns between protease and inhibitors, suggesting that Pain1a and EPICs may not overlap in time during *P. infestans* infection of tomato. Transcriptional induction of Pain1a occurs close to the bio-necrotrophic phase switch. Some PLCPs act upon PCD during plant development. Xylem cysteine proteases (XCPs) in Arabidopsis for instance, are required for protein degradation and amino acid recycling after the formation of tracheary elements[29,55,56]. Pain1a induction towards the necrotrophic switch indicates a similar role for Pain1a in dead plant tissues. Future Pain1a infection phenotyping experiments should be designed considering this evidence.

Material and methods

Pain1a orthologs search and alignment

Pain1a ortholog search was done using OrthoDB from EZlab[57] using the default parameters. Alignment of Pain1a and PITG_16276 was done using Geneious Software with following default parameters: free end gaps, a cost matrix of 65% similarity, a gap open penalty of 12 and a gap extension penalty of 3.

RNAseq expression analysis

Expression tables containing RPKM values from tomato var. Heinz infected with *P. infestans* isolate 88069[25] were analysed using voom and edgeR R packages (Supplementary file 1).

Phytophthora infestans and *Nicotiana benthamiana* growth conditions

Rye A agar plates were prepared using 60 grams of rye grain soaked in milliQ water for 24 hours in darkness at 22°C. Supernatant from germinating grains was put aside. Grain was blended with fresh miliQ water for 2 minutes. The blended grain was placed in glass beakers and heated at 68°C for 1 hour. The mixture was filtered through four layers of cheese cloth, and the sediment discarded. The supernatant kept was combined with the filtered rye. The mixture was added to

20g of sucrose and 15g of agar. Water was added up to 1 litre of volume. The mixture was autoclaved prior to use.

Starting culture of *P. infestans* isolate 88069 was kindly provided by Tolga Bozkurt's lab in Imperial College (London). Agar pieces of starting culture were grown in Rye A agar at 18°C in darkness for three weeks before being passes to fresh Rye A agar.

N. benthamiana plants were grown in a glasshouse at 21°C under long day light conditions (18/8h light/dark).

Cloning

PITG_12041 (Pain1a) coding sequence was amplified using forward primer 5'-TTGGTCTCAAGGTCTAACAACCGATCTCCCATCGTCTCTGA-3' and reverse 5'-TTGGTCTCAAAGCTTACATGATGCTGGCCAGCTCCGTCGTCT-3' from *P. infestans* isolate 88069 cDNA synthesised from 500ng of DNase-treated RNA using SuperScript Reverse Transcriptase (Thermo Fisher) following manufacturer instructions. These primers introduced to the sequence a BsaI restriction enzyme recognition site and a compatible Golden Gate system overhang for ligation. After digestion (37°C 40 minutes) and inactivation (80°C 20 minutes), the Pain1a amplicon was ligated into the BpiI digested binary vector pJK497 (21°C 10 minutes, 65°C 10 minutes). *E. coli* cells were transformed with the ligation product, and plasmids contained in 50 μM kanamycin resistant colonies were selected for sequencing. Full binary vector for Pain1a expression (pLOC001) and empty vector (EV) pJK497 were transformed into *Agrobacterium tumefaciens* strain GV3101 carrying the pMP90 helper plasmid. Agrobacterium transformants were selected in LB agar media (10 g/L NaCl, 10 g/L Tryptone, 5 g/L yeast extract, 15 g/L agar) with selection antibiotics (50 μM gentamycin, 25 μM rifampicin, 50 μM kanamycin). Colonies were grown in LB liquid media containing same mixture of antibiotics for further agroinfiltration and glycerol stock storage.

A summary of plasmids used in this chapter is provided in Supplementary table 1.

Agrobacterium-mediated *in planta* expression

Agrobacterium carrying pLOC001 or pJK497 were grown overnight in LB liquid media with selection antibiotics at 21°C in agitation. Cultures were centrifuged at 1000g for 10 minutes at

room temperature (RT). The pellet containing cells was resuspended in agroinfiltration buffer (10 mM MES, 10 mM $MgCl_2$, 100 μM acetosyringone, pH 5.6) until an OD_{600} of 0.5 was reached.

Leaves of four weeks old *Nicotiana benthamiana* plants grown as described before were infiltrated with OD_{600} 0.5 solution by hand with a 10 ml sterile syringe.

Four days after infiltration, leaves were collected and infiltrated with cold milli-Q water applying vacuum using a 50 ml syringe. After removing water excess from the surface with a tissue, leaves were placed in a 20 ml syringe without plunger inside a 50 ml tube. Leaves were then centrifuged at 1500Xg for 25 minutes. Apoplastic fluid was immediately snap frozen in liquid nitrogen for storage at -80°C before use.

ABPP and SDS-page

PLCP labelling was performed using fluorescent E-64 probes i912 and i916 (Schuster *et al.* in preparation). 200 µl of apoplastic fluid containing the protease of interest was buffered with 50 mM of sodium acetate pH5. Labelling was done in reducing conditions (5 mM DTT) during 4 hours with a probe concentration of 2 µM. Labelling reaction was stopped with 5 volumes of cold acetone. Samples were centrifuged at maximum speed in a benchtop centrifuge for 3 minutes. Supernatant was removed and protein pellets were left to dry at RT. Pellets were resuspended in 40 µl of PBS-SDS loading buffer (phosphate-buffered saline (PBS) pH 7.4, 1% (w/v) sodium dodecyl sulphate (SDS)), and denatured 5 min at 90°C.

10 µl of labelled proteins were loaded in 12% SDS-PAGE acrylamide gels and run at 180V for 1.5 hours approximately. Gels were scanned with an Amersham Typhoon 5 (GE Healthcare Life Sciences) fluorescence scanner (647 nm wavelength). After image acquisition, gels were stained with Coomassie Brilliant Blue G-250.

ROS burst assays

N. benthamiana leaf discs were excised using a cork borer of a 0.125 cm^2 area and left overnight in milli-Q water before the assay. Leaf discs were then placed in a 96 well COSTAR white plate with de adaxial side facing up. 100 µl of elicitin solution containing luminol 1X (Sigma-Aldrich), 0.25 µg/µl horse radish peroxidase (Pierce™ Horseradish Peroxidase) and 100 nM of flg22 were added

immediately before luminescence measurement. This measurement was done using a Tecan infinite 200 plate reader every minute for one hour.

EPIC2B *E. coli* expression and protein purification

Purified His-tagged EPIC2B was kindly provided by Sophie Eisele. *E. coli* carrying pJK157 was grown overnight at 37°C in 5 ml of LB medium supplemented with 50 µg/ml kanamycin. From this starting culture, 300 ml of fresh TB media 50µg/ml kanamycin (0.2% Tryptone 2.4% Yeast extract 0.5% glycerol, 17 mM KH_2PO_4, 72 mM K_2HPO_4) were inoculated and grown at 37°C in agitation until *E. coli* reached an OD_{600} 0.6. His-tagged EPIC2B expression was induced by 1 mM IPTG and grown for 24h at 37°C. The supernatant containing secreted EPIC2B was filtered and 1 ml of Ni-NTA beads (Qiagen Ni-NTA Superflow) was added. Beads incubation was performed at 4°C for 3 hours in rotation. Beads were harvested in a purification column. Resin washes were done with 10 volumes of washing buffer (50 mM Tris HCl pH 7.4, 50 mM NaCl, 50 mM imidazole). EPIC2B was eluted with 5 volumes of elution buffer (50 mM Tris HCl pH 7.4, 50 mM NaCl, 250 mM imidazole). EPIC2B was then concentrated, and the elution buffer was exchanged to 50 mM sodium acetate pH 5 using 3 KDa cut-off Amicon filters (Merck Millipore, Amicon Ultra-15 centrifugal filter unit) and following the manufacture's protocol. Purified protein concentration was measured with DC Protein Assay Kit (Biorad).

Plate reader inhibition assays

Pain1a and C14 activity in AF was measured using the Fluorogenic Peptide Substrate Z-LR-AMC 80 µM (Biotechne). AF activity was adjusted to similar values for both proteases before inhibition assays. AF containing Pain1a, C14 and EV controls were pre incubated with or without inhibitors for 30 minutes in 50 mM sodium acetate pH 5 and 5 mM DTT. Then Z-LR-AMC solution was added and fluorescence increase was measured over time with Tecan Infinite 200 plate reader.

Alphafold2 structural prediction

Pain1a sequence was 3D modelled using ColabFold notebook available online at https://colab.research.google.com/github/sokrypton/ColabFold/blob/main/AlphaFold2.ipynb and with default parameters.

Visualisation of the model generated by ColabFold was visualised using PyMOL software (https://pymol.org/2/).

Files used for the modelling can be found in Supplementary File 4.

Bibliography

1. England, R. A. S. of. *Journal of the Royal Agricultural Society of England*, (1876).

2. Goss, E. M. *et al.* The Irish potato famine pathogen *Phytophthora infestans* originated in central Mexico rather than the Andes. *Proc. Natl. Acad. Sci.* **111**, 8791–8796 (2014).

3. Boevink, *et al.* Devastating intimacy: the cell biology of plant–*Phytophthora* interactions. *New Phytol*, (2020).

4. Garry, G. *et al.* Genetic diversity and host differentiation among isolates of *Phytophthora infestans* from cultivated potato and wild solanaceous hosts in Peru. *Plant Pathol.* **54**, 740–748 (2005).

5. Raaymakers, T. M. & Van den Ackerveken, G. Extracellular recognition of oomycetes during biotrophic infection of plants. *Front. Plant Sci.* **7**, (2016).

6. Parniske, M. Intracellular accommodation of microbes by plants: a common developmental program for symbiosis and disease? *Curr. Opin. Plant Biol.* **3**, 320–328 (2000).

7. Wang, S. *et al.* The *Phytophthora infestans* haustorium is a site for secretion of diverse classes of infection-associated proteins. *mBio* **9**, e01216-18 (2018).

8. Wang, S. *et al.* Delivery of cytoplasmic and apoplastic effectors from *Phytophthora infestans* haustoria by distinct secretion pathways. *New Phytol.* **216**, 205–215 (2017).

9. Zhang, Z.-H. *et al.* A small cysteine-rich phytotoxic protein of *Phytophthora capsici* functions as both plant defense elicitor and virulence factor. *Mol. Plant-Microbe Interactions* **34**, 891–903 (2021).

10. Yin, J. *et al.* Conserved RXLR effector genes of *Phytophthora infestans* expressed at the early stage of potato infection are suppressive to host defense. *Front. Plant Sci.* **8**, (2017).

11. Schellenberger, R. *et al.* Apoplastic invasion patterns triggering plant immunity: plasma membrane sensing at the frontline. *Mol. Plant Pathol.* **20**, 1602–1616 (2019).

12. Godson, A. & van der Hoorn, R. A. L. The front line of defence: a meta-analysis of apoplastic proteases in plant immunity. *J. Exp. Bot.* **72**, 3381–3394 (2021).

13. Rooney, H. C. E. *et al.* Cladosporium Avr2 inhibits tomato Rcr3 protease required for Cf-2-dependent disease resistance. *Science* **308**, 1783–1786 (2005).

14. Ilyas, M. *et al.* Functional divergence of two secreted immune proteases of tomato. *Curr. Biol.* **25**, 2300–2306 (2015).

15. Kaschani, F. & Van der Hoorn, R. A. A model of the C14-EPIC complex indicates hotspots for a protease-inhibitor arms race in the oomycete-potato interaction. *Plant Signal. Behav.* **6**, 109–112 (2011).

16. Shindo, T *et al.* A Role in immunity for arabidopsis cysteine protease RD21, the ortholog of the tomato immune protease C14. *PLOS ONE* **7**, e29317 (2012).

17. Li, L. *et al.* Activation-dependent destruction of a co-receptor by a *Pseudomonas syringae* effector dampens plant immunity. *Cell Host Microbe* **20**, 504–514 (2016).

18. Misas-Villamil, J. C., Hoorn, R. A. L. & Doehlemann, G. Papain-like cysteine proteases as hubs in plant immunity. *New Phytol.* **212**, 902–907 (2016).

19. Bozkurt, T. O. *et al. Phytophthora infestans* effector AVRblb2 prevents secretion of a plant immune protease at the haustorial interface. *Proc. Natl. Acad. Sci.* **108**, 20832–20837 (2011).

20. Tian, M. *et al.* A *Phytophthora infestans* cystatin-like protein targets a novel tomato papain-like apoplastic porotease. *Plant Physiol.* **143**, 364–377 (2007).

21. Song, J. *et al.* Apoplastic effectors secreted by two unrelated eukaryotic plant pathogens target the tomato defense protease Rcr3. *Proc. Natl. Acad. Sci.* **106**, 1654–1659 (2009).

22. El-Banna, A. & Taller, J. Functional characterization of the silenced potato cysteine proteinase inhibitor gene (PCPI) in *Phytophthora infestans* resistance. *Physiol. Mol. Plant Pathol.* **100**, 23–29 (2017).

23. Meijer, H. J. G. *et al.* Profiling the secretome and extracellular proteome of the potato late blight pathogen *Phytophthora infestans*. *Mol. Cell. Proteomics MCP* **13**, 2101–2113 (2014).

24. Schoina, C. *et al.* Mining oomycete proteomes for metalloproteases leads to identification of candidate virulence factors in *Phytophthora infestans*. *Mol. Plant Pathol.* **22**, 551–563 (2021).

25. Huang, J. *et al. Phytophthora* effectors modulate genome-wide alternative splicing of host mRNAs to reprogram plant Immunity. *Mol. Plant* **13**, 1470–1484 (2020).

26. Law, C. W *et al.* voom: precision weights unlock linear model analysis tools for RNA-seq read counts. *Genome Biol.* **15**, R29 (2014).

27. Robinson, M. D., *et al.* edgeR: a Bioconductor package for differential expression analysis of digital gene expression data. *Bioinformatics* **26**, 139–140 (2010).

28. Zdobnov, E. M. & Apweiler, R. InterProScan--an integration platform for the signature-recognition methods in InterPro. *Bioinforma. Oxf. Engl.* **17**, 847–848 (2001).

29. Liu, H., *et al.* Role of papain-like cysteine proteases in plant development. *Front. Plant Sci.* **9**, (2018).

30. Shindo, T. & Hoorn, R. a. L. V. D. Papain-like cysteine proteases: key players at molecular battlefields employed by both plants and their invaders. *Mol. Plant Pathol.* **9**, 119–125 (2008).

31. Pourhajibagher, M., *et al.* Investigation of arginine A-specific cysteine proteinase gene expression profiling in clinical *Porphyromonas gingivalis* isolates against photokilling action of the photo-activated disinfection. *Lasers Med. Sci.* **33**, (2018).

32. Martin, R., *et al.* Leishmania metacaspase: an arginine-specific peptidase. *Methods Mol. Biol. Clifton NJ* **1133**, (2014).

33. Weber, E., *et al.* A modular cloning system for standardized assembly of multigene constructs. *PLOS ONE* **6**, e16765 (2011).

34. Brennan, P. drawProteins: a Bioconductor/R package for reproducible and programmatic generation of protein schematics. *F1000Research* **7**, 1105 (2018).

35. Mirdita, M. *et al.* ColabFold - Making Protein folding accessible to all. *bioRxiv* (2021).

36. Jumper, J. *et al.* Highly accurate protein structure prediction with AlphaFold. *Nature* (2021).

37. Chaparro-Garcia, A. *et al.* The receptor-like kinase SERK3/BAK1 is required for basal resistance against the late blight pathogen *Phytophthora infestans* in *Nicotiana benthamiana*. *PLOS ONE* **6**, (2011).

38. Benedyk, M. *et al.* Gingipains: critical factors in the development of aspiration pneumonia caused by porphyromonas gingivalis. *J. Innate Immun.* **8**, 185–198 (2016).

39. Zhang, R., *et al.* Effect of deletion of the rgpA gene on selected virulence of *Porphyromonas gingivalis*. *J. Dent. Sci.* **11**, 279–286 (2016).

40. Carmel, L. & Chorev, M. The Function of Introns. *Front. Genet.* **3**, (2012).

41. Haas, B. J. *et al.* Genome sequence and analysis of the Irish potato famine pathogen *Phytophthora infestans*. *Nature* **461**, 393–398 (2009).

42. Bentham, A. R. *et al.* A single amino acid polymorphism in a conserved effector of the multihost blast fungus pathogen expands host-target binding spectrum. *PLOS Pathog.* **17**, e1009957 (2021).

43. Kourelis, J. *et al.* Evolution of a guarded decoy protease and its receptor in solanaceous plants. *Nat. Commun.* **11**, 4393 (2020).

44. Tian, M., *et al.* CRISPR-Cas9-mediated gene editing of the plant pathogenic oomycete *Phytophthora palmivora*. *CRISPR-Cas Methods* 87–98, (2020).

45. Fang, Y., *et al.* Efficient genome editing in the oomycete *Phytophthora sojae* using CRISPR/Cas9. *Curr. Protoc. Microbiol.* **44**, 21A.1.1-21A.1.26 (2017).

46. Qiu, M *et al.* A CRISPR/Cas9-mediated in situ complementation method for mutants. *Mol. Plant Pathol.* **22**, 373–381 (2021).

47. Domazakis, E. *et al.* The ELR-SOBIR1 complex functions as a two-component receptor-like kinase to mount defense against *Phytophthora infestans*. *Mol. Plant-Microbe Interactions.* **31**, 795–802 (2018).

48. Du, J. *et al.* Elicitin recognition confers enhanced resistance to *Phytophthora infestans* in potato. *Nat. Plants* **1**, 1–5 (2015).

49. Chinchilla, D., *et al.* One for all: the receptor-associated kinase BAK1. *Trends Plant Sci.* **14**, 535–541 (2009).

50. Buendia, L., *et al.* LysM receptor-like kinase and LysM receptor-like protein families: an update on phylogeny and functional characterization. *Front. Plant Sci.* **9**, (2018).

51. Miya, A. *et al.* CERK1, a LysM receptor kinase, is essential for chitin elicitor signaling in Arabidopsis. *Proc. Natl. Acad. Sci.* **104**, 19613–19618 (2007).

52. Rebaque, D. *et al.* Cell wall-derived mixed-linked β-1,3/1,4-glucans trigger immune responses and disease resistance in plants. *Plant J. Cell Mol. Biol.* **106**, 601–615 (2021).

53. Mélida, H. *et al.* Non-branched β-1,3-glucan oligosaccharides trigger immune responses in Arabidopsis. *Plant J.* **93**, 34–49 (2018).

54. Robinson, S. M. & Bostock, R. M. β-glucans and eicosapolyenoic acids as MAMPs in plant–oomycete interactions: past and present. *Front. Plant Sci.* **5**, 797 (2015).

55. Avci, U., *et al.* Cysteine proteases XCP1 and XCP2 aid micro-autolysis within the intact central vacuole during xylogenesis in Arabidopsis roots. *Plant J. Cell Mol. Biol.* **56**, 303–315 (2008).

56. Han, J. *et al.* The papain-like cysteine protease CEP1 is involved in programmed cell death and secondary wall thickening during xylem development in Arabidopsis. *J. Exp. Bot.* **70**, 205–215 (2019).

57. OrthoDB presentation. https://www.ezlab.org/orthodb.html.

Supplementary materials

Supplementary table 1: plasmids description.

Plasmid ID	*Description*
pLOC001	2x35S::NtPR1a::Pain1a_CDS::t35S::P19
pJK137c	2x35S:: NtPR1a::EPIC1_CDS::t35S::P19
pJK157	pT7::LacOp::OmpA::6XHis::TEV_cleav::EPIC2B_CDS::tT7
pJK497	2x35S::NtPR1a::Cloning_site::t35S::P19

Supplementary files 1: RNAseq expression analysis scripts of *P. infestans* transcripts and data.

Supplementary files 2: ROS burst analysis script and data files.

Supplementary files 3: Kinetics assay analysis script and data files.

Supplementary file 4: Alphafold2 output files mature Pain1a modelling.

Chapter 5: General discussion, conclusions and future perspectives.

Apoplast hydrolases play a key role in antagonistic plant-pathogen interactions. Characterisation of apoplastic hydrolases or any other secreted protein can be done following a top-down approach. Candidates can be selected from a curated list based on *in silico* features for further characterisation. For instance, proteins showing adequate expression profiles (induced during infection), having predicted secretion motifs such as signal peptide[1] and those with conserved sequences among different species are usually considered for further characterisation. This targeted approach is very efficient when the goal is to provide a detailed description of proteins and hydrolases of interest, and it is adopted to characterise Pain1a in the third chapter of this thesis. For example, the small cysteine-rich protein secreted by *P. infestans* PC2 is a selected candidate from a list of predicted secreted proteins. Authors then narrow down that list based on other predictions such as subcellular localisation and motifs, and they choose PC2 after observing that it is able to trigger hypersensitive response (HR) in *N. benthamiana*[2]. Top-down approaches can be relatively limited as the candidate selection is usually based assumptions and on *in silico* predictions and these depend on the quality of the prediction tools. As a result, interesting candidates can be discarded during the selection process. In the first and second chapter of this thesis, we followed a bottom-up approach (from general to particular) to address the unsolved questions that arise from the chapter rationale. As such, in the first chapter we present the general proteomic changes occurring in the apoplast and the symplast upon detachment. Then, we addressed how specific immune responses are affected by detachment too. In the second chapter, we performed ABPP-MS and convolution ABPP-MS to assess the general activome changes in tomato apoplast upon *P. infestans* infection, providing a robust list of candidates subject of further experiments.

In the following discussion, we will summarise the main conclusions of each chapter and we will address the limitations encountered during the research, as well as the future perspectives.

Impact of leaf detachment in plant immunity: conclusions and future perspectives.

Nicotiana benthamiana is a frequently used species in plant pathology research due to its rapid growth and easy transient manipulation. In many cases, the impact of recombinant proteins on immunity is assessed by assaying detached *N. benthamiana* leaves[3]. There are, however, several reports describing an enhanced susceptibility of detached leaves compared to intact leaves in other species[4–6]. The first chapter of this thesis aimed to provide a series of robust observations on how

detachment could affect the immunity of *N. benthamiana* leaves. We started to give a general overview of the protein changes in the apoplast and in the cells using ABPP and shot-gun proteomics. Next, we focused on studying the impact of detachment on specific immune responses such as the rapid ROS burst elicited by flg22 in the apoplast (PTI)[7], the infection phenotype of WT and ΔHopQ *P. syringae* strains (ETI)[8,9], the cell death developed by the recognition of *P. infestans* secretome and lastly, *P. infestans* infection phenotype in WT and *sobir1 N. benthamiana* mutants[10]. We observed that all the studied processes were affected significantly by detachment. However, we could not give more specific answers about the actual components of plant immunity that are affected. A way to deconvolute our results and obtain a clearer picture of leaf detachment implications in immunity is to make use of mutant plants. For instance, the impact of the observed depletion of apoplastic subtilases activity could be further investigated in the context of detachment using subtilase mutants or using a transient gene silencing system such are antisense hairpin RNA[11] or VIGS. Such approach was followed to discover the subtilase that processes the GOLVEN1 signalling peptide hormone in Arabidopsis[12]. Furthermore, the fact that SOBIR1 does not contribute to dimmish *P. infestans* biomass in WT intact plants is a surprising observation that could only be partially explained in the chapter and that contradicts already published literature[13]. It could be possible that since *N. benthamiana* is not a natural host of *P. infestans*, the strong necrosis developed in intact plants helps preventing a compatible interaction in natural conditions, stopping the spread of the pathogen[14]. At the same time, this necrosis could have interfered with our genomic DNA measures reducing the level of host gDNA and thus, returning a relatively higher *P. infestans* biomass. It would be very interesting to test whether this pattern can be also observed using other measures of pathogen growth and in *sobir1* mutants of other Solanaceae species that are natural hosts of *P. infestans* such as potato and tomato, for intact and detached leaves[10]. Despite the limitations of our study, it proves that leaf detachment in *N. benthamiana* impacts plant immunity at several levels and we observed phenomena that are relevant for the phytopathology community.

Tomato apoplastic proteome and activome changes upon *P. infestans* infection: conclusions and future perspectives.

In this chapter, we followed a bottom-up strategy to describe the changes occurring in tomato apoplastic proteome and activome during *P. infestans* infection. In a similar way as in Planas-Marques *et al.* (2018)[15], we compared the apoplastic fraction extracted from mock treated tomato leaves with the one extracted from *P. infestans* infected leaves using total proteomics and ABPP coupled with mass spectrometry. It is the first study of this kind that uses more than 3 biological

replicates and that also includes convolution ABPP. Despite the relative high confidence of the proteins showing changes in activity, abundance or both, shot gun mass spectrometry is yet a technique used exclusively for discovery and further validation of the candidates is desired.

For instance, five *P. infestans* protein groups were identified robustly in 5 replicates of ISD samples. Among them, berberine-like PITG_02930 and the secreted cysteine-rich protein PITG_11060 are also identified by Meijer *et al.* (2014) in the secretome of *P. infestans* grown in minimum media[16]. PITG_02930 is studied in depth by Raffaele *et al.* (2010)[17] where the authors demonstrate that PITG_02930 is a conserved virulence factor of *P. infestans*. Altogether these data validate the quality of our analysis. However, to confirm the role of all robustly identified *P. infestans* proteins in infection, it would be needed to express them *in planta* and perform infection assays. It would be also necessary to consider the impact of leaf detachment in those assays if *N. benthamiana* is the chosen organism for transient expression.

In our study, we used a probe cocktail for labelling of PLCP and serine hydrolases. Despite the power of this technique in combination with total proteome analysis, we could observe that several hydrolase groups that were not targeted in the labelling step showed significant changes in the apoplast. Given the fact that we could identify interesting candidates using two probes, it would be very interesting to expand the probe repertoire used for labelling to obtain a more complete snapshot of the activome changes upon *P. infestans* infection and target other critical hydrolases such as carbohydrate-active enzymes or even metallo-proteases[18,19].

Among labelled proteins, a total of 161 proteins with no predicted PLCP or serine hydrolase activity were co-purified among the probe targets. This issue is due to nonspecific protein binding and is one of the main constrains of affinity purification protocols. For instance, a Contaminant Repository for Affinity Purification (or CRAPome) has been gathered by Mellacheruvu *et al.* (2013) for human and *Sacharomices cerevisiase* samples. This CRAPome aims to overcome partially the limitations derived from unspecific protein binding[20]. It would be interesting to create a customised CRAPome focused in plant and pathogen samples to improve previous and future analysis, from which the whole phytopathology community would benefit.

Among the labelled hydrolases, we could identify seven candidates which activity could be post-translationally regulated. Further *in vitro* confirmation of these observations is required to demonstrate such regulation. The candidates could be expressed including an affinity tag that would allow their purification. After purification, their activity can be tested in the presence of

infected apoplast. Hydrolase inhibitors can be small molecules[21] or proteins[22]. Separation of the small molecules present in infected apoplast from the protein fraction can be done using filters with molecular weight cut-off or using methanol-chloroform precipitation. These separation techniques could be used to give some hints about the nature of putative inhibitors. In the cases where the inhibitor is a protein, emerging mass spectrometry protocols that allow to identify protein-protein interactions (such as chemical crosslinking-MS) could help with the inhibitor identification[23]. Furthermore, these protocols could complement ABPP-MS experiments providing a snapshot of the interactome, shedding light in the regulation of the activome.

Convolution ABPP-MS analysis returned one significantly depleted hydrolase, SCPIP1[24]. Having a look at the distribution of logFC and intensity values in **Figure 6** (Chapter 2), we realised that the changes in activity between M&L and L&M samples are subtle and this could be one of the causes for having a reduced number of significant candidates. Moreover, *P. infestans* inhibitors are locally secreted and these are not abundant proteins. Once apoplastic fluid is extracted, inhibitors dilute in the samples, and this could be another cause of the observed subtle changes in activity. A proposed strategy to overcome this limitation would be to gain statistical power increasing the number of biological replicates.

Finally, these candidates for immune hydrolases represent an interesting data set for crop breeding programs. If their role in immunity against *P. infestans* is confirmed, breeding programs could be focused on the development of resistant varieties that for instance, would have a version of hydrolases that are not susceptible to *P. infestans* inhibition.

A role for Pain1a in *P. infestans* pathogenicity: conclusions and future perspectives.

In the third and last research chapter, we characterised a *P. infestans* secreted PLCP: Pain1a. We also assessed *in silico* Pain1a features. Previously, the role in immunity of secreted hydrolases from *Phytophthora* species such as XEG1 has been studied. XEG1 acts as a major virulence factor of *P. sojae* in infection of soybean and its secretion can be sensed by the host, triggering a immune response[25]. XEG1 is targeted by a plant aspartic protease for its degradation. It has been observed that XEG1 is glycosylated to prevent degradation from plant the aspartic protease and this reflects the molecular arms race between soybean and *P. sojae*[26]. Pain1a is the first PLCP from *P. infestans* that has been proven to be active in the plant apoplast. Moreover, we also demonstrated that EPICs can inhibit Pain1a. We hypothesised that the opposite expression between Pain1a and EPICs could be a regulatory mechanism that occurs during the switch from the biotrophic phase

to the necrotrophic phase. It would be very interesting to further confirm the sequential and non-overlapping expression of EPICs and Pain1a at the protein level using for instance, western blot analysis. We performed experiments aiming to describe Pain1a impact in *P. infestans* infection several times, using at least four biological replicates but unfortunately no conclusive results were obtained. This was mostly because using *P. infestans* zoospores for drop inoculation in detached *N. benthamiana* leaves was returning variable results in the controls and in Pain1a overexpressing leaves. Despite following strict protocols for infection conditions, the infection experiments were put on hold due to time constrains and our efforts focused on the *in vitro* characterisation of Pain1a. We have observed more homogeneous infections using spray inoculation instead of drop inoculation, and this method is suggested for future experiments.

Given the fact that Pain1a is a very well conserved PLCP among other *Phytophthora* species, it would be possible to generate mutants lacking Pain1a in species such as P. sojae[27]. These mutants would be very useful to study the impact of Pain1a in *Phytophthora* pathogenicity and biological function.

During the cloning of Pain1a, we tried to produce a histidine tagged version of Pain1a without success. It is possible that the tag interferes with the native protein folding and consequently, it does not accumulate in the apoplast. The availability of gene synthesis services in which codon optimisation is available, has simplified molecular cloning. Currently, one member of our team is working on a synthesised, codon-optimised His-tagged version of Pain1a that expresses well upon agroinfiltration and accumulates in the *N. benthamiana* apoplast. Tagged Pain1a will allow to monitor the accumulation of the recombinant protein in the apoplast with western blots and more importantly, will allow Pain1a purification. This is a key step to remove any endogenous PLCP activity from the plant and to conduct *in vitro* assays to further characterise the inhibition kinetics of Pain1a. Additionally, purified Pain1a can be used in terminomics experiments (such as TAILS or Hunter) to identify its substrates[28,29]. Furthermore, techniques such as PICS in which a purified protease is incubated with a library of well characterised *E. coli* peptides can be used to identify Pain1a cleavage site preference[30]. Moreover, the generation of catalytically inactive mutants of Pain1a will allow to have the correct control for infection assays, and to link the activity of Pain1a to any infection phenotype observed.

Altogether, we have initiated the characterisation of the first secreted PLCP by *P. infestans*, and we have set the basis for further experiments ideally more focused on deciphering the biological relevance during infection of this protease.

Conclusion

The present thesis has been focused on describing how plant immunity is affected by leaf detachment and on *P. infestans* pathogenicity.

The data set from Chapter 1 is of interest for the phytopathology community as conclusions made in *N. benthamiana* are usually extrapolated to other closely related species.

Moreover, this thesis introduces a full and comprehensive analysis of the tomato apoplastic activome upon *P. infestans* infection. This analysis has generated exciting perspectives as interesting candidates for further characterisation can be derived from it. The findings made in ABPP-MS of tomato apoplast can also be of great value for developing new crop protection strategies.

Finally, we made important progress in the characterisation of the first *P. infestans* secreted PLCP described to date: Pain1a. If its role in immunity is confirmed, further studies can be focused on analyse the biochemistry features of Pain1a.

Altogether, we think this thesis provides experimental support for interesting hypothesis for the scientific community and it also contains very interesting data-sets for further exploration.

1. Teufel, F. *et al.* SignalP 6.0 predicts all five types of signal peptides using protein language models. *Nat. Biotechnol.* **40**, 1023–1025 (2022).

2. Wang, S. *et al.* Cleavage of a pathogen apoplastic protein by plant subtilases activates immunity. *bio*R*xiv* doi:10.1101/2019.12.16.878272. (2019)

3. Bos, J. I. B. *et al. Phytophthora infestans* effector AVR3a is essential for virulence and manipulates plant immunity by stabilizing host E3 ligase CMPG1. *Proc. Natl. Acad. Sci. U. S. A.* **107**, 9909–9914 (2010).

4. Liu, G. *et al.* Detached and attached *Arabidopsis* leaf assays reveal distinctive defense responses against hemibiotrophic *Colletotrichum* spp. *Mol. Plant. Microbe Interact.* **20**, 1308–1319 (2007).

5. Michel, A. P. *et al.* Detached leaf and whole plant assays for soybean aphid resistance: differential responses among resistance sources and biotypes. *J. Econ. Entomol.* **103**, 949–957 (2010).

6. Miller-Butler, *et al.* Comparison of whole plant and detached leaf screening techniques for identifying anthracnose resistance in strawberry plants. *Plant Dis.* **102**, 2112–2119 (2018).

7. Chinchilla, D., *et al.* The arabidopsis receptor kinase FLS2 binds flg22 and determines the specificity of flagellin perception. *Plant Cell* **18**, 465–476 (2006).

8. Wei, C.-F. *et al.* A *Pseudomonas syringae* pv. tomato DC3000 mutant lacking the type III effector HopQ1-1 is able to cause disease in the model plant *Nicotiana benthamiana*. *Plant J. Cell Mol. Biol.* **51**, 32–46 (2007).

9. Schultink, A., *et al.* Roq1 mediates recognition of the *Xanthomonas* and *Pseudomonas* effector proteins XopQ and HopQ1. *Plant J.* **92**, 787–795 (2017).

10. Liebrand, T. W. H. *et al.* Receptor-like kinase SOBIR1/EVR interacts with receptor-like proteins in plant immunity against fungal infection. *Proc. Natl. Acad. Sci. U. S. A.* **110**, 10010–10015 (2013).

11. Brendolise, C. *et al.* A novel hairpin library-based approach to identify NBS–LRR genes required for effector-triggered hypersensitive response in *Nicotiana benthamiana*. *Plant Methods* **13**, 32 (2017).

12. Ghorbani, S. *et al.* The SBT6.1 subtilase processes the GOLVEN1 peptide controlling cell elongation. *J. Exp. Bot.* **67**, 4877–4887 (2016).

13. Domazakis, E. *et al.* The ELR-SOBIR1 complex functions as a two-component receptor-like kinase to mount defence against *Phytophthora infestans*. *Mol. Plant-Microbe Interactions®* **31**, 795–802 (2018).

14. Greenberg, J. T. & Yao, N. The role and regulation of programmed cell death in plant-pathogen interactions. *Cell. Microbiol.* **6**, 201–211 (2004).

15. Planas-Marquès, M. *et al.* Protease activities triggered by *Ralstonia solanacearum* infection in susceptible and tolerant tomato lines. *Mol. Cell. Proteomics MCP* **17**, 1112–1125 (2018).

16. Meijer, H. J. G. *et al.* Profiling the secretome and extracellular proteome of the potato late blight pathogen *Phytophthora infestans*. *Mol. Cell. Proteomics MCP* **13**, 2101–2113 (2014).

17. Raffaele, S., *et al.* Analyses of genome architecture and gene expression reveal novel candidate virulence factors in the secretome of *Phytophthora infestans*. *BMC Genomics* **11**, 637 (2010).

18. Wu, L. *et al.* An overview of activity-based probes for glycosidases. *Curr. Opin. Chem. Biol.* **53**, 25–36 (2019).

19. Morimoto, K., *et* al. Broad-range metalloprotease profiling in plants uncovers immunity provided by defence-related metalloenzyme. *New Phytol.* **235**(3): 1287-1301 (2022).

20. Mellacheruvu, D. *et al.* The CRAPome: a contaminant repository for affinity purification mass spectrometry data. *Nat. Methods* **10**, 730–736 (2013).

21. Buscaill, P. *et al.* Glycosidase and glycan polymorphism control hydrolytic release of immunogenic flagellin peptides. *Science* **364**, eaav0748 (2019).

22. Tian, M. & Kamoun, S. A two disulfide bridge Kazal domain from *Phytophthora* exhibits stable inhibitory activity against serine proteases of the subtilisin family. *BMC Biochem.* **6**, 15 (2005).

23. Götze, M *et al.* A simple cross-linking/mass spectrometry workflow for studying system-wide protein interactions. *Anal. Chem.* **91**, 10236–10244 (2019).

24. Chandrasekar, B., Hong, T. N. & van der Hoorn, R. A. L. Inhibitor discovery by convolution ABPP. *Activity-Based Proteomics: Methods and Protocols* (2017).

25. Ma, Z. *et al.* A *Phytophthora sojae* glycoside hydrolase 12 protein is a major virulence factor during soybean infection and is recognized as a PAMP. *Plant Cell* **27**, 2057–2072 (2015).

26. Xia, Y. *et al.* N-glycosylation shields *Phytophthora sojae* apoplastic effector PsXEG1 from a specific host aspartic protease. *Proc. Natl. Acad. Sci.* **117**, 27685–27693 (2020).

27. Cao, J., *et al. Phytophthora sojae* transformation based on the CRISPR/Cas9 System. *Bio-Protoc.* **12**, e4352–e4352 (2022).

28. Zhang, H. *et al.* N-terminomics reveals control of Arabidopsis seed storage proteins and proteases by the Arg/N-end rule pathway. *New Phytol.* **218**, 1106–1126 (2018).

29. Demir, F., *et al.* Sensitive plant N-terminome profiling with HUNTER. *Methods Mol. Biol. Clifton NJ* **2447**, 139–158 (2022).

30. Demir, F., *et al.* Quantitative proteomics in plant protease substrate identification. *New Phytol.* **218**, 936–943 (2018).